DOT/FAA/TC-20/22

Air Traffic Organization
NextGen & Operations Planning
Office of Research and
Technology Development
Washington, DC 20591

Effect of Jet Fuels Exposure on Aerospace Composites – Literature Review

April 2021

Final Report

U.S. Department of Transportation
Federal Aviation Administration

NOTICE

Technical Report Documentation Page

Form DOT F 1700.7 (8-72) Reproduction of completed page authorized

1. Report No.	2. Government Accession No.	3. Recipient's Catalog No.
DOT/FAA/TC-20/22		

4. Title and Subtitle Effect of Jet Fuels Exposure on Aerospace Composites – Literature Review	5. Report Date April 2021
	6. Performing Organization Code
7. Author(s) Rania Bassou, Naoufal Harich, Thomas Lacy, Charles Pittman, Matthew W. Priddy, and Santanu Kundu	8. Performing Organization Report No.
9. Performing Organization Name and Address Mississippi State University 479-1 Hardy Road Mississippi State, MS 39762	10. Work Unit No. (TRAIS)
	11. Contract or Grant No.
12. Sponsoring Agency Name and Address U.S. Department of Transportation Federal Aviation Administration Washington, DC 20591	13. Type of Report and Period Covered
	14. Sponsoring Agency Code AIR-600

15. Supplementary Notes

16. Abstract

Composites may display serious degradation of mechanical properties under extreme environments and exposure to organic fluids. In addition, the composite chemical structure and properties may be negatively impacted by exposure to and absorption of aeronautical fluids, hence the need to provide residual strength assessments as a function of jet fuel exposure to ensure overall aircraft flight safety. This document provides a survey of different types of aeronautical fluids that composites may encounter during their service life, with an emphasis on conventional jet fuels and alternative jet fuels. Also, state-of-the-art aerospace fiber/matrix composites are assessed. Then, the diffusion process of solvents into polymeric composites is explained kinetically and thermodynamically. Additionally, fundamental interaction mechanisms between the aeronautical fluids and aerospace composites, reinforcing fibers, and polymer matrices are investigated. Illustrative summaries are presented which show the scope of previous damage and composite property loss investigation parameters such as the type of aeronautical fluid, temperature and duration of exposure, the composite's or polymer's chemical composition, layup, and matrix type. Finally, the effects of matrix degradation and the loss of adhesion at thefiber-matrix interfaces on the mechanical properties as a function of fluid uptake were investigated.

17. Key Words	18. Distribution Statement
Solvent Diffusion, chemistry of diffusion, carbon/epoxy composites, mechanical properties, thermal properties	This document is available to the U.S. public through the National Technical Information Service (NTIS), Springfield, Virginia 22161. This document is also available from the Federal Aviation Administration William J. Hughes Technical Center at actlibrary.tc.faa.gov.

19. Security Classif. (of this report)	20. Security Classif. (of this page)	21. No. of Pages	22. Price
Unclassified	Unclassified	98	

Contents

Figures

Tables

Acronyms

Acronym	Definition
FAA	Federal Aviation Administration
DMA	Dynamic Mechanical Analysis
T_g	Glass Transition Temperature
NDI	Non-Destructive Inspection
NIAR	National Institute for Aviation Research
ILT	inter-laminar tension
ASTM	American Society for Testing and Materials
ATJ	Alcohol-to-Jet
SPK	Synthetic Paraffinic Kerosene
FT	Fischer Tropsch
HEFA	Hydroprocessed Esters and Fatty Acids
HFS-SIP	Hydroprocessed Fermented Sugars to Synthetic IsoParaffins
RH	Relative Humidity
E'	Storage Modulus
E''	Loss Modulus
tan(δ)	Tangent Delta
DMA T_g	T_g from storage modulus curve
DMA T_t	T_g from Tangent Delta curve
GA	General aviation
PEEK	Poly(etheretherketone)
JP	Jet Propellant
BMI	Bismaleimide
AS4	Carbon fibers
IM7	Carbon fibers
IM8	Carbon fibers
APC(HTA)	Aromatic Polymer Composite (High Temperature Amorphous)
PPS	Polyphenylene Sulfide
MeCl	Methylene Chloride
MEK	Methyl Ethyl Ketone
f_T	Ultimate strength in tension
f_{OT}	Open-hole ultimate strength in tension
f_{OC}	Open-hole ultimate strength in compression

Acronym	Definition
E_T	Young's modulus in tension
f_S	Interlaminar shear strength
GC	Gas Chromatography
MS	Mass Spectrometry
TGA	Thermogravimetric Analysis
TD	Thermal Desorption
HSPs	Hansen Solubility Parameters
AFCESA	Air Force Civil Engineer Support Agency
HRJ	Hydrotreated Renewable Jet
FTIR	Fourier Transform Infrared Spectroscopy
DSHC	Direct-Sugar-to-HydroCarbon
ACI	Advanced Composites Institute
NCAMP	National Center for Advanced Materials Performance
ILT	InterLaminar Tension
NIAR	National Institute for Aviation Research
CDT	Cold Temperature Dry
DiEGME	Diethylene Glycol Monomethyl Ether
AVGAS	Aviation Gasoline
CAL	Continental Airlines
ANZ	Air New Zealand
JAL	Japan Airlines
UOP	Universal Oil Products
CLEEN	Continuous Lower Energy Emissions and Noise
CAAFI	Commercial Aviation Alternative Fuel Initiative
NREL	National Renewable Energy Laboratory
RFS	Renewable Fuel Standard
RRB	Red Rock Biofuels
SAJF	Sustainable Alternative Jet Fuels
DEFSTAN	Defense Standard
FT-SPK/A	Fischer Tropsch- Synthetic Paraffinic Kerosene with increased aromatic content
CHJ	Catalytic Hydrothermolysis Jet
HC	Hydroprocessed Hydrocarbons
Bb-oil	Botryococcus braunii oil

Acronym	Definition
PMC	Polymer Matrix Composite
PMR	Polymerization of Monomeric Reactants
DGEBA	Diglycidyl Ether Bisphenol A
DDM	Diaminodiphenyl Methane
DETA	Diethylenetriamine
IPD	Isophorone
MDA	Methylenedianiline
HMTA	Hexamethylenetetramine
BTDE	Benzophenone Tetracarboxylic Dialkyl Ester
p-DCB	Para-Dichlorobenzene
NaSH	Sodium Hydro Sulfide
Na_2S	Sodium Sulfide
HDM	Hindered Diffusion Model
DDA	Dicyandiamide
DGEBF	Bisphenol F Diglycidyl Ether
DSC	Differential Scanning Calorimetry
SEM	Scanning Electron Microscopy
PEI	Poly (etherimide)
SAXS	Small-Angle X-ray Scattering
WAXS	Wide-Angle X-ray Scattering
AFCESA	Air Force Civil Engineer Support Agency

Executive summary

Composite materials have increasingly been used as an alternative to metals over the last few decades due to the plethora of advantages they offer, such as tailorability. These materials may display serious degradation of mechanical properties under extreme environments and exposure to organic fluids. In addition, the composite chemical structure and properties may be negatively impacted by exposure to and absorption of aeronautical fluids, hence the need to provide residual strength assessments as a function of jet fuel exposure to ensure overall aircraft flight safety. This document provides a survey of different types of aeronautical fluids that composites may encounter during their service life. Some of these fluids are basic in nature, such as hydraulic fluids and cleaning solvents, while other fluids are highly acidic service-fluids. Polymeric composites used in aircraft are typically highly resistant to the basic fluids and less resistant to the highly acidic fluids. Hence, understanding the effects of service-fluids that structural composites may encounter is of utmost importance.

The aeronautical fluids emphasized in this survey are conventional jet fuels and alternative jet fuels. Commercial conventional fuels such as Jet A, Jet A-1, and Jet B, as well as military jet fuels such as JP-4 and JP-8 are usually derived from a crude oil-based feedstock comprised of a mixture of several hydrocarbons. Depending on their major chemical compositions, these hydrocarbons are characterized as paraffinic, naphthenic, or aromatic. Alternative jet fuels are usually blended with Jet A fuel in a specified amount following American Society for Testing and Materials (ASTM) standards to be approved as drop-in fuels. This would allow the usage of these alternative jet fuel blends directly in aircraft without the need for recertification and without compromising the aircraft's operability, performance, and safety. These alternative jet fuels are derived through different processes and feedstocks including the Fischer-Tropsch Synthetic Paraffinic Kerosene (FT-SPK), the Hydroprocessed esters and fatty acids (HEFA-SPK), and the Alcohol-to-Jet synthetic paraffinic kerosene (ATJ-SPK) processes.

Additionally, state-of-the-art aerospace fiber/matrix composites are assessed. Carbon, graphite, aramid, and glass are the reinforcing fibers commonly used in aerospace applications. Matrices used in aerospace applications are usually polymers, which bind the reinforcements together and transfer the load to the reinforcements. The matrix prevents damage from fiber-to-fiber friction. The matrix also provides a protective surface finish from harsh chemicals and other foreign substances. The matrix can either be a thermoplastic or a thermoset polymer. Common aerospace-grade thermoset polymers include epoxies, phenolics, and bismaleimides (BMI), while common thermoplastics are poly(ether ether)ketone (PEEK) or polyphenylene sulfide (PPS).

The diffusion process of solvents into polymeric composites is explained kinetically and thermodynamically. Kinetically, diffusion is a process in which matter is transported from one part of a system to another due to random molecular motions. These molecules diffuse into the free volume present in the polymer. The most used diffusion model is the Fickian model, where the governing equations are based on Fick's second law. Thermodynamically, the amount of a fluid that will diffuse into a material at equilibrium is determined by the free energy change in the system. This free energy change is the driving force that causes the diffusion to occur. The overall free energy change between the sum of the free energies of the starting components (fluid and the starting matrix polymer or composite) and the sum of the free energies of the polymer (or composite) containing the absorbed fluid plus the fluid that remains of the original starting amount is the driving force.

Additionally, fundamental interaction mechanisms between the aeronautical fluids and aerospace composites, reinforcing fibers, and polymer matrices are investigated. Illustrative summaries are presented, which show the scope of previous damage and composite property loss investigation parameters such as the type of aeronautical fluid, temperature and duration of exposure, the composite's or polymer's chemical composition, layup, and matrix type. Finally, the effects of matrix degradation and the loss of adhesion at the fiber/matrix interfaces on the mechanical properties as a function of fluid uptake were investigated. Aeronautical fluids effects on aerospace composites comprise mechanical property degradation (e.g., stiffness, tensile strength, flexural strength, compressive strength, etc.), thermal degradation (e.g., T_g), and can lead to the degradation of the structural integrity of the composite (e.g., delamination, fiber/matrix debonding, matrix cracking, etc.).

1 Introduction

Composite materials are increasingly being used in the aerospace industry as an alternative to metals, primarily due to their high specific mechanical properties (stiffness, strength, etc.), and tailorability. Composites have applications in primary aerospace structures such as the fuselage, wings, and fuel tanks for general aviation (GA) aircraft, commercial aircraft, and unmanned aerial vehicles. As the composites are of lower density compared to the metals, application of these result in a lower vehicle mass, which in turn can lead to improved fuel efficiency. In fact, utilizing fiber-reinforced polymers in aircraft structures can lead to an overall weight reduction of 20-40% compared to the metallic structures (Mazumdar, 2001). In addition, composite structures display exceptional corrosion and fatigue resistance properties.

During their lifetime, composite materials can be subjected to water, fuels, or other types of aeronautical fluids. These fluids can diffuse through the matrix phase leading to liquid uptake into the composite; however, the amount of diffused fluid depends on the contact timescale, fluid type, matrix composition (fiber/matrix content), fiber dimensions, and specimen dimensions. In addition, chemical compositions of the fluid and matrix, and the interactions between them affect the diffusion process. For example, for the same matrix material, the uptake amount of two different aeronautical fluids can vary, because of different chemical compositions of these two distinct fluids. Uptake of liquids into the composites' matrices (thermoplastics or cured crosslinked resins) can plasticize the matrix, change the nature of the fiber-to-matrix interface, etc. All of these can have a profound effect on the composites' mechanical, thermal, and physicochemical properties, potentially leading to various failure mechanisms.

In comparison to the tensile-dominated flaw growth in metals, composites display a multitude of failure mechanisms depending on the loading conditions. For example, when loaded in tension and/or shear, failures are typically due to matrix cracking, fiber/matrix debonding, delamination, fiber rupture, etc. Stability-related failures such as fiber micro-buckling, face sheet crimping, delamination buckling, and core instabilities under compression loading are also observed. Matrix-related failure mechanisms can be aggravated as aeronautical fluids are diffused into the matrix and to the fiber/matrix interface.

This literature review provides a survey of different types of aeronautical fluids that composites may encounter during their service life, with an emphasis on conventional and alternative aviation jet fuels . In addition, this review will assess state-of-the-art bare aerospace fiber/matrix composites, meaning that the presence of protective barriers on composites will not be investigated within the scope of this study. Then, the diffusion process of solvents into polymeric composites is explained kinetically and thermodynamically. Finally, this review investigates fundamental interaction mechanisms between the aeronautical fluids and aerospace composites, reinforcing fibers, and polymer matrices.

2 Literature review

2.1 Types of aeronautical fluids

Composite materials in the aerospace industry encounter many service-related aeronautical fluids. These structural composites generally have an epoxy matrix known to be highly fluid resistant, specifically to service fluids that are basic in nature, such as hydraulic fluids and cleaning solvents, and less fluid resistant to some highly acidic service-fluids. Also, the structural composites level of exposure to service-fluids (whether they were in contact with fluids for long periods of time or if they were in contact with fluids periodically for short amounts of time) plays a role in how these aeronautical fluids affect composites with which they come in contact. Hence, understanding the effects of service-fluids which composites may come in contact with is of utmost importance (Handbook, 2002).

2.1.1 Anti-icing and deicing fluids

Anti-icing fluid is a fuel additive that prevents water dissolved in the fuel from freezing at low temperatures. The currently accepted anti-icing additive is diethylene glycol monomethyl ether (DiEGME) with a chemical formula of $HOCH_2CH_2OCH_2CH_2OCH_3$. Isopropyl Alcohol can also be used as an anti-icing additive in avgas but not jet fuel. Its chemical formula is $CH_3CHOHCH_3$. Deicing fluid is applied to the outside of aircraft to remove ice and snow on the aircraft. Deicing fluids are usually composed of ethylene glycol or propylene glycol, as well as other components such as thickening agents, surfactants, corrosion inhibitors, and UV-sensitive dye. Propylene glycol-based fluid is used more frequently since it is less toxic than ethylene glycol (Pillard & DuFresne, 1999).

2.1.2 Hydraulic fluids

(Aircraft Hydraulic Fluids Types, Intermixing, Contamination, Flushing and Handling, n.d.). Only qualified hydraulic fluids (FAA regulations) can be used in a certified aircraft (Shell, n.d.). There are three principal categories of hydraulic fluids. The first category is mineral oil-based, which provides excellent operational properties over the temperature range of –54 °C to 135 °C, though it is highly flammable (Hydraulic fluid: Aircraft hydraulic systems, n.d.). The second category is polyalphaolefin based, which is compatible with mineral-based hydraulic fluids and was developed to address the low flash point drawback of mineral-based hydraulic fluids (Hydraulic fluid: Aircraft hydraulic systems, n.d.). The third type is phosphate ester based, such as Skydrol (fire-resistant hydraulic fluid), which is used in the most commercial aircraft and are extremely fire-resistant (Aircraft Hydraulic Fluids Types, Intermixing, Contamination, Flushing and Handling, n.d.; Parts, 1979).

2.1.3 Conventional jet fuels

Common aviation fuels are usually derived from a crude oil-based feedstock comprised of a mixture of several hydrocarbons. Depending on their major chemical compositions, these hydrocarbons are characterized as paraffinic, naphthenic, or aromatic. The most significant stage in the standard oil refining process is distilling the crude oil to the desired fuel range. Similar to any distillation process, the quality of the generated product is affected by the temperature at which the process is occurring. The most widely used distillate as a fraction of contemporary jet fuels like JP-8 and Jet A-1 is Kerosene, which is distilled at around 204.5 °C (Pond & Company, Inc., 2012).

There are two main types of aviation fuels: reciprocating-engine fuel (also referred to as "aviation gas" AVGAS, or simply gasoline), and aviation turbine fuel (Aviation Maintenance Technician Book Vol. 2 , 2012). AVGAS is highly volatile, intensely flammable, and specifically formulated for spark-ignited internal-combustion aircraft engines. Some AVGAS contains lead and is not used in commercial jet aircraft.

For jet aircraft, three types of jet fuels (A, A-1, and B) are available. Jet A is mostly used in the contiguous United States and some parts of Canada, while Jet A-1 is used in the rest of the world. Jet B is a more volatile jet fuel that is formulated for use in cold climates but is rarely used today. Table 1 illustrates components present in different types of fuels, where Jet A fuel components are highlighted, and Table 2 illustrates the typical overall weight percentage content of the n-paraffin, iso-paraffin, olefin, naphtene, and aromatic fractions.

Both Jet A and Jet A-1 have historically been obtained by fractional distillation of crude oil, but other refining processes such as hydrocracking and fluid catalytic cracking are now utilized more often. These fuels are similar to kerosene and consist of hydrocarbons with 8-12 carbon atoms, shown in Figure 1. In addition to linear and branched alkanes, some amount of naphthenic and aromatic compounds are also present. Note that gasoline and diesel have physical properties inadequate for airplanes: the shorter hydrocarbons in gasoline can cause the fuel to be too volatile. The longer hydrocarbons in diesel can increase the fuel's freezing point, constraining the operating conditions of the aircraft (Fellet, 2016).

Table 1. Main components of regular fuels (Pires, Han, Kramlich, & Garcia-Perez, 2018).

Component	**Molecular Form**	**Classification**
Heptane	C_7H_{16}	Paraffin
Heptane, 2-methyl	C_8H_{18}	Paraffin
Heptane, 3-methyl	C_8H_{18}	Paraffin
Octane	C_8H_{18}	Paraffin
Cyclohexane, ethyl-	C_8H_{16}	Naphthene
Octane, 4-methyl-	C_9H_{20}	Paraffin
Octane, 2-methyl-	C_9H_{20}	Paraffin
Heptane, 2,5-dimethyl-	C_9H_{20}	Paraffin
Octane, 3-methyl	C_9H_{20}	Paraffin
Heptane, 2,2,4-trimethyl	$C_{10}H_{22}$	Paraffin
Cyclopenthane, butyl	C_9H_{18}	Naphthene
Nonane	C_9H_{20}	Paraffin
Hexane, 3-ethyl-2,5-dimethyl-	$C_{10}H_{22}$	Paraffin
Benzene, 1,3-dimethyl-	C_8H_{10}	Aromatic
Cyclohexane, propyl-	C_9H_{18}	Naphthene
Octane, 2,5,6-trimethyl	$C_{11}H_{24}$	Paraffin
Nonane, 2-methyl-	$C_{10}H_{22}$	Paraffin
Nonane ,3-methyl-	$C_{10}H_{22}$	Paraffin
Heptane, 2,2,4,6,6-pentamethyl	$C_{12}H_{26}$	Paraffin
Nonane, 2,3-dimethyl-	$C_{11}H_{24}$	Paraffin
Decane	$C_{10}H_{22}$	Paraffin
Cyclohexane, 1-methyl-2-propyl-	$C_{10}H_{22}$	Naphthene
Heptane, 5-ethyl-2,2,3-trimethyl-	$C_{12}H_{26}$	Paraffin
Benzene, 1-ethyl-2-methyl-	C_9H_{12}	Aromatic
Decane, 3-methyl-	$C_{11}H_{24}$	Paraffin
Benzene,1,2,3 – trimethyl-	C_9H_{12}	Aromatic
Decane,3,7-dimethyl-	$C_{12}H_{26}$	Paraffin
Undecane, 4-methyl-	$C_{12}H_{26}$	Paraffin
Undecane	$C_{11}H_{24}$	Paraffin
Benzene, 1-ethenyl-2-methyl-	C_9H_{14}	Aromatic
Benzene, 1,2-diethyl-	$C_{10}H_{14}$	Aromatic
Benzene, 1-methyl-4-(2-propenyl)-	$C_{10}H_{12}$	Aromatic
Benzene, 1-ethyl-2,4-dimethyl-	$C_{10}H_{14}$	Aromatic

Component	Molecular Form	Classification
1-Methyl-2-(4-methylpentyl)cyclopentane	$C_{12}H_{24}$	Naphthene
Undecane, 3-methyl	$C_{12}H_{26}$	Paraffin
Benzene, 1,2,3,5-tetramethyl	$C_{10}H_{14}$	Aromatic
1,1'-Bicyclohexyl, 2-methyl-, cis	$C_{13}H_{24}$	Naphthene
Z-1,6-Tridecadiene	$C_{13}H_{24}$	Olefin
Dodecane	$C_{12}H_{26}$	Paraffin
Benzene, 1-ethenyl-4-ethyl-	$C_{10}H_{12}$	Aromatic
Benzene, 1-methyl-2-(2-propenyl)-	$C_{10}H_{12}$	Aromatic
Undecane, 2,6-dimethyl	$C_{13}H_{28}$	Paraffin
Naphtalene, 1,2,3,4-tetrahydro-	$C_{10}H_{12}$	Aromatic
Benzene, 2-ethenyl-1,3,5-trimethyl-	$C_{11}H_{14}$	Aromatic
Cyclohexane, hexyl-	$C_{12}H_{24}$	Naphthene
Dodecane, 3-methyl-	$C_{13}H_{28}$	Paraffin
Naphtalene, 1,2,3,4-tetrahydro-2-methyl-	$C_{11}H_{14}$	Aromatic
Tridecane	$C_{13}H_{28}$	Paraffin
Nonane, 2,2,4,4,6,8,8-heptamethyl-	$C_{16}H_{34}$	Paraffin
Naphtalene, 1,2,3,4-tetrahydro-5-methyl-	$C_{11}H_{14}$	Aromatic
Tridecane,3-methyl-	$C_{14}H_{30}$	Paraffin
Dodecane, 2, 6, 10-trimethyl	$C_{15}H_{32}$	Paraffin
Naphtalene, 1,2,3,4-tetrahydro-2,7-dimethyl-	$C_{12}H_{16}$	Aromatic
Tetradecane	$C_{14}H_{30}$	Paraffin
Pentadecane, 7-methyl-	$C_{16}H_{34}$	Paraffin
Tetradecane, 3-methyl-	$C_{16}H_{34}$	Paraffin
Pentadecane	$C_{15}H_{32}$	Paraffin
Hexanedecane	$C_{16}H_{34}$	Paraffin
Heptadecane	$C_{17}H_{36}$	Paraffin

Table 2. Typical Overall wt. % content of the fractions (Reproduced from reference (Pires, Han, Kramlich, & Garcia-Perez, 2018)).

Fuel	n-paraffin	Iso-paraffin	Olefin	Naphthene	Aromatic

Jet A fuel	28.1	38.8	1.2	15.1	14.4

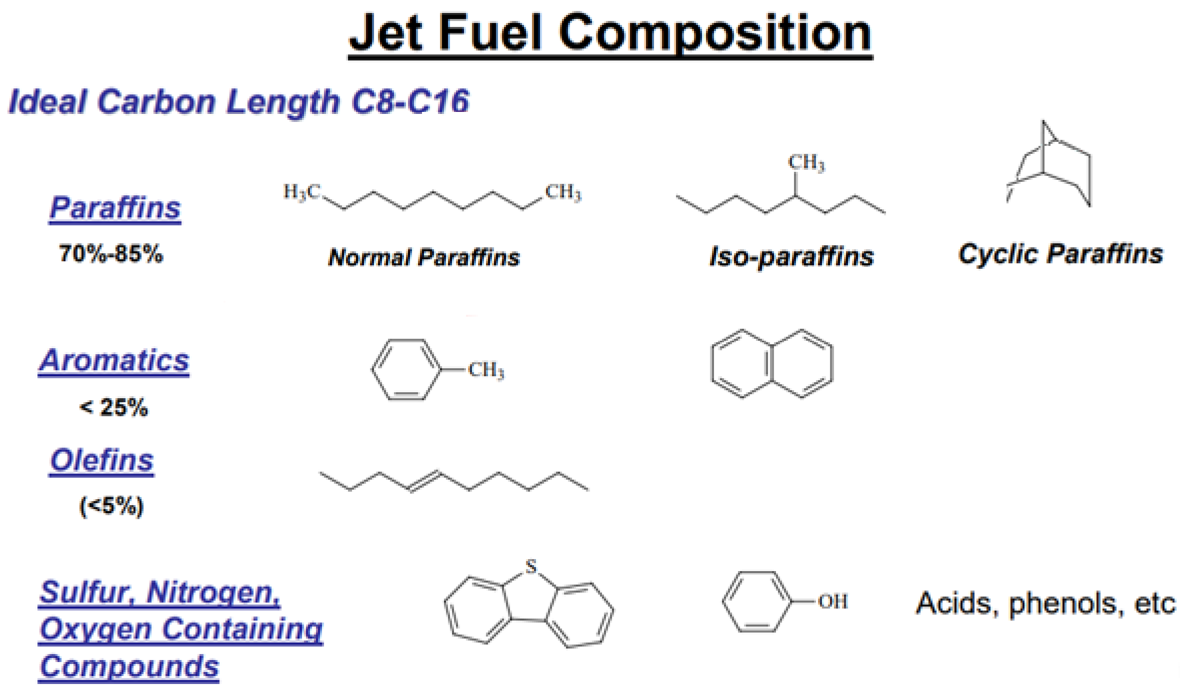

Figure 1. Jet fuel and blends of Bio-SPK and conventional Jet fuel composition (Rahmes, et al., 2009).

Both Jet A and Jet A-1 have low volatility with flashpoints ranging between 110-150 °F. The only difference between Jet A and Jet A-1 is the freezing points of -40 °C and -47 °C, respectively (Aviation Maintenance Technician Book Vol. 2 , 2012). Jet B is well suited for colder areas (e.g., Alaska, Canada) because of its higher volatility and lower freezing point (-50 °C) relative to Jet A and Jet A-1. This leads to better performance in cold weather. Jet B is a blend of light naphtha/gasoline and denser kerosene (Aviation fuel: Jet fuel, n.d.). In Jet B, hydrocarbons with 5-15 carbon atoms are present. Also, military Jet Propellant (JP) classification numbers are used to define fuels that are similar to commercially available ones (Aviation fuel: Jet fuel, n.d.). For example, JP-8 and JP-4 are similar to Jet A-1 and Jet B, respectively, although slight differences can be seen in the flash point, volume of aromatics and olefins, and distillation range for Jet A-1 and JP-8, as illustrated in Table 3.

Table 3: Typical characteristics of Jet A-1, and JP-8 fuels (Cheng, Zhou, Chow, Watson, & Frazier, 2001).

Fuel	**JA-1 jet fuel**	**JP-8 jet fuel**

Cetane index		45.3	43.3
Distillation Range	IBP, °F	350.6	341.7
	10%-point, °F	375.6	362.9
	50%-point, °F	414.0	395.9
	90%-point, °F	468.0	448.1
	End-point, °F	495.1	482.5
Flash point, °F		130.0	132.0
Gravity, °API		43.1	44.2
Density, g/ml		0.8104	0.8054
Viscosity	cSt @40 °C	1.435	1.319
Aromatics	Vol. % aromatics	20.9	17.0
	Vol. %olefins	2.4	1.5
Hydrocarbons	Vol. % saturates	76.7	81.5
Sulfur, mass %		0.0119	0.0245
Lead, ppm		<0.1	<0.1
Net heat, kJ/L		34,908	34,743

2.1.4 Alternative jet fuels

The aviation industry has aimed at reducing its greenhouse gas footprint through decreasing overall fuel usage, increasing fuel efficiency, and embracing renewable fuels (Wyman, 2017). In recent years, commercial airlines have started using small amounts of alternative jet fuels. United Airline flights out of Los Angeles International Airport to San Francisco beginning March 2016, Alaska Air flights between Seattle-Tacoma International Airport and Washington D.C beginning November 2016, Singapore airlines on non-stop trans-Pacific flights between Singapore and San Francisco are examples (Wyman, 2017; Aviation Biofuel, n.d.). Air transport companies—such as Boeing, Continental Airlines (CAL), Air New Zealand (ANZ), Japan Airlines (JAL), CFM International, General Electric Aviation, Pratt & Whitney, Honeywell's Universal Oil Products (UOP), and Rolls-Royce—have been vigorously contributing to the development of new aviation alternative fuels. This development will advance aviation industry objectives to decrease life cycle CO_2 emissions, while still meeting or exceeding the existing jet fuel specification properties and being cost-competitive (Rahmes, et al., 2009).

The FAA, in collaboration with the aviation industry, aims to approve alternative aviation fuels following American Society for Testing and Materials (ASTM) standards -which aims to enhance performance and ensure safety of materials usage- through the Continuous Lower

Energy Emissions and Noise (CLEEN) partnership (New alternative jet fuel approved, 2016) and the Commercial Aviation Alternative Fuel Initiative (CAAFI) (CAAFI Fuel Qualification, n.d.). Benefits of developing and approving more alternative jet fuels include the increased potential for low-cost production and extensive use (Biofuels for Aviation: Technology Brief, 2017). Since fuel accounts for about 30% of the total expense of operating an airline, airline companies prefer fossil-derived jet fuels, as they are lessexpensiveOne of the main reasons for the limited use of alternative jet fuels is their high cost of production and feedstock and limited availability (New alternative jet fuel approved, 2016).

The term feedstock is used to describe raw materials needed in industrial processes, such as the production of alternative jet fuels. Common feedstock sources are plants, e.g., Camelina, which is part of the mustard or cabbage family group. It is grown mostly in Northern Europe, Central Asia, and some parts of the U.S. It is considered as feedstock in some conversion to alternative jet fuels processes since its seed generates a large amount of oil. Also, Camelina doesn't require the use of large amounts of water or nitrogen to grow and involves reduced upkeep and weed regulation, thus requiring low overhead costs (Pond & Company, Inc., 2012). KLM Royal Dutch Airline used standard jet fuel and an alternative jet fuel made from Camelina oil in a 50/50 blend for the first commercial passenger flight powered by alternative jet fuels, and studies have claimed that bio-derived fuels produced using Camelina feedstock generate 80% fewer net carbon emissions compared to standard jet fuels (Pond & Company, Inc., 2012).

Another appealing candidate used in making alternative jet fuel is Jatropha, because of its capability to produce large amounts of oil. The Jatropha seed consists of up to 40% refinable oil. Jatropha is a Central and South America native plant. It is easy to grow due to its resistance to drought. Furthermore, potentially over 1,600 gallons of fuel could be produced from Jatropha per acre per year, while capturing four tons of Carbon Dioxide per acre. Also, jatropha oil is very cost competitive to crude oil. In 2008, the actual price of a barrel of jatropha was 43 USD, compared to 122 USD for a barrel of crude oil (Pond & Company, Inc., 2012). Since Jatropha presents many advantages, Air New Zealand operated a test flight using 50/50 blends of Jatropha-based alternative jet fuel with Jet-A1 in 2008. The same airline plans on using larger amounts of the novel alternative jet fuel to cover roughly 10% of the company's overall fuel needs over the next few years (Pond & Company, Inc., 2012).

Other than plants, other types of feedstock are increasingly used in the alternative jet fuel production process, such as algae. The photosynthetic creatures are abundant in nature and specifically thrive in environments with plenty of light, warm water, and carbon dioxide. In the U.S, specifically in water-rich states such as Alabama, up to three billion gallons of biofuel can be generated while merely using 3% of its entire land area (Pond & Company, Inc., 2012). Currently there are multiple projects and corporations engaged in making algae a viable source for alternative jet fuel production. The National Renewable Energy Laboratory (NREL) projected that algae could help generate up to 10,000 gallons of alternative jet fuel per acre every year at a relatively reduced cost (Pond & Company, Inc., 2012). Animal sources, such as tallow, can also be used as feedstock. Although both plants and animals are sources of tallow, the latter is produced mostly from animal fat. Conversion of tallow is not an efficient process due to ensuing complications involved in the esterification stage (separation of esters) (Pond & Company, Inc., 2012).

Other sources of feedstock include sugar-based and starch-based feedstocks. Here, sugars can easily be extracted and fermented, leading to inexpensive large-scale ethanol production. Corn is the primary U.S. crop used as feedstock to generate most domestic ethanol. Corn ethanol is considered a renewable fuel by the Renewable Fuel Standard (RFS) and is restricted to 15 billion gallons. The challenges related to sugar-based and starch-based crops is the struggle to balance needs regarding food production and energy production in a sustainable manner (Ethanol feedstocks, n.d.; Feedstocks for Biofuel Production, 2019). Cellulosic feedstocks comprise crop wastes, wood wastes, and industrial residues. These feedstocks contain cellulose, hemicellulose, and lignin. Typically, the latter is removed and transformed into heat and electricity during the conversion procedure. Cellulosic feedstocks present various advantages compared to sugar-based and starch-based feedstocks. They exist in extensive amounts and can be utilized to generate cellulosic alternative jet fuels (Ethanol feedstocks, n.d.; Feedstocks for Biofuel Production, 2019). LanzaTech (a biotech start-up) was able to use bacteria usually found in rabbits to ferment gas waste of factories and generate ethanol, which is then used in the Alcohol-To-Jet Synthetic Paraffinic Kerosene (ATJ-SPK) process as a feedstock to obtain an alternative jet fuel.

Several companies have initiated a series of projects trying to efficiently convert household garbage and cellulosic woody biomass into jet fuel, including Fulcrum BioEnergy, Red Rock Biofuels, Total, and Velocys, as illustrated in Table 4 (The race is on to repurpose garbage, 2019).

Table 4: Companies seeking to turn waste into jet fuel (Reproduced from reference (The race is on to repurpose garbage, 2019)).

Company	Project location	Completion date	Feedstock	Output
Fulcrum BioEnergy	Gary, Indiana	2022	Household garbage	Renewable crude, jet fuel, and diesel
Red Rock Biofuels	Lakeview, Oregon	2020	Woody biomass	Naphta, jet fuel, and diesel
Total	Dunkerque, France	2020	Woody biomass	jet fuel and diesel
Velocys	Immingham, England	Mid-2020s	Household and office waste	jet fuel and diesel
	Natchez, Mississippi	2004	Woody biomass	Jet fuel and gasoline

Red Rock Biofuels (RRB) is combining gasification with Fischer-Tropsch process to produce jet fuel and diesel gas, utilizing wood residues from sawmill and logging plants. The company is establishing a gasification factory in Lakeview, Oregon, that will use 125,000 t per year of wood residue to produce jet fuel, diesel, and naphtha up to 55 million L. RRB had established deals earlier with Southwest Airlines and FedEx for jet fuel. The firm is incorporating gasifiers with Fischer-Tropsch units to transform syngas into liquid hydrocarbons through catalysis and will hydroprocess the hydrocarbons to jet fuel, diesel, and naphtha. Although significant strides have been made towards using waste to generate jet fuel and other sources of energy, the production of jet fuel using garbage feedstocks is still in its early stages. Financial hurdles, technological obstacles, a challenging market for recycled materials, problems getting environmental permits, low-cost rival petroleum-based fuels, and trouble satisfying engine performance criteria have led some of the initiatives to failure (The race is on to repurpose garbage, 2019).

Engine performance criteria are strict and must be met to guarantee aircraft safety. Engine manufacturers determine what fuel types meet these criteria through fuel specifications. For certified aircraft, changing the fuel type would necessitate recertification of the aircraft to prove that performance, operability, and safety did not deteriorate by employing the new fuels. Recertification may necessitate alterations to the aircraft's engine fuel systems or the fuel, or any other part of the current fuel infrastructure (tanks, pipelines, equipment, etc.). This would expectedly be extremely expensive. Therefore, fuels that can be used "as is"; that satisfy relevant fuel specifications and prevent any unnecessary recertification or great financial investment in aircraft modifications are highly desirable (National Academies of Sciences, 2016). These fuels are referred to as drop-in alternative jet fuels. To be approved as drop-in fuels, ASTM D4054, the "Standard Practice for Qualification and Approval of New Aviation Turbine Fuels and Fuel Additives," must be followed. This standard was established to guarantee the safe and dependable operation of aircraft using alternative aviation fuels for engine and airplane manufacturers and owners (CAAFI Fuel Qualification, n.d.). This ASTM standard covers the four-level process for testing alternative aviation fuels and fuel additives (ASTM International, 2012), as given in Figure 2. First, the alternative fuel must be specified, and then the "fitness for purpose" is determined, followed by testing components. Finally, the engine and auxiliary power unit are tested. At the end of the D4054 tests, the D7566 "Standard Specification for Aviation Turbine Fuel Containing Synthesized Hydrocarbons" (ASTM International, 2011) approval process starts. In this process, the ASTM subcommittee compares the alternative jet fuels properties and characteristics to conventional fossil-derived fuels using data produced under the D4054 testing protocols. If the alternative jet fuel is estimated to be equivalent to conventional jet fuel, then it is designated as a "drop-in fuel," and the process used to produce the fuel can be listed in ASTM D7566. A provision in D7566 recognizes that any fuel meeting the requirements of this specification can be reidentified as conventional fuel. With this addition, any alternative jet fuel can be added to the aircraft without requiring separate tracking or regulatory approval (Office of Energy Efficiency & Renewable Energy, n.d.).

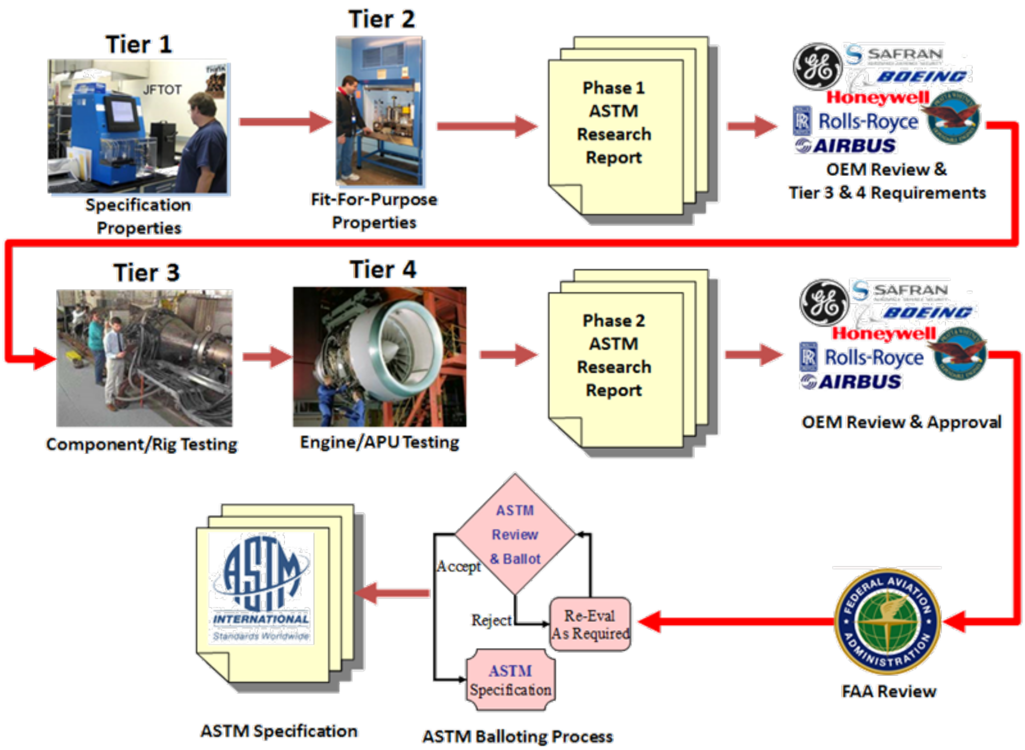

Figure 2. Initial step for drop-in specification process of alternative jet fuels (SAJF) (Office of Energy Efficiency & Renewable Energy, n.d.).

Some alternative jet fuel blending components may be approved as "drop-in" only after being mixed with conventional fuel in a specified amount. This is the case for seven specified alternative jet fuel pathways for air travel use, which are developed through different conversion processes approved by ASTM International, and are related to several feedstock types, such as algae, as discussed above. As an example, these processes from algae feedstock are shown in Figure 3.

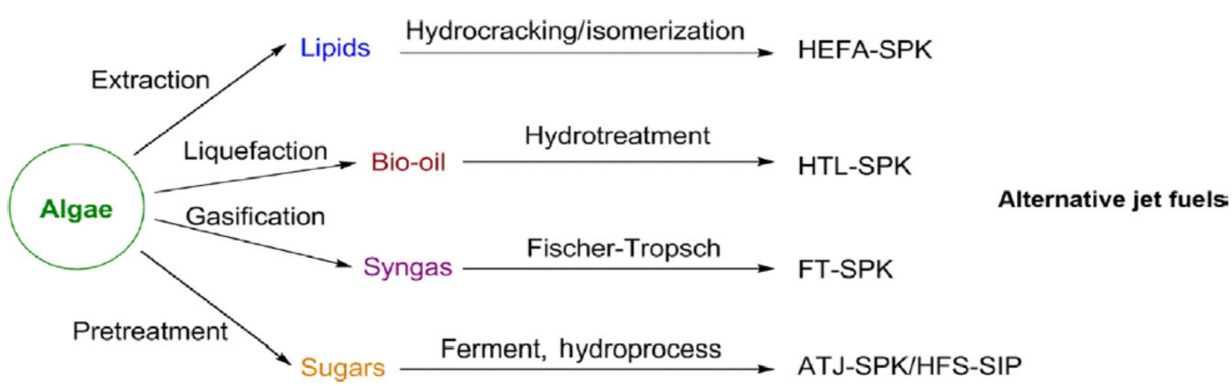

Figure 3. Pathways for alternative fuel production from algae (O'Neil, Knothe, & Reddy, 2019).

Each one of the pathways for alternative fuel production forms some of the hydrocarbons found in petroleum-based jet fuels, which consists of aromatic compounds as well as linear, branched, and cyclic paraffins-saturated hydrocarbons with 8 to 16 carbon atoms, as shown in Figure 4 for hydroprocessed esters and fatty acids (HEFA), Alcohol-to-Jet (ATJ), and Fischer-Tropsch (FT) processes. This mixture generates a fuel with the freezing point, energy density, and lubricity among other properties that resist freezing, boiling, or absorbing water in fuel tanks and fuel lines during in-flight conditions.

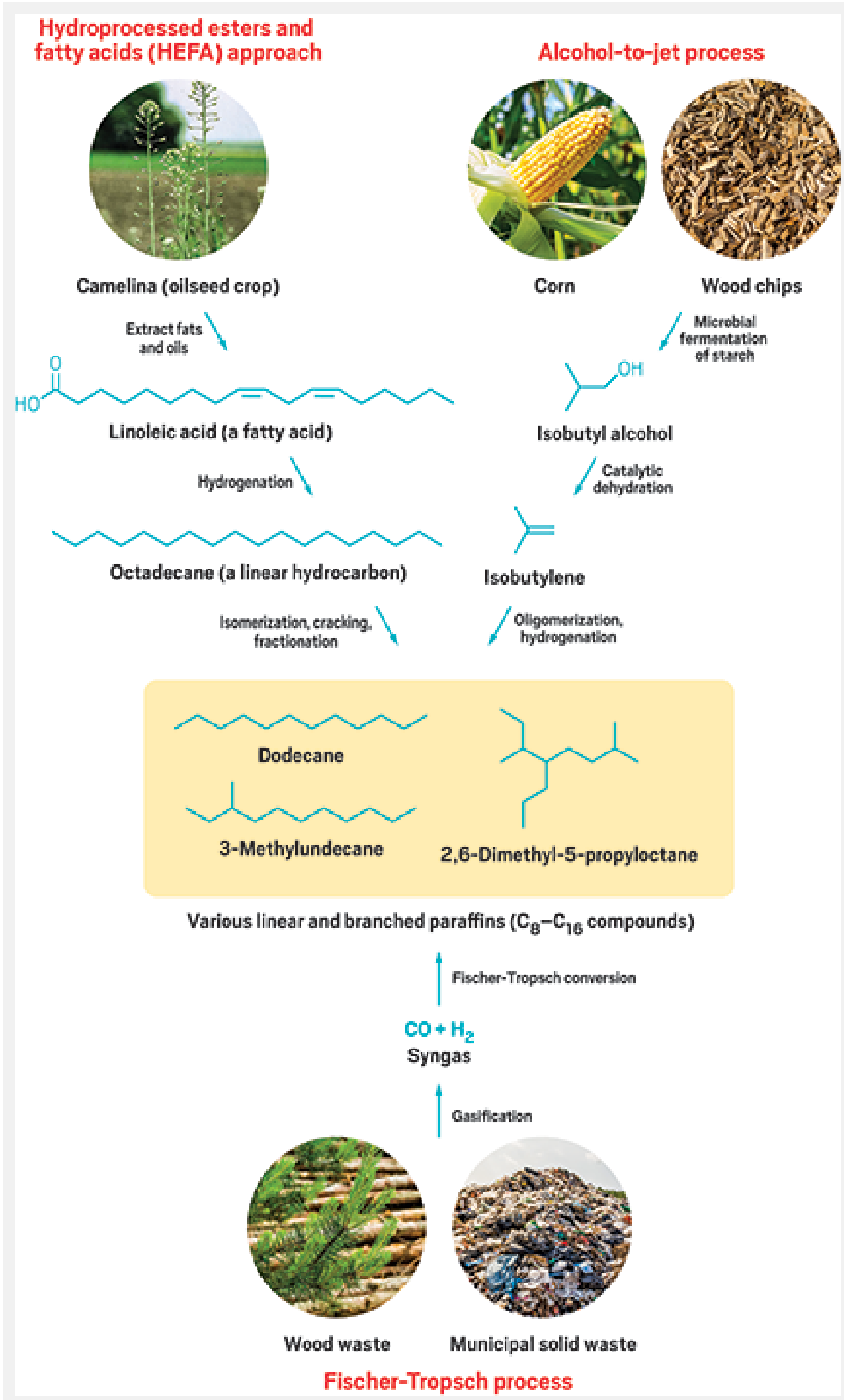

Figure 4. HEFA, ATJ, and FT processes pathways (Fellet, 2016).

- The Fischer-Tropsch Synthetic Paraffinic Kerosene (FT-SPK) process illustrated Figure 5, was approved in 2009 for use in up to 50% blends by volume with conventional fuels, such as Jet A or Jet A-1 fuels. A carbonaceous feedstock source is mainly gasified at high temperatures of 1200-1600 °C into carbon monoxide and hydrogen, thus generating syngas. An FT reactor is then used to convert this syngas into long carbon chain waxes through the FT synthesis. The wax-like product is then cracked and isomerized to develop drop-in fuels similar to the paraffins in petroleum-based jet fuels, but it does not have aromatic compounds. The FT-SPK process combines multiple catalytic processes using cobalt or iron-based catalysts contingent on the synthesis temperature and the goal end products, e.g., jet fuel, bio-diesel, gasoline, olefins, or paraffins. Preferably, FT-SPK feedstocks would contain large concentrations of carbon and hydrogen to boost the effectiveness of the thermochemical FT process. Common suitable feedstock sources for aviation fuel production during this process are biomass like forestry products, or grasses. Biomass is renewable but often varies in carbon content. A less frequently used, yet still renewable feedstock source, is biogas generated from anaerobic digestion of organic matter, e.g., animal manure, landfills, etc (Biofuels for Aviation: Technology Brief, 2017; CAAFI Frequently Asked Questions, n.d.; BENEFITS, 2009; Fellet, 2016).

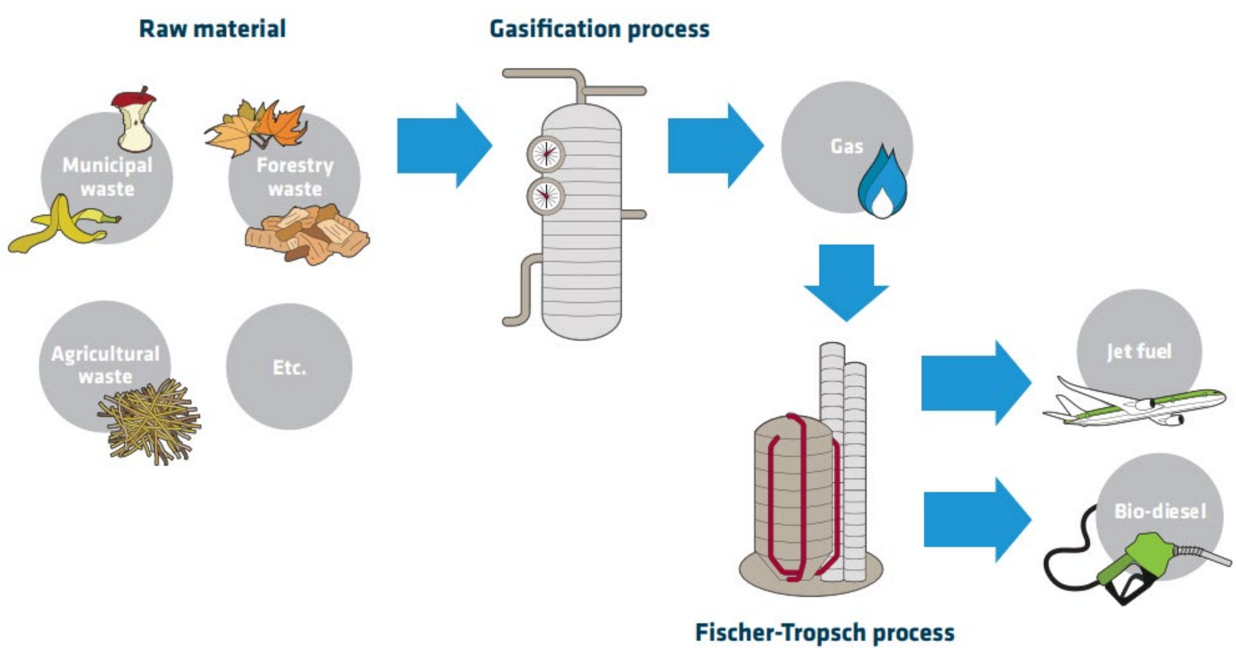

Figure 5. Production of Jet fuel and Bio-Diesel through the Fischer-Tropsch process (ATAG, 2009).

- Hydroprocessed esters and fatty acids (HEFA-SPK) fuel is a type of synthetic paraffinic kerosene fuel made from bio-based oil feedstocks. The four preferable feedstock sources are jatropha, camelina, algae, and tallow (Pond & Company, Inc., 2012). The terms Hydrotreated Renewable Jet (HRJ) and Bio-SPK have been used to refer to HEFA, but all rely on hydroprocessing as the key step in the conversion process. In hydroprocessing, a feedstock reacts with hydrogen at high pressure and temperatures, over a catalyst. The process leads to medium-length (9 to 16 carbon atoms) straight-chain hydrocarbon molecules that are completely saturated. Chemically, the novelty in HEFA/HRJ jet fuel resides in the absence of both aromatics and impurities, and a minimum amount of cycloparaffins (Pond & Company, Inc., 2012). The absence of sulfur, along with a decrease in the hydrocarbons maximum size used in the combustion process leads to cleaner emissions.

  Distillation is used to separate products produced from crude oil into the different types of fuels (diesel, jet, gasoline, etc.), each with different properties suited to their intended use. However, unlike crude oil, the feedstock for HEFA/HRJ must first be hydroprocessed to reduce the number of triglycerides and other impurities (Pond & Company, Inc., 2012). These impurities contain oxygen, nitrogen, and sulfur. Triglycerides are a class of triesters formed from three fatty acids and glycerol (Pond & Company, Inc., 2012).

  Hydroprocessing consists of deoxygenation and hydrocracking and is aimed at reducing the triglycerides to single-chain hydrocarbons and removing feedstock impurities. These processes eliminate +/-90% of these imperfections in the HEFA/HRJ feedstock using standard oil cleaning procedures (Pond & Company, Inc., 2012). The oils are then converted to shorter chain diesel-range paraffins through deoxygenation, which is the elimination of oxygen molecules from the oil and conversion of olefins to paraffins by adding hydrogen as a reactant. The elimination of oxygen increases the fuel's heat of combustion. The elimination of the olefins and the lack of heteroatoms (O, N, S) increases the fuel's thermal stability (Rahmes, et al., 2009; Pond & Company, Inc., 2012). Consequently, the resulting fuel has a higher combustion heat and greater thermal stability than conventional jet fuel. The added hydrogen here acts as a reactant while pressurized in a catalytic reactor and heated to 315-426°C. After deoxygenation, selective cracking/isomerization occurs, as seen in Figure 6, where diesel range paraffins are cracked to mainly branched jet fuel range paraffins, thus improving the freezing point. Upon completion of the hydrocracking, the resulting hydrocarbon paraffin mixture is distilled and processed similarly to Jet A-1 or JP-8. Hydrocracking is most efficient when occurring before the distillation so that the impurities do not interfere with the subsequent subprocesses (Rahmes, et al., 2009; Pond & Company, Inc., 2012).

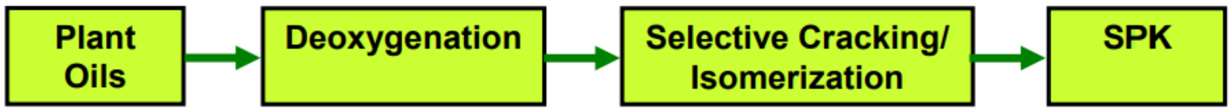

Figure 6. The bio-derived oil-to-SPK conversion process path (Rahmes, et al., 2009).

Since hydrocracking processes do not generate aromatic compounds that are commonly present in up to 25% in volume in regular jet fuel, a 50% blending ratio of HEFA/HRJ with regular jet fuel is needed to meet the ASTM standards discussed previously, as well as the current aviation turbine fuel specification requirements, namely: ASTM D1655 20c (Standard Specification for Aviation Turbine Fuels) (ASTM International, 2020); DEFSTAN 91-91 (the Defense Standard for Turbine Fuel, Kerosene Type, Jet A-1) (Defence Standard, 2002); and the military JP-8 specification for numerous fuel properties such as density (Rahmes, et al., 2009). The resulting HEFA/HRJ is made of molecules, which already exist in conventional jet fuel. The resulting HEFA/HRJ product depends on the processing conditions and is mostly independent on the source of the bio-derived feedstocks (Rahmes, et al., 2009).

- Hydroprocessed fermented sugars to synthetic iso-paraffins (HFS-SIP) (formerly called DSHC (Direct-Sugar-to-HydroCarbon)), was approved in 2014 for use in up to 10% blends with conventional jet fuel. This pathway is specified in D7566 Annex A3 and was issued in June 2014. The development of this pathway was led by Amyris who has a biorefinery in Brazil's São Paulo area that allows the production of up to 50 000 m^3 of the intermediary product farnesene per year while still supplying its renewable diesel product to large areas in Brazil (Michel, 2016).

  The HFS-SIP process, shown in Figure 7, was originally developed from sugar cane and corn. When the feedstock consists of sugars, it can be treated in the synthetic biologic step with micro-organisms and fermentation reaction straightforwardly, transforming the carbohydrates to β-farnesene, an iso–C_{15} tetra-olefin (a sesquiterpene molecule 7,11-dimethyl-3-methylene-1,6,10-dodecatriene, chemical formula $C_{15}H_{24}$). Afterward, the olefin is slightly hydrotreated to the corresponding iso-paraffin known as farnesane (2,6,10-trimethyldodecane, with chemical formula $C_{15}H_{32}$) that can be straightforwardly used as a base jet fuel constituent. If the feedstock is the entire biomass, it is obligatory to isolate the cellulose and hemicellulose from the lignin as a pretreatment stage. Then the cellulose is converted to sugars through hydrolysis, and sugars are transformed through fermentation to farnesene (Michel, 2016). Farnesene has a density of 0.77 kg/l, a kinematic viscosity of 2.325 mm^2/s and a flash point of 110 °C. SIP characteristics generally resemble FT-SPK and HEFA-SPK, but with the major difference that it is a nearly pure molecule and not a complex mixture of normal and isoparaffins.

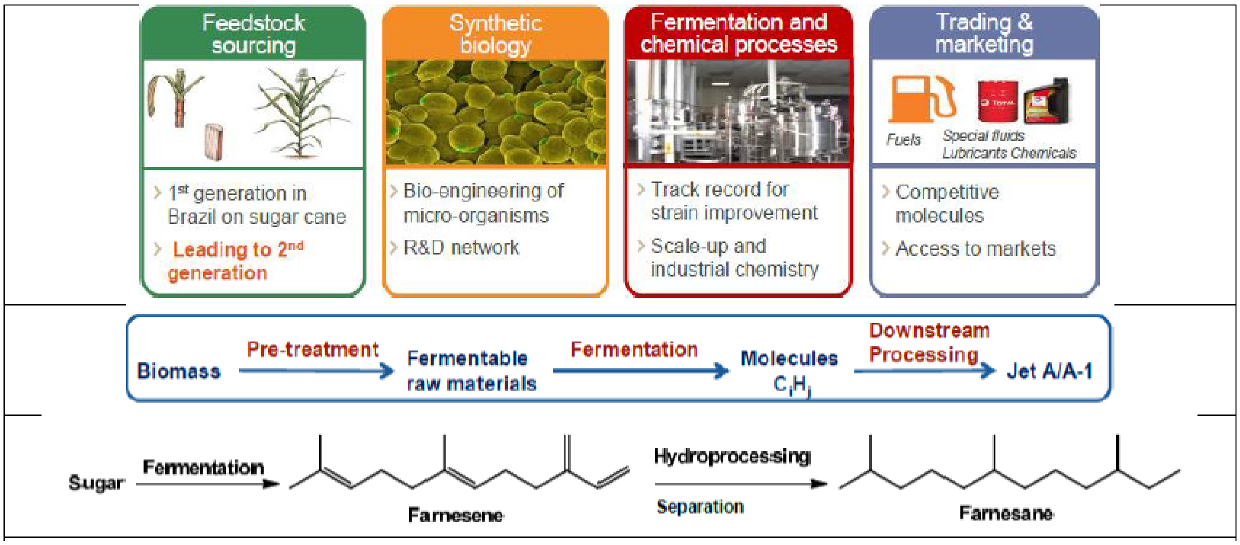

Figure 7. Amyris/TOTAL SIP ASTM certified route (Michel, 2016).

- FT-SPK with increased aromatic content (FT-SPK/A) was approved in 2015 for use in up to 50% blends with conventional jet fuel. The FT synthesis process is used to generate a hydrocarbon blend that comprises aromatic compounds. A minimum of 8% aromatics is needed to guarantee elastomer seal swell in aircraft components. Aromatics may ensure that shrinkage of aged elastomers seals (from dissolving the elastomer components due to fuel) and associated fuel leakage is prevented. Analogous feedstocks to those utilized to generate FT-SPK fuel are utilized with complementary processing steps necessary to generate aromatics. Following the ASTM D7566 specification, the SPK/A synthetic blending elements should contain FT-SPK mixed with synthesized aromatics produced from the alkylation of non-petroleum (coal) derived light aromatics, mainly benzene (Fellet, 2016; O'Neil, Knothe, & Reddy, 2019; Biofuels for Aviation: Technology Brief, 2017; CAAFI Frequently Asked Questions, n.d.; BENEFITS, 2009). This is not considered a bio-derived alternative jet fuel because the benzene stream is extracted from coal, which is a fossil-derived carbon source.

- The Alcohol-to-Jet synthetic paraffinic kerosene (ATJ-SPK) process, illustrated in Figure 8, was approved in 2016 for use in up to 30% blends by volume with conventional jet fuel. Its blend ratio was increased to 50% in 2018. This process uses the fermentation of cellulose and sugar feedstock, e.g., sugar cane, sugar beet, hydrolysed corn or wheat grain starch, hydrolysed polysaccharides derived from lignocellulosic biomass. Numerous bacteria, yeasts, or microbes are utilized to process waste from agricultural products (crop straws, grasses, forestry waste) to be converted either to jet fuel directly or through a group of alcohol conversion pathways. Feedstocks necessary for this process can easily be obtained at a cheaper cost, converting them to fuel doesn't necessitate much energy, making this process an efficient one (New alternative jet fuel approved, 2016; CAAFI Frequently Asked Questions, n.d.; Five Jet Biofuels Now Approved, FAA Says, 2016). Although both the ATJ-SPK and HFS-SIP processes are based on the fermentation of sugars to hydrocarbons, the main difference remains that instead of generating ethanol like in the ATJ-SPK process, HFS-SIP produces substances such as farnesene (synthetic iso-paraffin (SIP)). The initial version of the Annex issued in 2016 was limited to isobutanol as the feedstock. In 2018, the annex was revised to add ethanol as a feedstock.

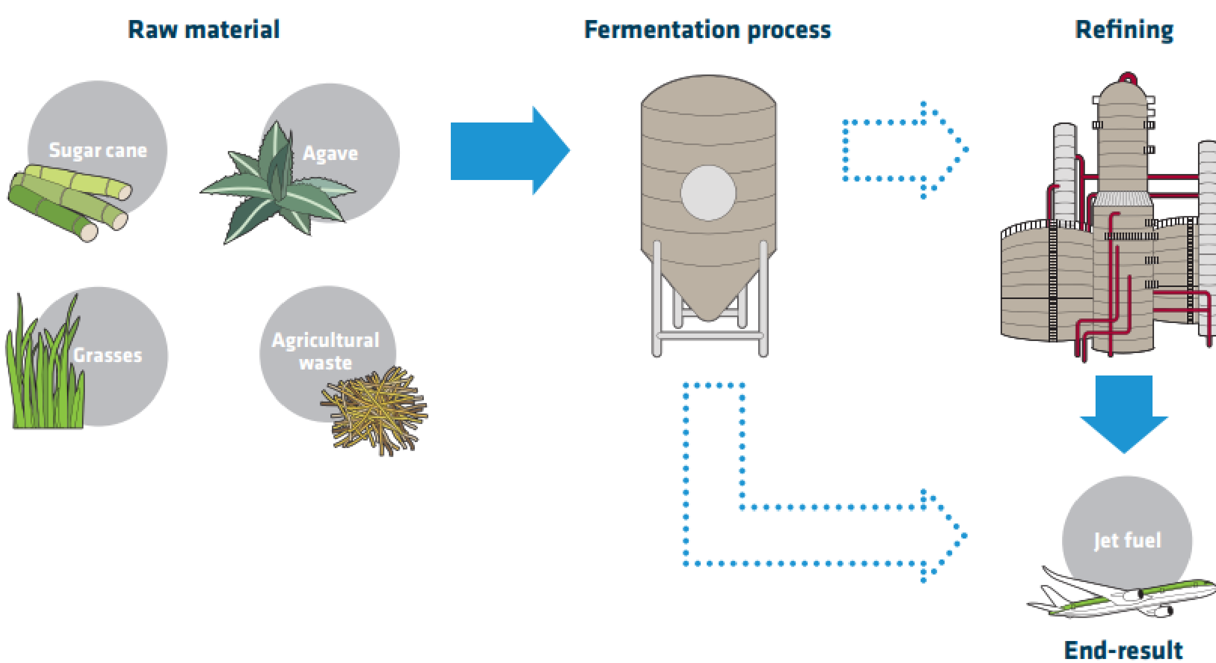

Figure 8. Production of Jet fuel through the ATJ process (ATAG, 2009).

- Synthesized kerosene from hydrothermal conversion of fatty acid esters and fatty acids, identified as catalytic hydrothermolysis jet (CHJ) was approved in December 2019. The process for making CHJ fuels is defined by three integrated unit operations as depicted in Figure 9. The first unit operation is the hydrothermal conversion of fatty acid esters and fatty acids into renewable crude oil via the Catalytic Hydrothermolysis (CH) process. The renewable crude produced by the CH process is referred to as CH crude. The CH process reduces the molecular weight of the feed stock into kerosene and diesel boiling-range compounds and generates all hydrocarbon types present in petroleum jet fuels including aromatic and cycloparaffin compounds. The second unit operation is the hydroprocessing step. Hydroprocessing is necessary to remove residual oxygenates and saturate olefins that were present or formed during CH conversion. The hydroprocessed product is a pure hydrocarbon mixture of naphtha, kerosene, and diesel-boiling-range hydrocarbons. The hydroprocessed product is then fractionated by conventional distillation into specification fuels (ASTM, 2019).

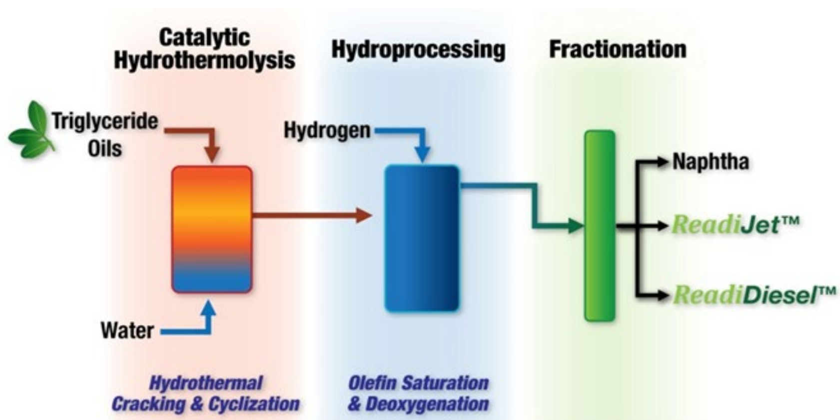

Figure 9. The CHJ process (ASTM, 2019).

- Hydroprocessed hydrocarbons, esters and fatty acids (HC-HEFA) was approved May, 2020. HC-HEFA utilizes the HEFA conversion process to convert a strain of microalgae called Botryococcus braunii (Bb) into an SPK jet fuel blending component. This algae strain has been improved to efficiently produce algal oil, hereafter called Bb-Oil, which is composed primarily of hydrocarbons with a smaller amount of free fatty acids resulting in much lower oxygen content than traditional HEFA feedstocks. The standard HEFA process described in ASTM D7566 Annex A2 can be used to convert the hydrocarbon rich Bb-Oil to a high quality SPK blending component (designated Bb-SPK). HC-HEFA was evaluated under a new provision in D4054 called the Fast Track process. This allowed for an expedited evaluation and approval, but the blend concentration with conventional jet fuel is limited to 10%.

2.2 Introduction to polymeric composites and polymers

2.2.1 Polymeric composites

Composite materials are made from a combination of two or more components that are dissimilar in form and/or material composition and have different properties (Mangalgiri, 1999). These components, when combined, produce a material with superior properties compared to traditional aircraft materials. Composites offer numerous advantages such as light weight, high specific strength and stiffness, the ability to tailor the directional strength and stiffness, high fatigue and corrosion resistance and the ability to mold large intricate parts in a short period of time (Mangalgiri, 1999). However, composites are prone to weaknesses such as a weak interface between phases, low resistance to out-of-plane tensile loading, and highly sensitive to environmental effects, with subsequent property degradation and overall performance losses. Manufacturing defects can also lead to a degradation of material properties (Mangalgiri, 1999).

Composite manufacturing processes require high precision. These processes include filament winding, resin infusion, and usage of prepregs. Filament winding is common when making shell-like parts such as rocket motor casings used in missiles and launch vehicles. Resin infusion is a composite manufacturing process used to make low-defect large-scale parts. First, dry fabric preforms are placed in an open mold, which in turn is placed within a plastic vacuum bag. The one-sided mold is linked to a resin source and a vacuum pump. Then the liquid resin infuses into the continuous reinforcing fibers through a vacuum drawn through the mold. During the last step, the resin-infused fibers are cured and de-molded (Daniel, 1978). Resin infusion molding can also be used to make special parts such as radomes (Mangalgiri, 1999).

Prepregs are sheets of fibers pre-impregnated with resin (Mangalgiri, 1999). These single-layered sheets are stacked following the hand lay-up process. They are the most used raw materials in aerospace composites. The thickness of the composite depends on the number of layers used. Placing sheets at different angles allows different orientations of fibers between plies, which improves the overall properties of the composite (Brown, 2013). After stacking prepreg layers, air is often removed from the layered composite under vacuum in a vacuum bag to make sure no air bubbles remain between the layers. Then, the stacked sheets are cured using either an autoclave or a regular oven. An autoclave controls both the curing pressure and temperature. Oven-curing is mainly used for glass fiber composites utilized in low-speed small aircraft. Oven-cured composites contain a higher percentage of voids leading to low hygrothermal sensitivity, higher moisture content, and higher diffusivity, as opposed to autoclave-cured composites (Akay, Mun, & Stanley, 1997). During the last step, the resin-infused fibers are cured and de-molded (Daniel, 1978).

The majority of aerospace-grade composite materials used in commercial aircraft principal structures are autoclave-cured and are made of continuous carbon fiber reinforcements and a matrix. The main function of the reinforcement in a polymer matrix composite (PMC) is to carry the load and provide stiffness, strength, and other structural properties. Carbon fiber reinforcements are generally 5–10 micrometers diameter or fibers made of carbon, graphite (higher modulus than carbon fibers), glass, or aramid (such as Kevlar), as seen in Table 5 (Johnson, 2019). Carbon fibers are mostly used in aerospace applications due to their high modulus, specific modulus, strength, specific strength and fatigue strength (Huang, 2009).

Table 5: Reinforcing fibers used in aerospace applications (Reproduced from reference).

Fiber	Density (g/cc)	Modulus (GPa)	Strength (GPa)	Application areas
Glass				
E-glass	2.55	65-7 (Mangalgiri, 1999)5	2.2-2.6	Small passenger aircraft parts, aircraft interiors, secondary parts, radomes, rocket motor casings
S-glass	2.47	85-95	4.4-4.8	Highly loaded parts in small passenger aircraft
Aramid[1]				
Low modulus	1.44	80-85	2.7-2.8	Fairings, non-load bearing parts
Intermediate modulus	1.44	120-128	2.7-2.8	Radomes, some structural parts, rocket motor casings
High modulus	1.48	160-170	2.3-2.4	Highly loaded parts
Carbon				
Standard modulus (high strength)	1.77-1.80	220-240	3.0-3.5	Widely used for almost all types of parts in aircraft, satellites, antenna dishes, missiles, etc.
Intermediate modulus	1.77-1.81	270-300	5.4-5.7	Primary structural parts in high performance fighters
High modulus	1.77-1.80	390-450	2.8-3.0 4.0-4.5	

[1] Kevlar composites are almost nonexistent in aviation due to their high thermal mismatch and extensive matrix cracking issues.

Fiber	Density (g/cc)	Modulus (GPa)	Strength (GPa)	Application areas
Ultra-high strength	1.80-1.82	290-310	7.0-7.5	Space structures, control surfaces in aircraft Primary structural parts in high performance fighters, spacecraft

Developments in carbon and aramid fibers properties for aircraft applications are mostly aimed at achieving higher strength (>5 GPa for carbon fibers) as well as improvements in modulus to a reasonable level (>300 GPa for carbon fibers). Improvements for space applications mostly focus on a higher modulus (>500 GPa for carbon fibers) with reasonable strength (3.5 GPa for carbon fibers). Aramid fibers property improvements also aim at higher modulus with an increase in strength (Mangalgiri, 1999).

2.2.2 Polymers

The matrix phase of composites may be a polymer, ceramic, metal, etc. Matrices used in aerospace applications are usually polymers, which bind the reinforcements together and transfer the load to the reinforcements. The matrix prevents damage from fiber-to-fiber friction. The matrix also provides a protective surface finish from harsh chemicals and other foreign substances (Mangalgiri, 1999). The PMC matrix can be either a thermoplastic or a thermoset polymer. Thermoset polymers have a cross-linked structure with covalent bonds. The cross-link density is defined as the density of polymer chains or segments that link two infinite parts of the polymer network (La Scala & La Scala, 2005). The density of polymer cross-links is related to mechanical properties. A higher cross-link density will lead to higher stiffness (high Young's modulus) yield strength, etc (Chua & Tu, 2018). Thermoset polymers are subject to decomposition under heating, which causes permanent structural hardening and char formation. Thermoplastics, on the other hand, tend to soften or melt with high temperatures, and can be reshaped at temperatures below where thermal decomposition begins to occur. These differences often make thermoset polymers more effective for higher temperature applications. Thermoset polymers strengthen when heated as crosslinking reactions advance but cannot be remolded or heated after their initial formation, while thermoplastics can be reheated, remolded, and cooled as needed without leading to any chemical changes at temperatures below where decomposition can occur (Comparison of Thermoset Versus Thermoplastic Materials, n.d.). Common aerospace-grade thermoset polymers include epoxies, phenolics, bismaleimides (BMI), and other systems involving polymerization of monomeric reactants (PMR), while common thermoplastics are poly(ether ether)ketone (PEEK) or polyphenylene sulfide (PPS), as seen in Table 6.

Table 6: Commonly used matrices in aerospace applications (Reproduced from reference (Mangalgiri, 1999)).

Thermosets				**Thermoplastics**
Forms cross-linked networks in polymerization curing by heating				**No chemical change**
Epoxies	**Phenolics**	**Polyester**	**Polyimides**	**PPS, PEEK**
▪ Most popular ▪ 80% of total composite usage ▪ Moderately high temp ▪ Comparatively expensive	▪ Cheaper ▪ Lower viscosity ▪ Easy to use ▪ High temp usage ▪ Difficult to get good quality composites	▪ Cheap ▪ Easy to use ▪ Popular for general applications at room temp	▪ High temp application 300℃ ▪ Difficult to process ▪ Brittle	▪ Good damage tolerance ▪ Difficult to process as high temp 300-400℃ is required
▪ Low shrinkage (2-3%) ▪ No release of volatile during curing	▪ More shrinkage ▪ Release of volatile during curing	▪ High shrinkage (7-8%)		
▪ Can be polymerized in several ways giving varieties of structures, morphology and wide range of properties	▪ Inherent stability for thermal oxidation ▪ Good fire and flame retardance ▪ Brittle than epoxies	▪ Good chemical resistance ▪ Wide range of properties but lower than epoxies ▪ Brittle ▪ Lower T_g		
▪ Good storage stability to make prepregs	▪ Less storage stability-difficult to prepreg	▪ Difficult to prepreg		▪ Infinite storage life. But difficult to prepreg
▪ Absolute moisture (5-6%) causing swelling and degradation of high temp properties ▪ Also, ultraviolet degradation in long-term	▪ Absorbs moisture but no significant effect of moisture in working service range	▪ Less sensitive to moisture than epoxies		▪ No moisture absorption

Epoxies are the most widely used resins used in aerospace-grade composites. Three main reactions can occur in an epoxy system during curing, as seen in Figure 10. Initially, the epoxide and a primary amine function of the hardener will react. Hardeners (curing agents) are difunctional or higher (tri- or tetrafunctional) amines. This amine/epoxy reaction proceeds through a nucleophilic attack of the primary amine and a beta- alcohol group on epoxide leading to ring-opening and the generation of a secondary amine (Step 1 in Figure 9). That secondary amine can also react with another epoxide group, thus generating a tertiary amine (Step 2 in Figure 10). The rate constant for a secondary amine to open an epoxide ring is typically slower than that of a primary amine. Hence, k_1 is greater than k_2. Next, the secondary hydroxyl groups, previously generated by ring-opening epoxide, can also react to ring-open another epoxide to produce an ether linkage, as seen in Step 3 of Figure 9. This reaction is typically slower than the amine/epoxide opening. As the reaction progresses, a crosslink network structure forms (Li, et al., 2013; Singh, Panda, Mohanty, Nayak, & Gupta, 2017).

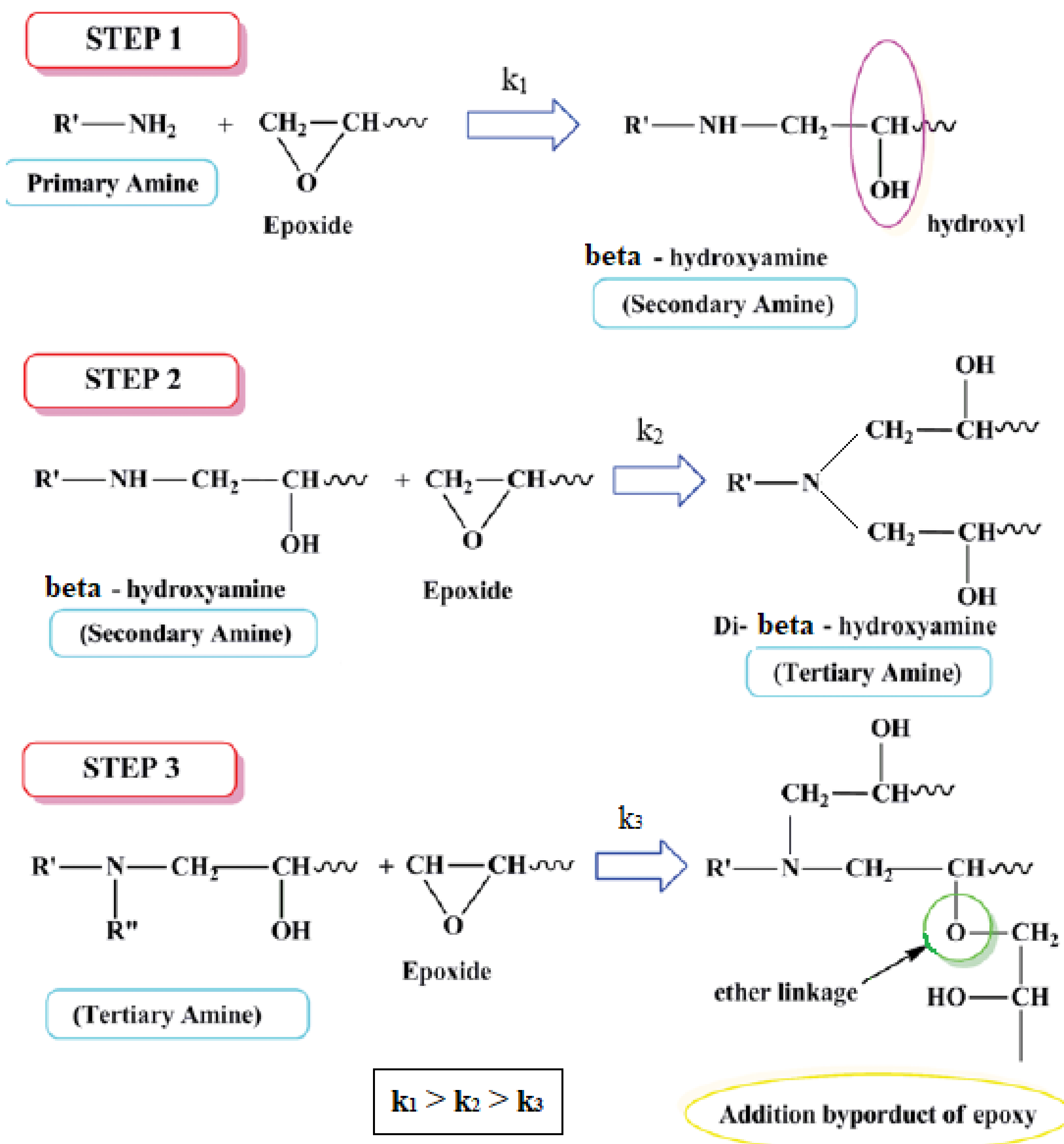

Figure 10. Three principal reaction paths in general for epoxy curing (Li, et al., 2013; Singh, Panda, Mohanty, Nayak, & Gupta, 2017).

Many epoxies used in the aerospace industry are based on diglycidyl ether Bisphenol A (DGEBA), which can be cured using different curing agents. Chemical structures for a DGEBA monomer, DGEBA monomer with its oligomer, and curing agents are illustrated in Figure 11, Figure 12 and Figure 13, respectively (Abdelkader & White, 2005).

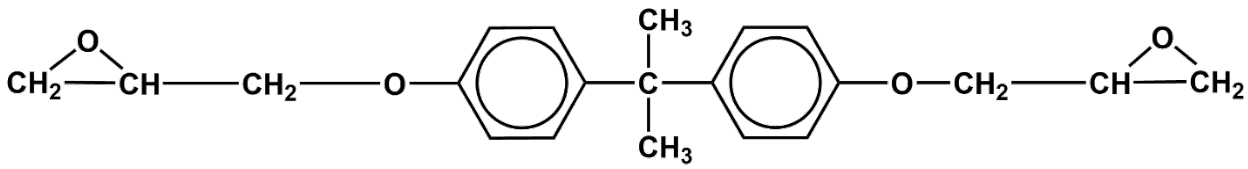

Figure 11. Chemical structure of a DGEBA epoxy monomer

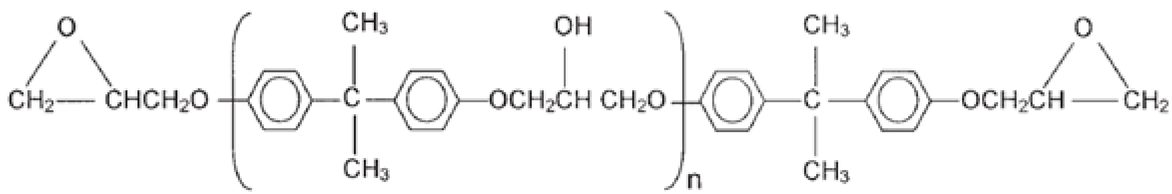

Figure 12. Chemical structure of a DGEBA epoxy monomer and its oligomer (Abdelkader & White, 2005).

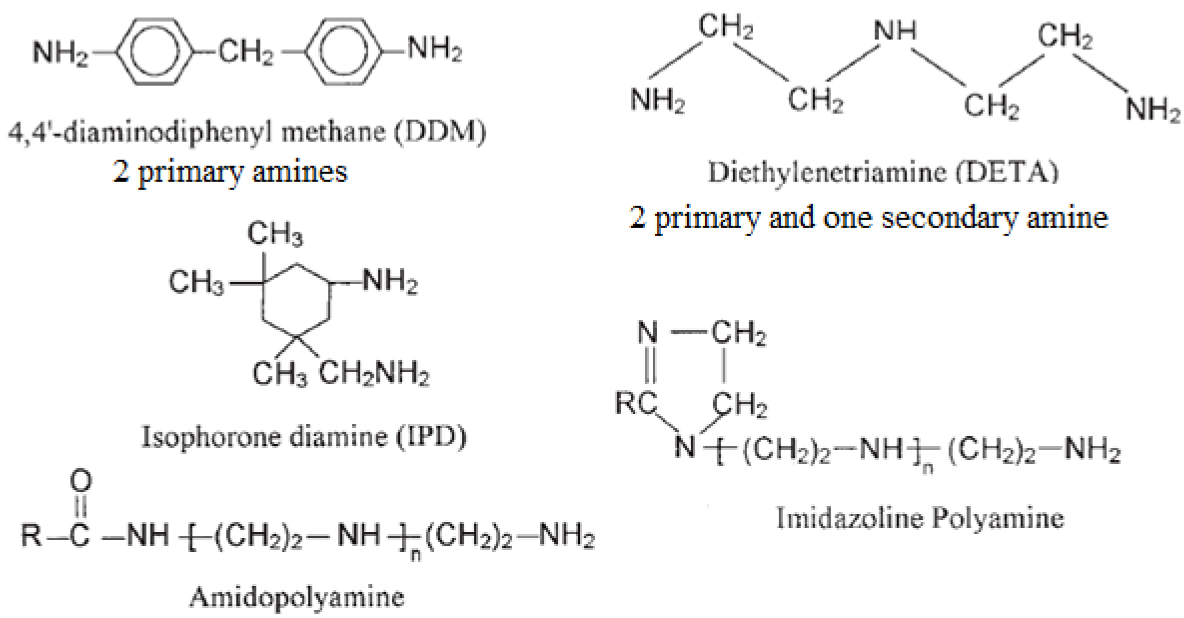

Figure 13. Chemical structures of curing agents for DGEBA epoxy (Abdelkader & White, 2005).

Figure 14 and Figure 15 show the reaction of epoxy monomer DGEBA with the 4,4'- Methylenedianiline (MDA) curing agent, where nucleophilic attack by the amine groups ring-open the epoxy monomer, extending and crosslinking growing polymer chains. These figures show both secondary and tertiary amine group formation during curing.

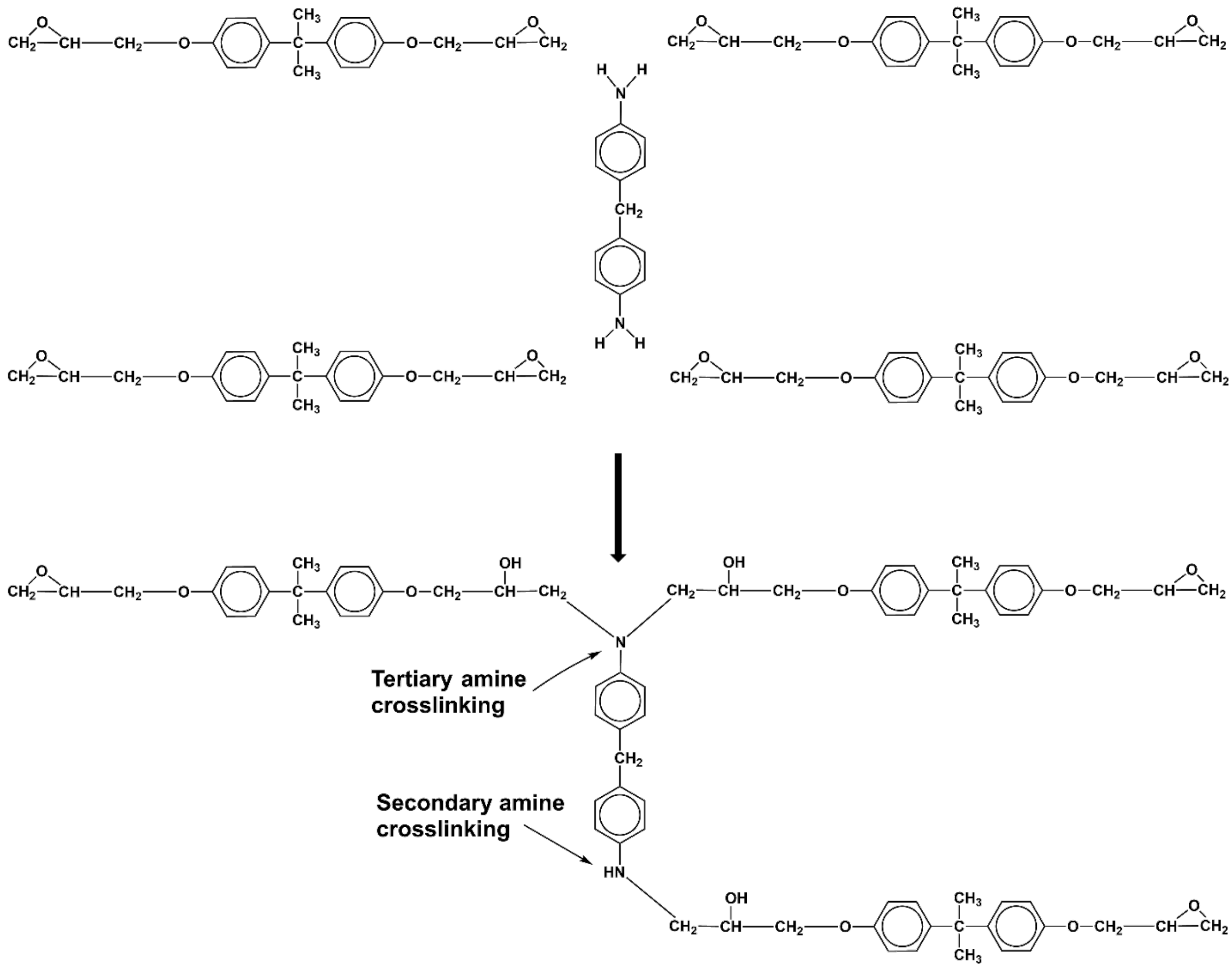

Figure 14. Reaction of curing agent with three epoxide groups.

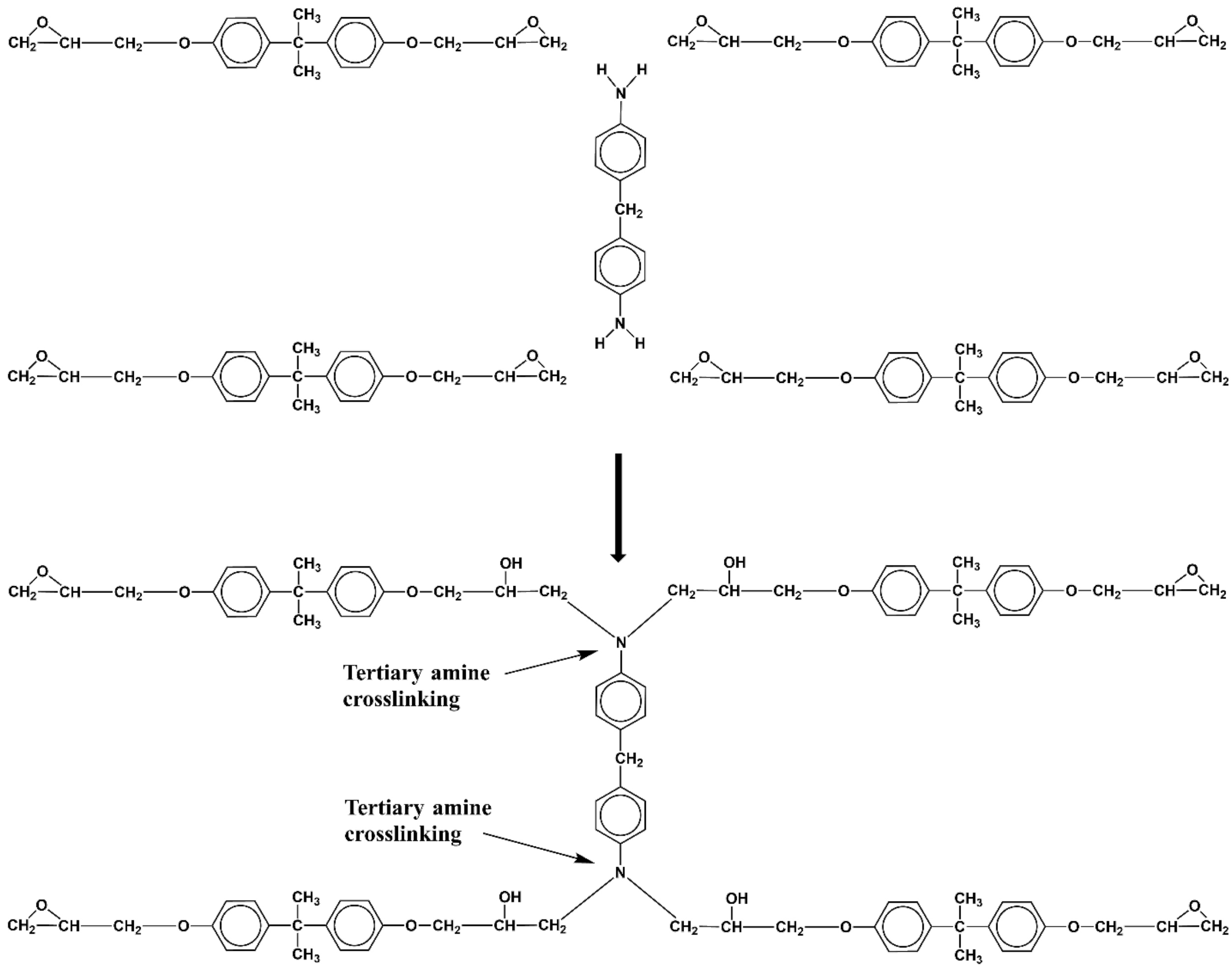

Figure 15. Curing agent reaction with epoxy groups at high curing temperature and conversion.

A sample region of a fully cured crosslinked epoxy is illustrated in Figure 16. In this figure, oligomeric units of DGEBA, as well as DGEBA itself are shown in the structure. This better represents the real structure of epoxy resins rather than simply using DGEBA. The reader should note that a variety of other epoxy monomers (di-, tri-, and perhaps tetrafunctional) will sometimes be used. Also, many other amine curing agents (again di-, tri-, and tetrafunctional) have been employed in various ratios. Finally, to control curing rates, sterically hindered amine curing agents are used, so resin preforms can be made without the liquid resin's viscosity becoming too high.

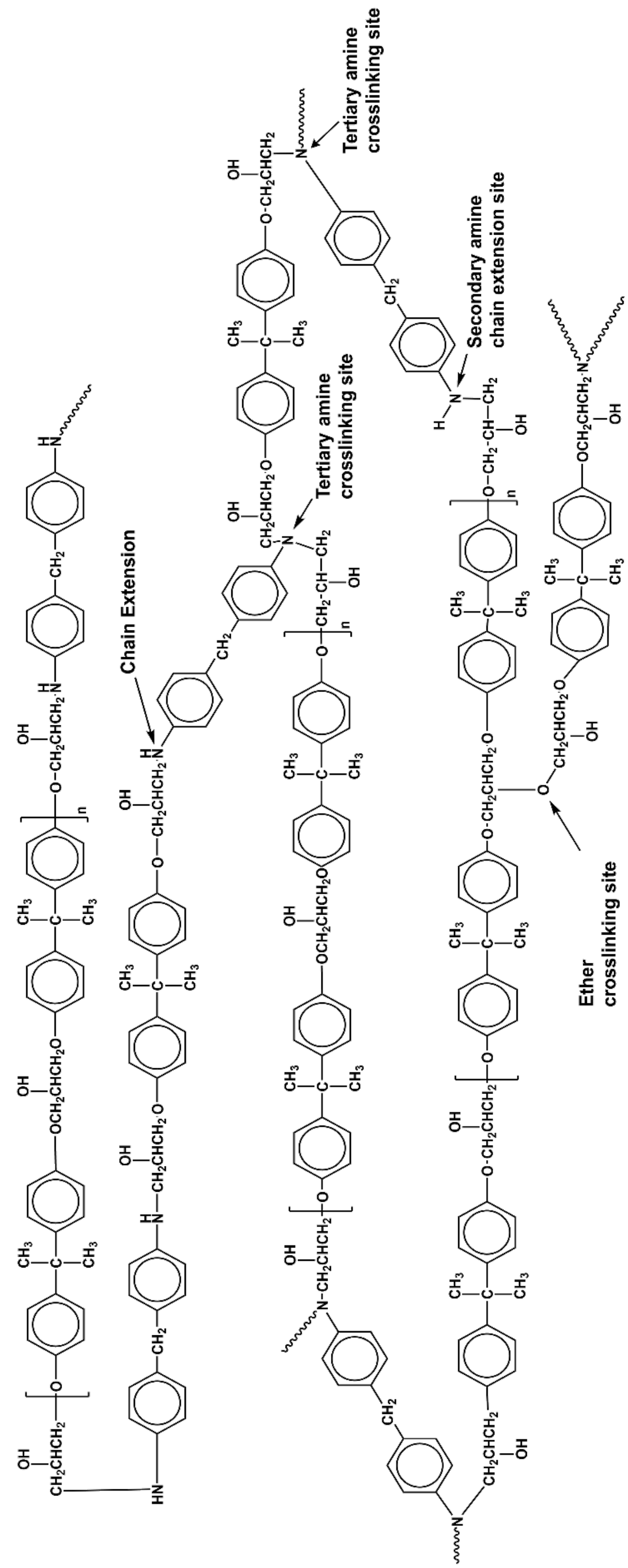

Figure 16. A sample cured and crosslinked cured DGEBA-MDA epoxy.

Phenolic resins are another form of thermosets used in the aerospace industry. Phenolic resins are synthetic polymers resulting from condensation of phenols and aldehydes. This step-growth polymerization reaction can either be acid or base catalyzed, forming either novalac or resole resin classes, respectively. Novolac resins necessitate a curing agent and are not sensitive to heat. Resole resins are produced by the polymerization reaction in alkaline solution. These resins are sensitive to heat, acid, do not necessitate curing agents, and have comparatively short shelf lives (What are phenolic resins?, n.d.). The higher formaldehyde (F) to phenol (P) ratio used in Resole synthesis gives a higher degree of phenol ring hydroxymethylation, as seen in Figure 17. Thus, no more formaldehyde or formaldehyde equivalent needs to be added to generate a crosslinked network upon curing (Zhang, 2014; What are phenolic resins?, n.d.).

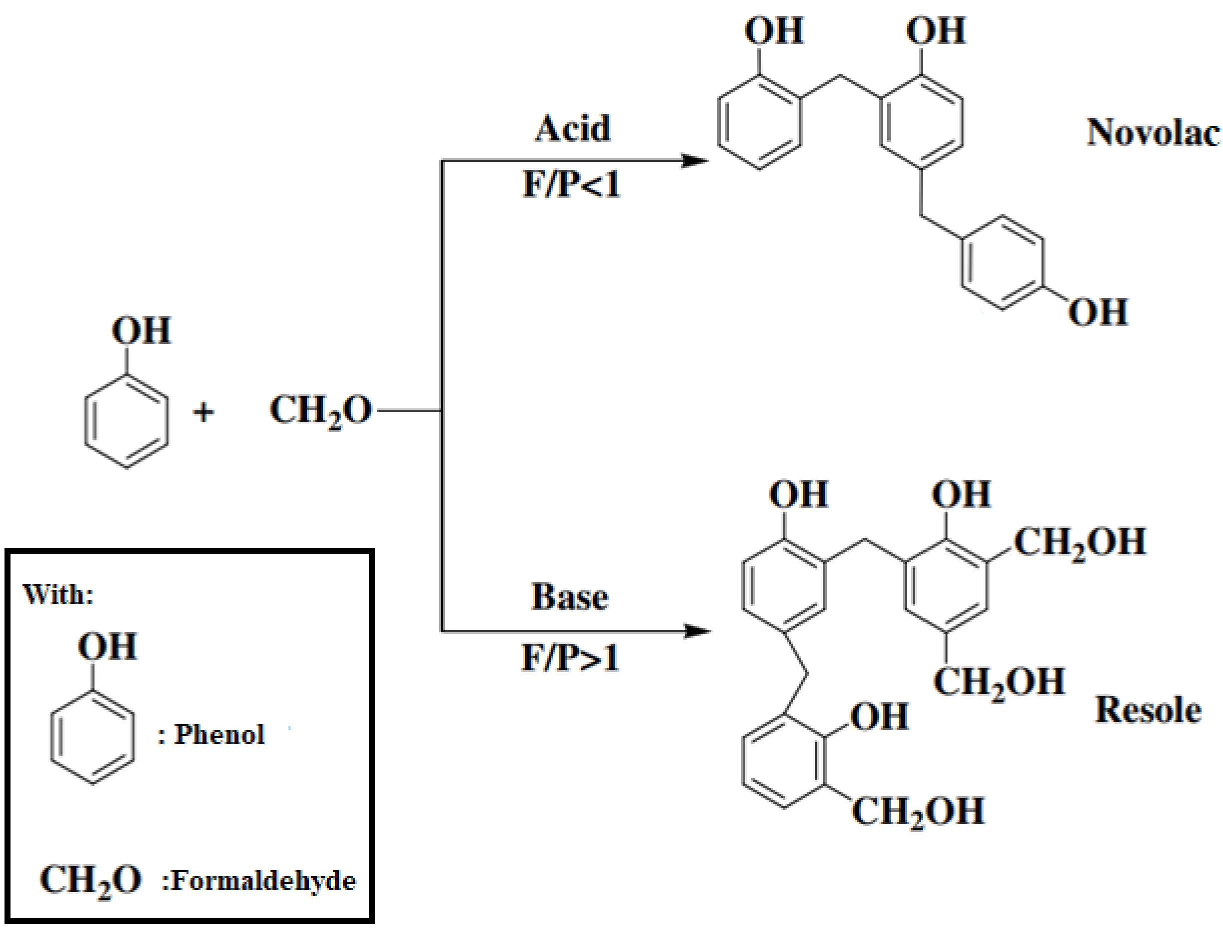

Figure 17. Synthetic route to phenolic resins formation (Zhang, 2014).

Phenolic resins are further categorized into alkylphenol novolacs (alkylidene bridge) and alkylphenol resoles (hydroxymethyl group, dimethylene ether bridge). Polycondensation of formaldehyde (F) and phenol (P) in a molar ratio of F/P less than one with acidic catalysts leads to the formation of novolacs. The first stage in novolac polycondensation is the electrophilic attack of carbonyl compound on the *para*- and/or *ortho*-positions of phenol, favorably at the para-position to the phenolic hydroxyl, as shown in Figure 18.

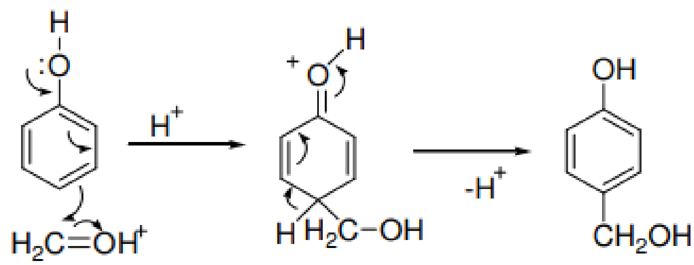

Figure 18. First stage in novolac polycondensation.

High-ortho novolacs are generated when polymerization is catalyzed by salts of specific carboxylic acids or divalent metal salts, such as zinc, calcium, and magnesium at a pH of 4-7. High ortho novolac PF resins typically have many ortho-ortho repeat units. The reactions between the hydroxymethyl groups and aromatic ring carbons of phenol or another hydroxymethyl group lead to the formation of methylene linkages, as seen in Figure 19 (Zhang, 2014; Allen & Ishida, 2001; Phenolic novolac and resole resins, n.d.).

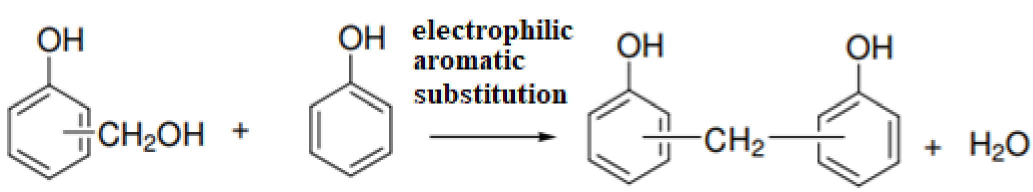

Figure 19. Reactions between the hydroxymethyl groups and aromatic ring carbons

Novolacs are alkylidene bridges (typically methylene)-linked phenols, with no extra remaining hydroxymethyl functional groups. Therefore, novolacs cannot cure without adding additional curing agents. The frequently used curing agent hexamethylenetetramine (HMTA) and novolacs cross-link according to Figure 20 (Zhang, 2014).

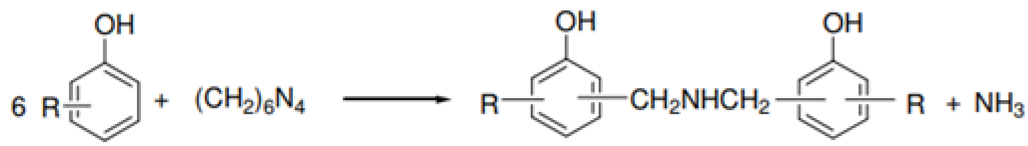

Figure 20. HMTA and novolacs cross-link.

Typically, resoles generate at an F/P molar ratio higher than one using basic catalysts. Sodium hydroxide is the most frequently used catalyst, though sodium carbonate, alkaline oxides and hydroxides, ammonia, and other base catalysts can be used as well. The nucleophilic attack of the para- and ortho-positions of a phenolate anion on electrophilic formaldehyde occurs in the initial stage in resole polycondensation, as seen in Figure 21. During the synthesis, mono-, di-, and trihydroxymethyl derivatives of phenol are formed at first. Then, methylene or ether linkages between monomeric phenol components are produced by condensation of hydroxymethyl derivatives, as this continues larger aggregated molecules form and finally the entire mass becomes consolidated. Resole polymers have a more highly branched structure compared to novolac polymers (Zhang, 2014; Allen & Ishida, 2001).

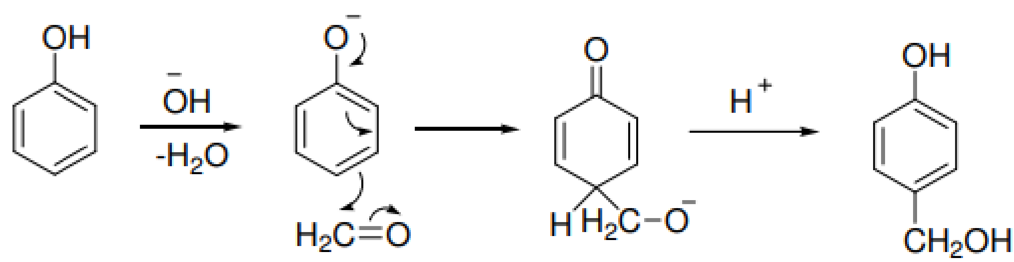

Figure 21. Resole polymer synthesis.

Hydroxymethyl groups can react to create dimethylene ether bridges with the formation of water molecules, as seen in Figure 22. Hydroxymethyl groups of resoles can undergo condensation with other phenol molecules directly as given in Figure 19 (Zhang, 2014).

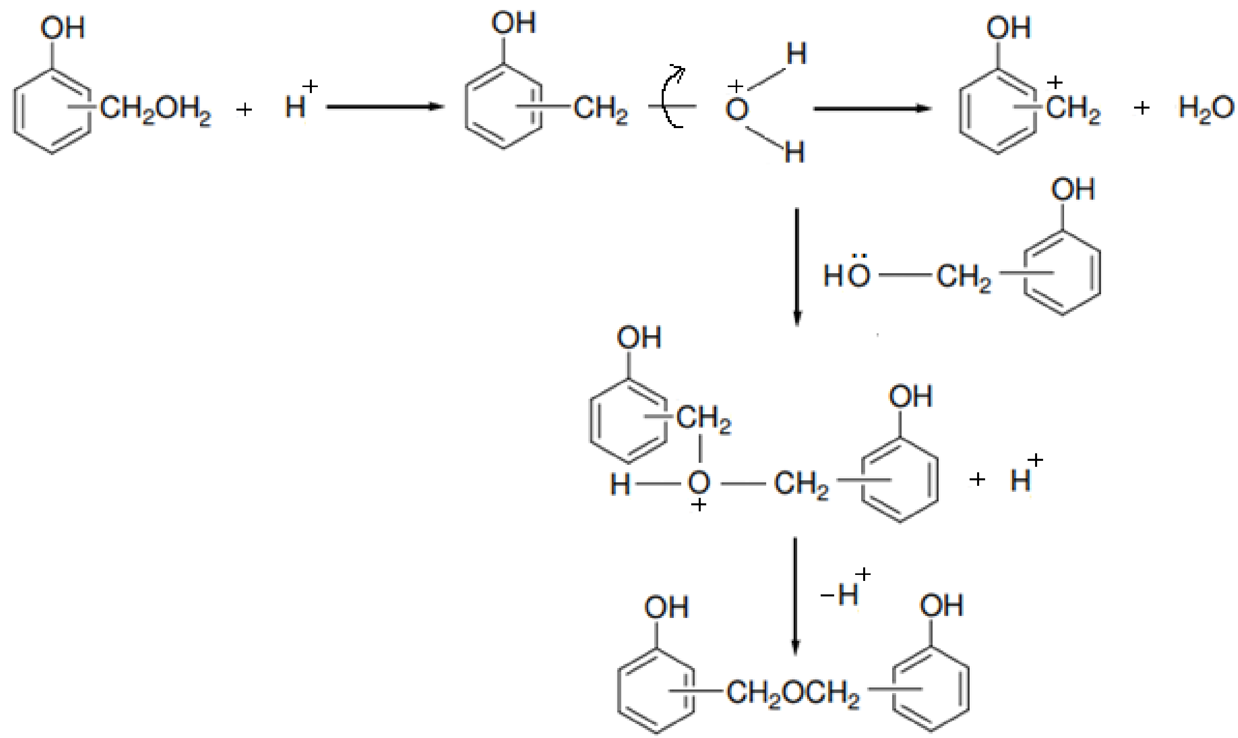

Figure 22. Creation of dimethylene ether bridge.

Other thermosets used in aerospace industry are polyester resins, which can refer to various types of resins typically created through the condensation of polybasic acids with polyhydride alcohols or from by-products of these materials. The conventional chemical structure of a bisphenol-A fumarate polyester resin is seen in Figure 23.

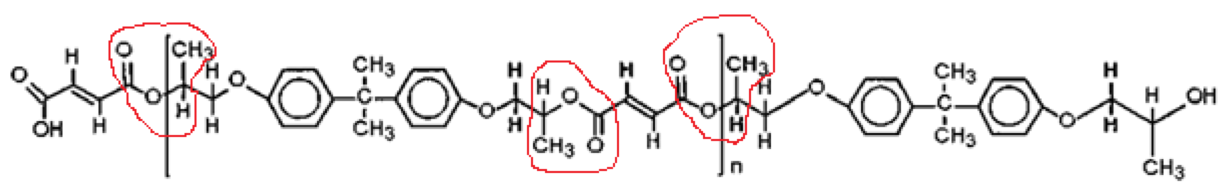

Figure 23. Chemical structure of a bisphenol-A fumarate polyester resin.

The ester groups (circled in red) represent sites that can undergo hydrolysis via nucleophilic acyl substitution under acidic or basic conditions. Unsaturated bonds at the end of and in the molecule can co-polymerize with styrene to generate cross-links between neighboring styrene chains. Polymerization is realized by means of free radical initiators. Styrene monomer and the polyester resin rarely react entirely, and the matrix will contain some trapped unreacted molecules (Boinard, Pethrick, Dalzel-Job, & Macfarlane, 2000; Yang & Lee, 2002).

Thermosetting imide resins (used in aerospace) are difunctional monomers or prepolymers, or their mixtures with low molecular weight. Reactive sites that can undergo homopolymerization can include endomethylenetetrahydrophthalic acid, benzocyclobutene units, ethynylphenyl groups, allyl nadic imide groups (Figure 24) or activated vinyls (such as bismaleimides). In all these reactive sites, the reactive groups are, or comprise, numerous carbon carbon bonds that are distant from the imide groups. Bismaleimides are the exception since the vinyl group is a constituent of the five membered maleimide ring and is consequently highly activated by two neighboring carbonyl groups (Stenzenberger H. , 1988).

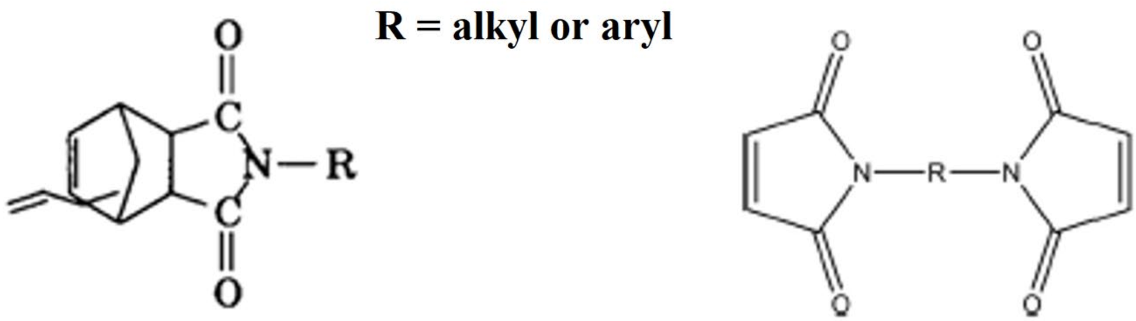

Figure 24. Allyl nadic imide monomer (left), and bismaleimide monomer (right) structures (Abdelkader & White, 2005; Renner & Kramer, 1989).

Bis-nadic imides are subjected to a retro-Diels-Alder reaction in the 250-270 °C temperature range, leading to the release of cyclopentadiene prior to an almost immediate polymerization of the maleimide function generated. This reaction can sometimes be denoted as pyrolytic polymerization since the first stage in the cure reaction is the norbornene group's decomposition, as seen in Figure 25. LARC-13 a polyimide adhesive based on 3,3'- diaminodiphenylmethane, benzophenonetetracarboxylic acid dianhydride and norbornene anhydride as seen in Figure 26 (Stenzenberger H. , 1988).

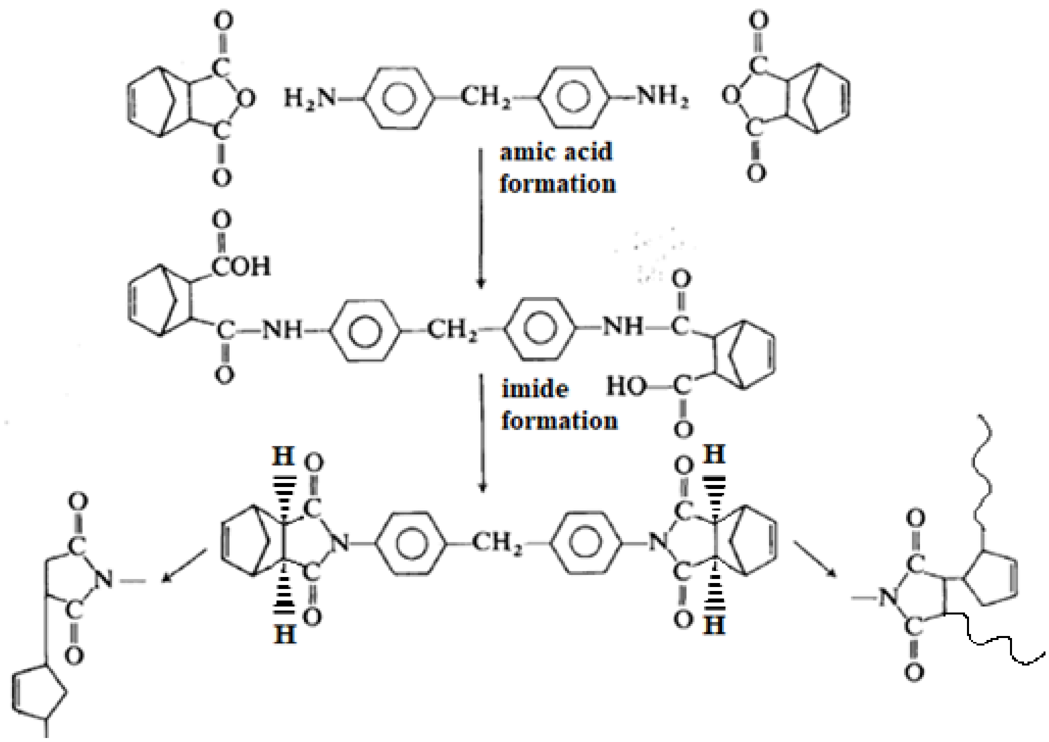

Figure 25. Synthesis and cure of endomethylenetetrahydrophthalimides (Stenzenberger H. , 1990; Wilson, Stenzenberger, & Hergenrother, 1990; Polyether ether ketone, n.d.).

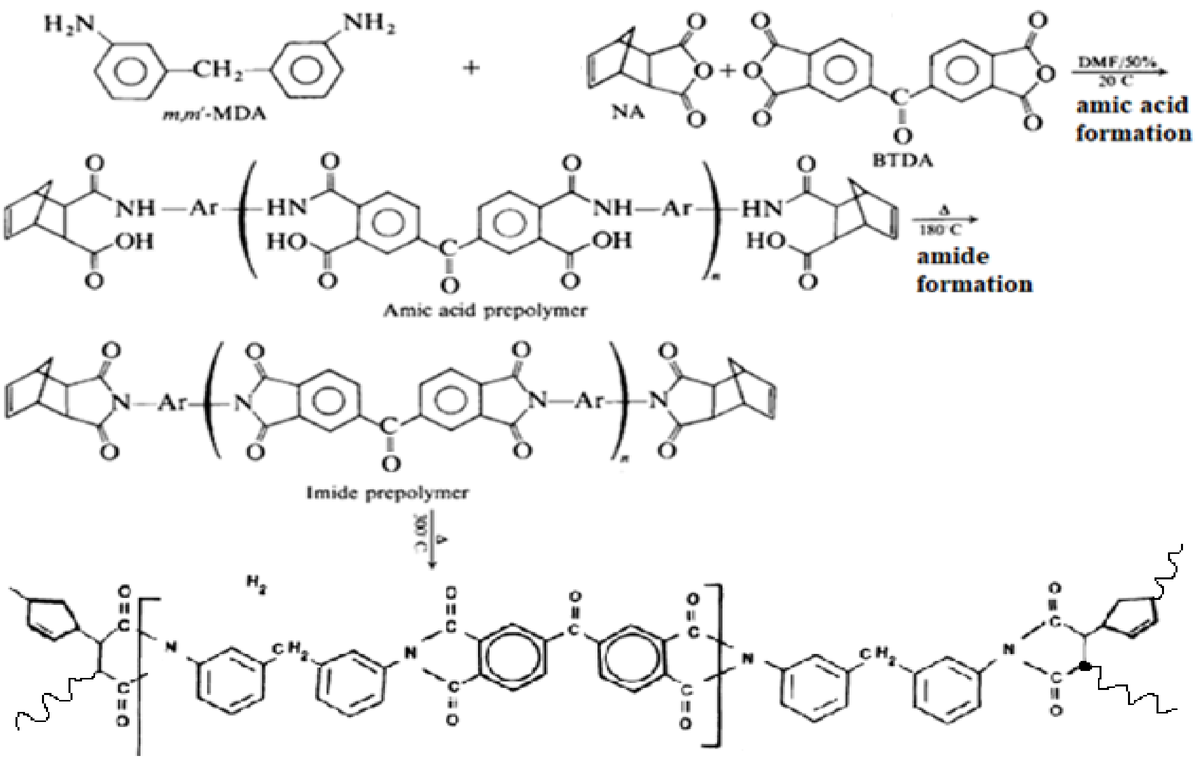

Figure 26. LARC-13 resin chemistry (Stenzenberger H. , 1988; Iredale, Ward, & Hamerton).

The norbornene aerospace-grade resin commonly used is PMR-15. The polymerization of monomeric reactants (PMR) is achieved during the resin processing and cure stages. The aromatic diamine (4,4'-methylenedianiline), the dialkylester of benzophenonetetracarboxylic acid (BTDE), and the monoalkylester of norbornene 2,3-dicarboxylic acid react together. In this reaction, a molar ratio is used leading to a prepolymer with a molecular weight of 1500 (Boinard, Pethrick, Dalzel-Job, & Macfarlane, 2000). That prepolymer can be further reacted to form the continuous matrix after infusion into fiber preforms, as depicted in the last step of Figure 27.

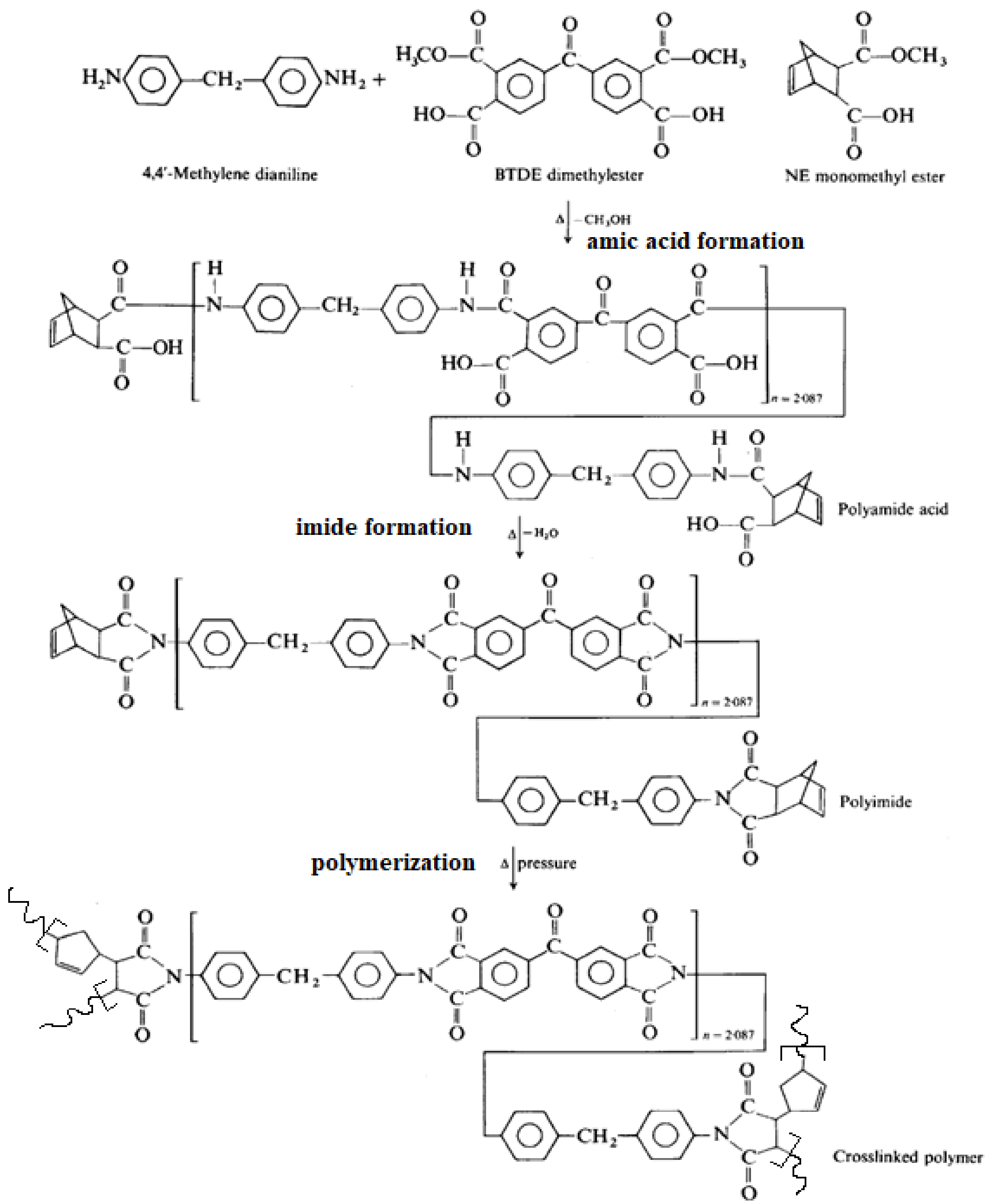

Figure 27. PMR-15 resin chemistry (Stenzenberger H. , 1988).

Copolymers based on bismaleimide/comonomer blends offer substantially enhanced properties over bismaleimide homopolymers, mainly in the areas of toughness, hygrothermal performance, and moisture absorption. The most commonly utilized bismaleimide is 4,4'-bismaleimidodiphenylmethane, which is synthesized from 4,4'-diaminodiphenylmethane and maleic acid anhydride, as seen in Figure 28 (Stenzenberger H. , 1988; Iredale, Ward, & Hamerton).

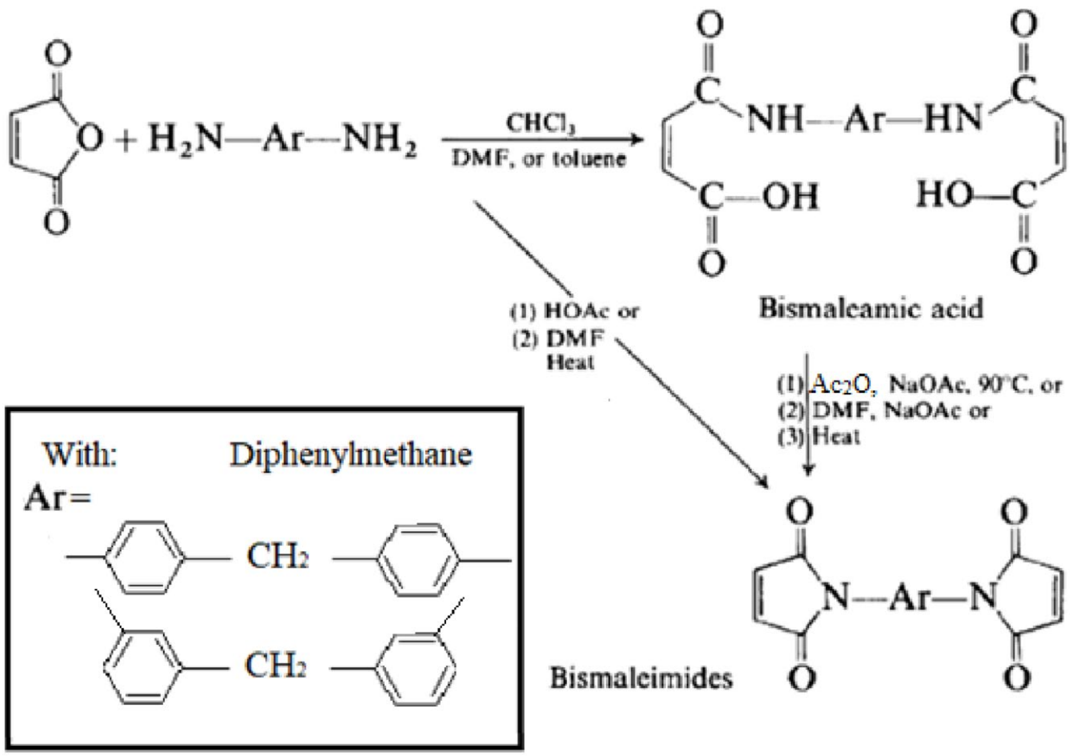

Figure 28. Synthesis of an aryl bismaleimide (Stenzenberger H. , 1988).

Thermoplastic polymers are also used in the aerospace industry. The most common thermoplastics are polyetheretherketone (PEEK) and polyphenylenesulfide (PPS). The PEEK polymer illustrated in Figure 29 is one of a class of semicrystalline polyethers obtained by step-growth polymerization during the dialkylation of bisphenolate salts, typically through the reaction of 4,4'-difluorobenzophenone and the disodium salt of hydroquinone. This salt is produced by deprotonation of p-dihydroxybenzene with sodium carbonate. The polymerization reaction occurs at around 300 °C in polar aprotic solvents such as diphenyl sulphone (Polyether ether ketone, n.d.; Melton, Peters, & Arisman, 2011). The high melt-viscosity of thermoplastic PEEK polymers makes its infusion into fiber preforms difficult. To lower the viscosity, different methods are used, such as molecular weight control of polymer chains during polymerization (Yuan, Galloway, Hoffman, & Bhatt, 2011), or melt blends of long, rigid, rod-like liquid crystal polymer molecules (Demeuse & Kiss, 2014).

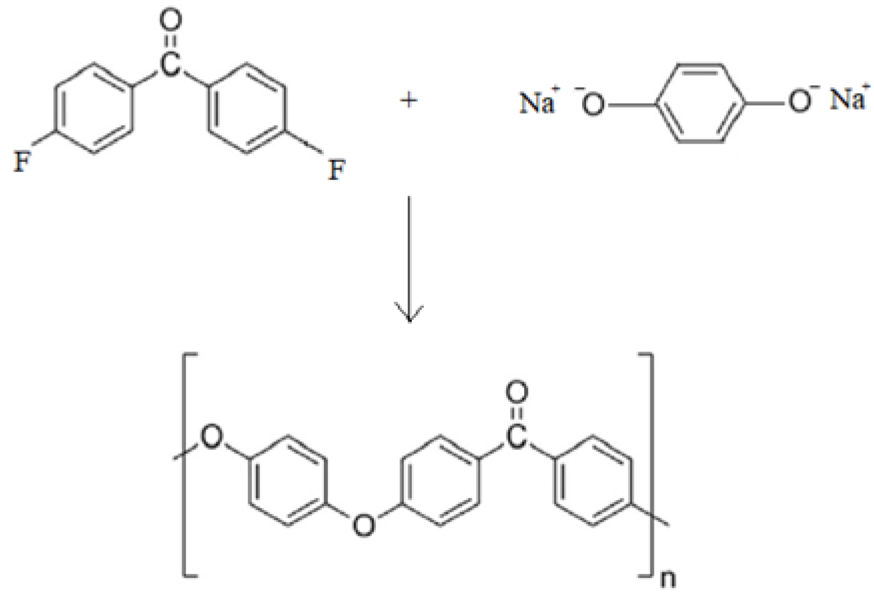

Figure 29. Chemical reaction forming PEEK (Puhan & Wong, 2019).

PPS is a semi crystalline thermoplastic polymer, represented in Figure 30, that is generally used with glass fiber reinforcement. The aromatic rings separated by sulfur atoms and the high degree of crystallinity lead to remarkably high chemical resistance of the material (Collyer, 1989). PPS can be polymerized through the polycondensation reaction of para-dichlorobenzene (p-DCB) and sodium hydro sulfide (NaSH) or sodium sulfide (Na_2S) in a polar solvent at high pressure and temperatures. PPS is produced through several reactions: dehydration, sodium chloride removal, exothermic, and high temperature pressurization reactions. The PPS polymerization reaction is shown in Figure 30. By thermal processing, thermal cross-linking can occur leading to branched PPS and later on crosslinking (What is PPS?, n.d.).

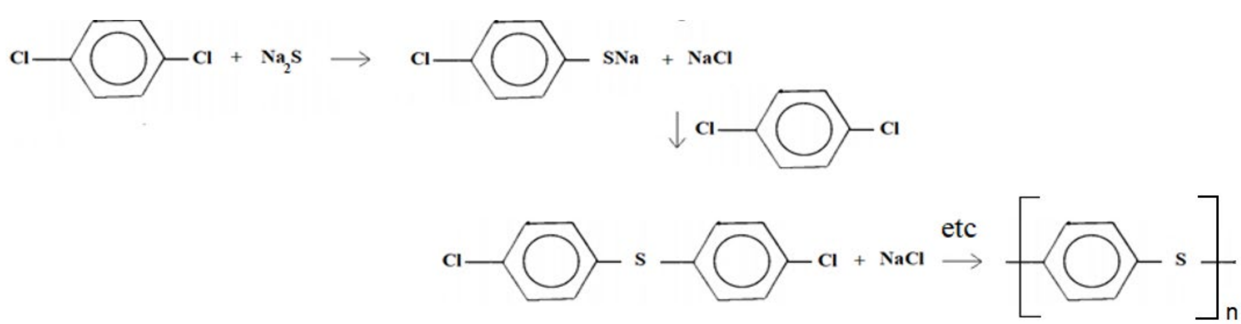

Figure 30. The repeat unit forming polyphenylenesulphide (PPS) (Collyer, 1989).

A significant effort to improve composites has been made through the improvement of matrix materials. Specifically, the two main concerns motivating this improvement are impact damage tolerance and hygro-thermal degradation. Improving the toughness will lead to higher resistance against delamination and impact. High failure strain of the matrix will improve translating the higher properties of the improved fibers to the overall composite. Higher resin shear modulus will lead to a better load transfer from the fibers to the resin and again to the fibers, thus improving compression strength (Mangalgiri, 1999). The use of thermoplastic resins and their blends is being investigated to improve hygro-thermal degradation. PEEK has shown promising results, though the problems related to the high processing temperature of the material still need to be solved (> 350 °C). Recent approaches have been directed towards the development of polymeric systems such as polymerizable liquid crystalline monomers and phthalonitrile resins for high temperature applications, these can be processed similarly to composites (such as autoclave curing up to 180 °C) (Mangalgiri, 1999).

2.3 Kinetics and thermodynamics of diffusion

Fluids diffuse into polymers at different rates and different total amounts to reach equilibrium. The rate at which the diffusion occurs is controlled by the kinetics, while the amount of fuel absorbed at equilibrium is controlled by the thermodynamics.

2.3.1 Kinetics of diffusion

Kinetically, diffusion is a process in which matter is transported from one part of a system to another due to random molecular motions. These molecules diffuse into the free volume present in the polymer (Crank, 1979; Vanlandingham, Eduljee, & Gillespie Jr, 1999). The most used diffusion model is the Fickian model, where the governing equations are based on Fick's second law. In the three-dimensional form, where the geometry has finite length "l", width "w", and thickness "h" (as shown in Figure 31).

The unsteady form of the equation is as follows (Equation 1):

$$\frac{\partial c}{\partial t} = D(\frac{\partial^2 c}{\partial x^2} + \frac{\partial^2 c}{\partial y^2} + \frac{\partial^2 c}{\partial z^2})$$

Equation 1

- D: spatially uniform diffusion coefficients (Figure 30)
- c: concentration of the diffused substance

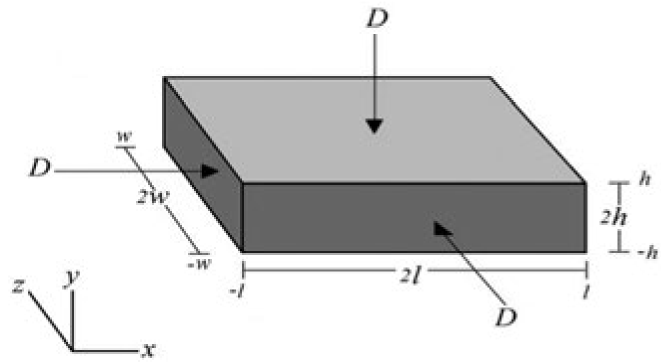

Figure 31. Dimensions and configuration for the 3D case.

The solution to this equation in terms of the concentration is given as (Equation 2):

$$\frac{c(t)-c_0}{c_1-c_0} = 1-\frac{64}{\pi^3}\sum_{p=0}^{\infty}\sum_{q=0}^{\infty}\sum_{r=0}^{\infty} e^{-\pi^2 t\left(\frac{D(2r+1)^2}{4l^2}+\frac{D(2q+1)^2}{4h^2}+\frac{D(2p+1)^2}{4w^2}\right)}\frac{(-1)^r}{2r+1}\frac{(-1)^q}{2q+1}\frac{(-1)^p}{2p+1}\cos(\frac{(2r+1)\pi x}{2l})\cos(\frac{(2q+1)\pi y}{2h})\cos(\frac{(2p+1)\pi z}{2w})$$

Equation 2

- c_1: the constant concentration at the outer surfaces
- c_0: the concentration at the center of geometry at t =0
- c(t): the concentration at a given time t

The mass of the specimen at a given time is obtained by (Equation 3):

$$M(t) = \int_{-w}^{w}\int_{-h}^{h}\int_{-l}^{l} c(t)\, dxdydz$$

Equation 3

The solution in terms of mass at a given time is obtained by (Equation 4)

$$\frac{M(t)}{M_\infty} = 1-\frac{512}{\pi^6}\sum_{p=0}^{\infty}\sum_{q=0}^{\infty}\sum_{r=0}^{\infty} e^{-\pi^2 t(\frac{D(2r+1)^2}{l^2}+\frac{D(2q+1)^2}{h^2}+\frac{D(2p+1)^2}{w^2})}\frac{1}{(2r+1)^2}\frac{1}{(2q+1)^2}\frac{1}{(2p+1)^2}$$

Equation 4

- M(t): mass of the specimen at a given time.
- M_∞: mass of the specimen at saturation

For the 3D case, all three dimensions are finite. If one of the dimensions is larger than the other two (w >> l and w>>h), as seen in Figure 32, the governing equation then becomes two-dimensional (Equation 5):

$$\frac{\partial c}{\partial t} = D(\frac{\partial^2 c}{\partial x^2} + \frac{\partial^2 c}{\partial y^2})$$

Equation 5

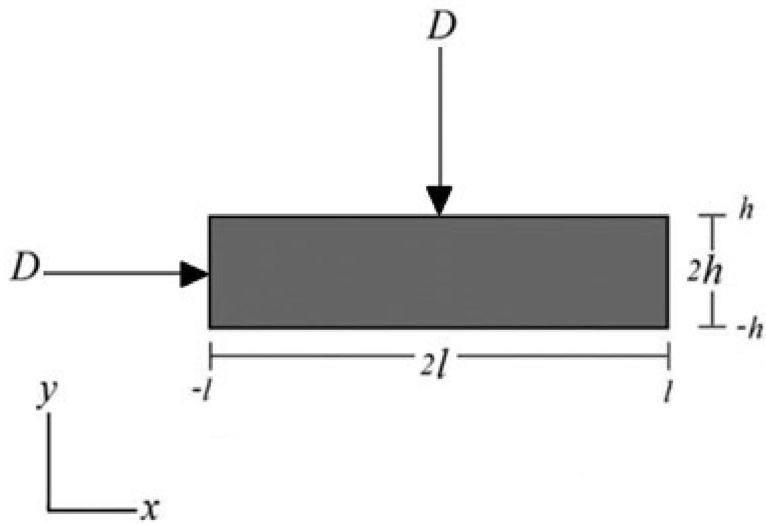

Figure 32. Dimensions and ingress direction for the 2D case.

With a solution in terms of concentration given as (Equation 6):

$$\frac{c(t) - c_0}{c_1 - c_0} = 1 - \frac{16}{\pi^2}\sum_{q=0}^{\infty}\sum_{r=0}^{\infty} e^{-\pi^2 t\left(\frac{D(2r+1)^2}{4l^2} + \frac{D(2q+1)^2}{4h^2}\right)} \frac{(-1)^r}{2r+1}\frac{(-1)^q}{2q+1}\cos(\frac{(2r+1)\pi x}{2l})\cos(\frac{(2q+1)\pi y}{2h})$$

Equation 6

- c_1: the constant concentration at the outer surfaces
- c_0: the concentration at the center of geometry at t=0
- c(t): the concentration at a given time t

To obtain the mass of the specimens at a given time is obtained by (Equation 7):

$$M(t) = \int_{-h}^{h}\int_{-l}^{l} C\, dxdy$$

Equation 7

The solution in terms of mass at a given time is obtained by (Equation 8):

$$\frac{M(t)}{M_\infty} = 1 - \frac{64}{\pi^4}\sum_{q=0}^{\infty}\sum_{r=0}^{\infty} e^{-\pi^2 t(\frac{D(2r+1)^2}{l^2}+\frac{D(2q+1)^2}{h^2})}\frac{1}{(2r+1)^2}\frac{1}{(2q+1)^2}$$

Equation 8

In the one-dimensional case (h >> l), as seen in Figure 33, the governing equation then becomes (Equation 9):

$$\frac{\partial c}{\partial t} = D\frac{\partial^2 c}{\partial x^2}$$

Equation 9

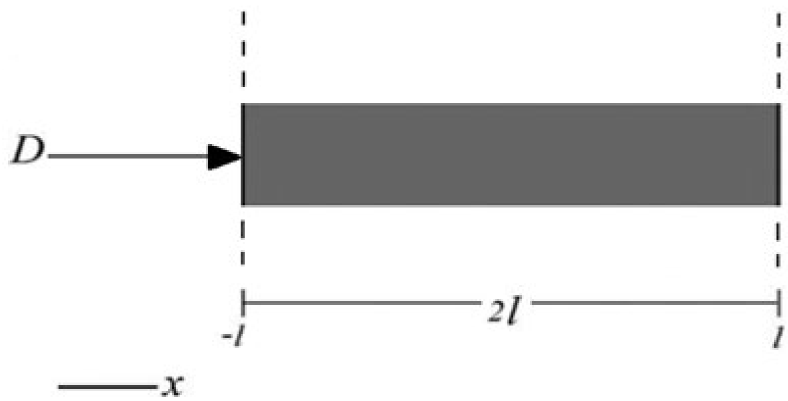

Figure 33. Dimensions and ingress direction for the 1D case.

The solution to this equation in terms of concentration was given in to be (Equation 10):

$$\frac{c(t)-c_0}{c_1-c_0} = 1 - \frac{4}{\pi^2}\sum_{r=0}^{\infty} e^{-\pi^2 t\left(\frac{D(2r+1)^2}{4l^2}\right)}\frac{(-1)^r}{2r+1}\cos(\frac{(2r+1)\pi x}{2l})$$

Equation 10

- c_1: the constant concentration at the outer surfaces
- c_0: the concentration at the center of geometry at t=0
- c(t): the concentration at a given time t

The mass of the specimens at a given time is obtained by (Equation 11):

$$M(t) = \int_{-l}^{l} C\,dx$$

Equation 11

The solution in terms of mass at a given time is obtained by (Equation 12):

$$\frac{M(t)}{M_\infty} = 1 - \frac{8}{\pi^2}\sum_{r=0}^{\infty} e^{-\frac{D(2r+1)^2\pi^2 t}{l^2}} \frac{1}{(2r+1)^2}$$

Equation 12

It must be noted that in some cases, the edges are sealed with impermeable coating that ensures that no diffusion happens through the edges (Shen & Springer, 1976). When neglecting the effects through the edges, the diffusion coefficient D (obtained from equation 12) is defined as (Equation 13):

$$D = \pi\left(\frac{h}{4M_\infty}\right)^2\left(\frac{M_2 - M_1}{\sqrt{t_2} - \sqrt{t_1}}\right)^2$$

Equation 13

- M_2: Mass at time t_2
- M_1: Mass at time t_1

Since diffusion is a thermally driven process, the diffusion coefficient can be defined as a function of temperature by the Arrhenius equation (Equation 14). The exponential component of diffusivity and its relation to $\frac{1}{T}$ leads to a high-temperature dependency, and the pre-exponential factor conforms to the activated transition state principle (Bao & Yee, 2002):

$$D = D_0 exp(\frac{-E_a}{RT})$$

Equation 14

Where:

- D_0 is the pre-exponential factor and is a constant coefficient defined as the diffusion coefficient when the temperature approaches infinity
- E_a is the diffusion activation energy can be defined as the energy required to produce the diffusive motion on one mole
- R is the universal gas constant
- T is the temperature.

The 1D Fickian diffusion model remains the most used model since it provides a very accurate prediction of diffusion into semi-infinite isotropic materials. However, it is known to neglect diffusion through the edges, which introduces errors to the solution when the edges have finite dimensions and when the material is anisotropic. Shen and Springer (Shen & Springer, 1976) introduced an edge correction to the Fickian diffusion model accounting for diffusion through the edges, where the diffusion coefficient is a function of all three dimensions of the specimen.

Fickian diffusion does not account for the interaction between the polymer and the absorbed substance, which may potentially slow the diffusion (known as “hindrance effect”). The hindrance effect was noticeable in some studies (Grace & Altan, 2013), where the weight gain data from the experiment always lagged behind the one predicted by the Fickian model.

Diffusion modeling in composites represents a significant challenge since composites are anisotropic materials, and it is expected that diffusion will be higher along the fiber direction than other directions (e.g., through-thickness) since the interface between fibers and the matrix can represent a pathway for diffusion (Korkees, Alston, & Arnold, 2018).

In many studies of moisture absorption in polymeric composites and polymers, non-Fickian behavior was reported as illustrated in Figure 33. The dual-diffusivity model (Jacobs & Jones, 1989) considers a diffusivity of the two-phases of the composite (matrix and fiber). Here, the diffusion coefficient is a function of the diffusion coefficient of the matrix and fibers, and the volume fraction of the fibers. The time-varying diffusivity model is another non-Fickian diffusion model (Roy, Xu, Park, & Liechti, 1999), it accounts for time-dependent behavior of the polymer which is analogous to viscoelastic relaxation. In this case, a new term is added to the diffusion coefficient that accounts for relaxation of the polymer upon absorption of moisture.

The coupled diffusion relaxation model (Berens & Hopfenberg, 1979), accounts for relaxation effects as well. In this case, the absorbed amount at any given time accounts for both contributions from the Fickian diffusion and relaxation.

$$M(t) = M_F(t) + M_R(t)$$

Equation 15

- $M(t)$: mass at a given time t
- $M_F(t)$: mass from Fickian diffusion process at a given time t
- $M_R(t)$: mass from relaxation process at a given time t

The Langmuir-type model is a one-dimensional isotropic non-Fickian model that introduces the hindrance effect by adding a new term to the Fickian diffusion model (see Equation 16). This term accounts for the binding and unbinding of molecules which represent the interaction between the polymer and absorbed substance (Carter & Kibler, 1978) (Figure 34).

$$D\frac{\partial^2 n}{\partial x^2} = \frac{\partial n}{\partial t} + \frac{\partial N}{\partial t}$$

Equation 16

Where:

$$\frac{\partial N}{\partial t} = \gamma n - \beta N$$

Equation 17

- n: represents the mobile molecules per unit volume
- N: represents the bound molecules per unit volume
- γ: represents probability per unit time that a mobile molecule will become bound
- β: represents probability per unit time that a bound molecule will become mobile

Grace and Altan (Grace & Altan, Three-dimensional anisotropic moisture absorption in quartz-reinforced bismaleimide laminates, 2014), developed a three-dimensional hindered diffusion model (3D HDM) based on the "Langmuir-type" which accounts for the interaction between the polar molecules of the polymer and the polar molecules of the absorbed substance (hindrance effect).

The three-dimensional form of the 3D HDM is given in Equation 18:

$$D_x \frac{\partial^2 n}{\partial x^2} + D_y \frac{\partial^2 n}{\partial y^2} + D_z \frac{\partial^2 n}{\partial z^2} = \frac{\partial n}{\partial t} + \frac{\partial N}{\partial t}$$

Equation 18

Where:

$$\frac{\partial N}{\partial t} = \gamma n - \beta N$$

Equation 19

- n: represents the mobile molecules per unit volume
- N: represents the bound molecules per unit volume
- γ: represents probability per unit time that a mobile molecule will become bound
- β: represents probability per unit time that a bound molecule will become mobile

At equilibrium: $\frac{dN}{dt} = 0$ meaning that: $\gamma n = \beta N$. Equation 18 then becomes the three-dimensional Fickian diffusion model. In Figure 35, the 3D HDM model is fitted for two set of experimental data, showing good agreement.

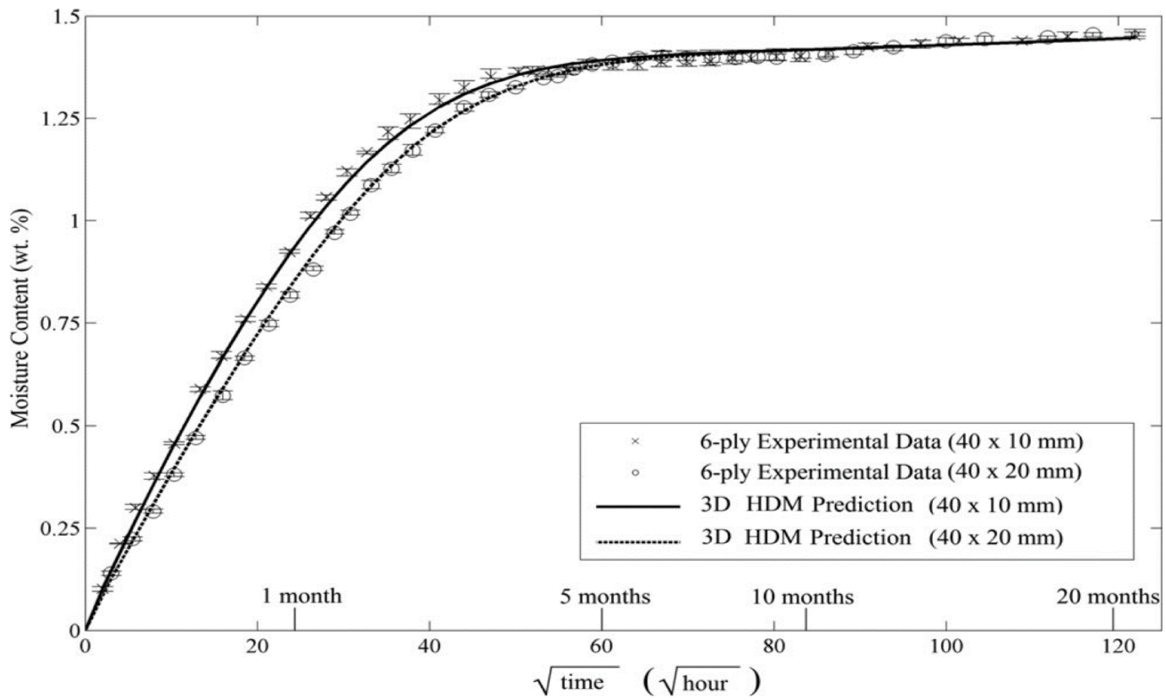

Figure 34. Weight tracking for moisture uptake and 3D HDM fitting for quartz/BMI laminates.

All these non-Fickian diffusion models will converge at equilibrium to the same solution predicted from Fickian diffusion.

The effect of the moisture absorption and diffusivity differ depending on the types of fluids being absorbed, and the type of matrices into which they are being absorbed; which can lead to swelling, plasticization, and degradation on the mechanical and thermomechanical properties level. Therefore, understanding all the underlying mechanisms behind fluid absorption in polymer matrices such as epoxies is of the utmost importance, chemically, thermodynamically, and kinetically.

2.3.2 Thermodynamics of fuel diffusion into aerospace epoxy composites

The amount of a fluid that will diffuse into a material at equilibrium is determined by the free energy change in the system. This free energy change is the driving force that causes the diffusion to occur. The overall free energy change between the sum of the free energies of the starting components (fluid and the starting matrix polymer or composite) and the sum of the free energies of the polymer (or composite) containing the absorbed fluid plus the fluid that remains of the original starting amount is the driving force (see Equation 20). Fluid uptake will occur until the value of ΔG reaches zero, where equilibrium is reached. The amount of fluid uptake at equilibrium determines the uptake of fluid per unit weight of the polymer when that polymer (or composite) is immersed in the fluid. Here, the composite's matrix polymer will be considered since the carbon fibers or glass fibers of a composite will not take up fluid. The fluid considered is jet fuel.

$$\Delta G = \left[G_{pure\ fluid} + G_{polymer}\right] - \left[G_{polymer\ with\ absorbed\ fluid}\right]$$

Equation 20

Where $\Delta G = 0$ at equilibrium.

In some cases, matrix components may extract into the fluid (fuel) in which the polymer is immersed. However, for this discussion, such extraction will not be considered. This is reasonable because the extent of fuel uptake by aerospace composites is typically small and the matrix resins are relatively highly crosslinked and contain only small amounts of extractable components.

The change in free energy of any system can be written as (Equation 21):

$$\Delta G = \Delta H - T\Delta S$$

Equation 21

Here ΔS is the entropy change, and ΔH is the enthalpy change between the starting and final states. The equilibrium uptake of fluid is reached when the change in free energy becomes zero. After fuel diffusion into the matrix begins, the process involves both diffusion into and out of the resin since this process is moving towards a final equilibrium. Diffusion in exceeds diffusion out of the matrix until equilibrium is reached. At that point, the diffusion rates, in and out, become equal, and the change in free energy becomes zero. The equilibrium constant, K_{eq}, is related to the free energy by: $\Delta G = -RT \ln K_{eq}$. Thus, at equilibrium $-RT \ln K_{eq} = 0$.

Upon spontaneous adsorption of a fuel into a polymer, the overall entropy change increases since both the fuel and the polymer proceed from a more ordered state to a more disordered state. This is the thermodynamic component of the driving force permitting the fuel to diffuse into the polymer until equilibrium is reached. The sum of the order in (1) the final swollen matrix polymer and (2) the remaining fuel is more disordered (less ordered) than at the start of the diffusion. Also, there is less remaining fuel in the sample of starting fluid than existed at the start of the process. Therefore, the total ΔS (entropy change) of the system is positive. For ΔG to reach zero during solvent diffusion then requires the net final ΔH to be positive (hence endothermic) to counteract the magnitude of the $-T\Delta S$ term in Equation 21 at equilibrium where $\Delta G = 0$. So, the enthalpic changes must be understood as fuel leaves the initial body of fuel's location and moves into the polymer matrix. This is represented in Figure 36.

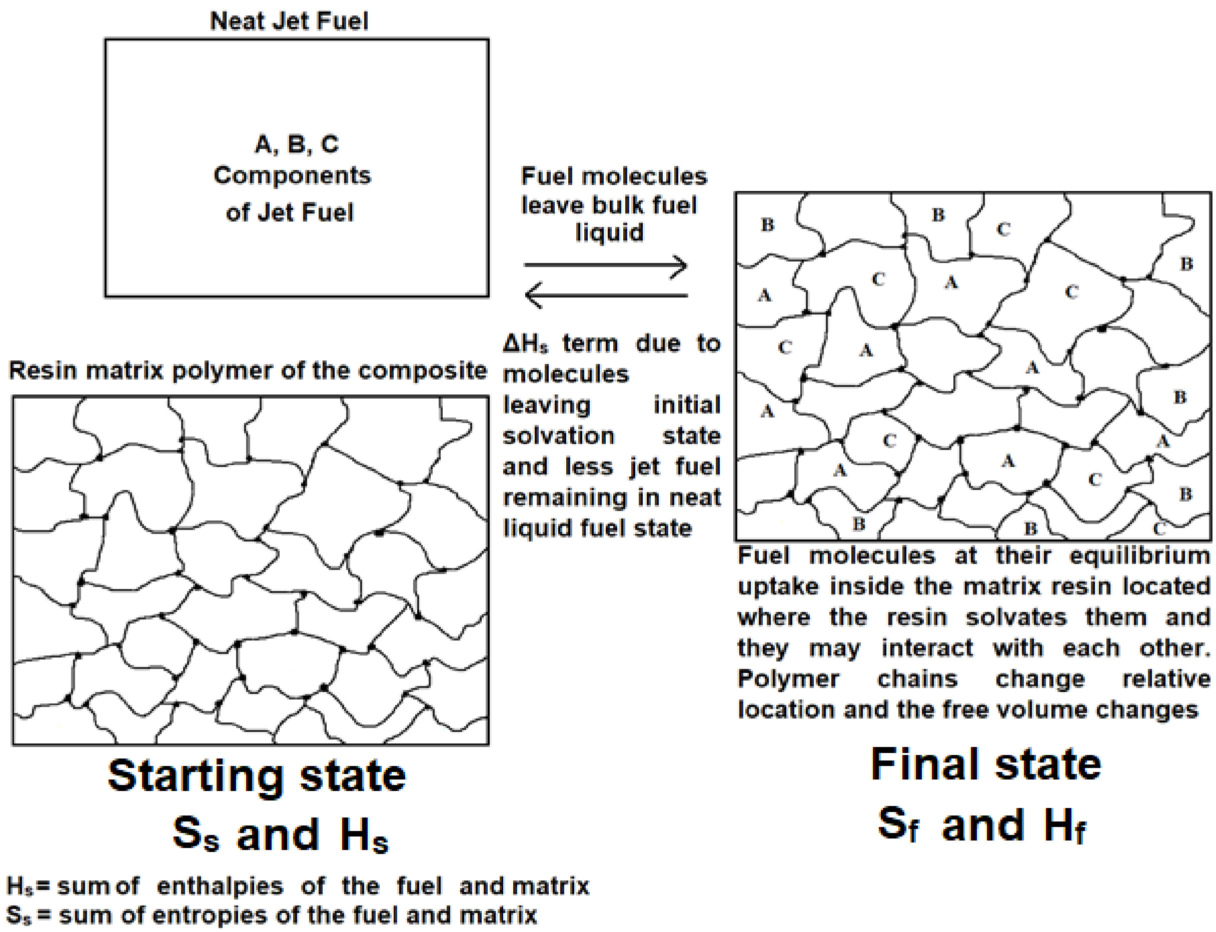

Figure 35. Representation of starting and final states of diffusion.

At equilibrium:

$$\Delta G = (H_F - H_S) - T(S_F - S_S) = 0$$

Equation 22

Here, the sub letters F and S represent the final and starting states of the system.

As seen in Figure 36, the starting state (fuel and polymer before mixing) is more ordered compared to the final state (fuel mixed with the polymer). This means that $S_F > S_S$, implying that $\Delta S > 0$. For diffusion to happen, attractive forces between fuel molecules in the starting state must be broken for these molecules to be able to leave this liquid state. This is an endothermic process (H_S>0) and it requires the input of energy. Creating new attractive forces between fuel molecules and the fuel with polymer components is an exothermic process (H_F<0) in which energy is released. For ΔG to be zero at equilibrium requires the net enthalpy change ($\Delta H = H_F - H_S > 0$) to be positive making it an overall endothermic process. Thus, the exothermic release of energy during solvation interactions within the matrix resin must have a smaller magnitude than the magnitude of enthalpic input (endothermic) that is required to be expended within the starting state.

The energy released during the creation of new attractive forces between fuel molecules and the polymer components as well as the energy absorbed during the separation of fuel molecules in the starting state will depend on the structure of the components of the fuel and of the polymer matrix. For fuel molecules to be separated from the bulk of fuel molecules in the starting state, attractive forces connecting different fuel molecules need to be broken; these attractive forces are mainly π- π stacking between the aromatic compounds, as well as Van der Waals forces between aromatic and aliphatic molecules with all fuel components. To break these attractive forces, this needs an energy input, making it an endothermic process ($H_S > 0$). The creation of new attractive forces between fuel molecules and the polymer components involves π- π stacking attractive forces between aromatic fuel and aromatic epoxy components and Van der Waals forces between all the non-polar fuel components (aromatic and aliphatic) with the epoxy resin which creates attractive forces. Upon creation of new attractive forces, this process is exothermic since energy is released ($H_F < 0$). The overall diffusion process is endothermic, since the net enthalpy change needs to be positive ($\Delta H = H_F - H_S > 0$) for ΔG to be zero at equilibrium.

The diffusion of Jet A fuel into a cured crosslinked epoxy is used here as an illustration. Jet A fuel components include aliphatic molecules (such as octane and heptane) and aromatics (such as 1,2,3-trimethylbenzene) shown in Figure 37.

The three sample Jet A fuel components structures are:

A: octane

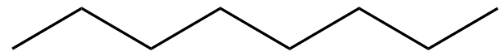

B: heptane

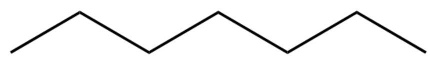

C: 1, 2, 3-trimethylbenzene

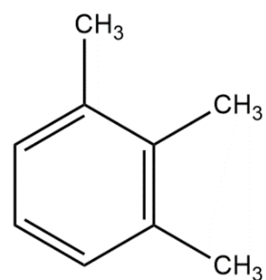

Figure 36. Three sample Jet A fuel components.

Figure 38 illustrates some simple concepts of solvation forces contributing to enthalpic effects during fuel diffusion into an epoxy resin. The cured epoxy used is illustrated in Figure 16. This helps illustrate some portions of the ΔH effects, which occur during fuel uptake by the matrix epoxy, resin thereby contributing to the thermodynamics. Figure 38 shows component fuel molecules (in red) diffused into the epoxy structure. Figure 38 is used only as an illustration for the final state of the epoxy chain after fuel components are diffused. This figure exaggerates the number of fuel components diffused, which may represent a lower weight percentage in the actual final state.

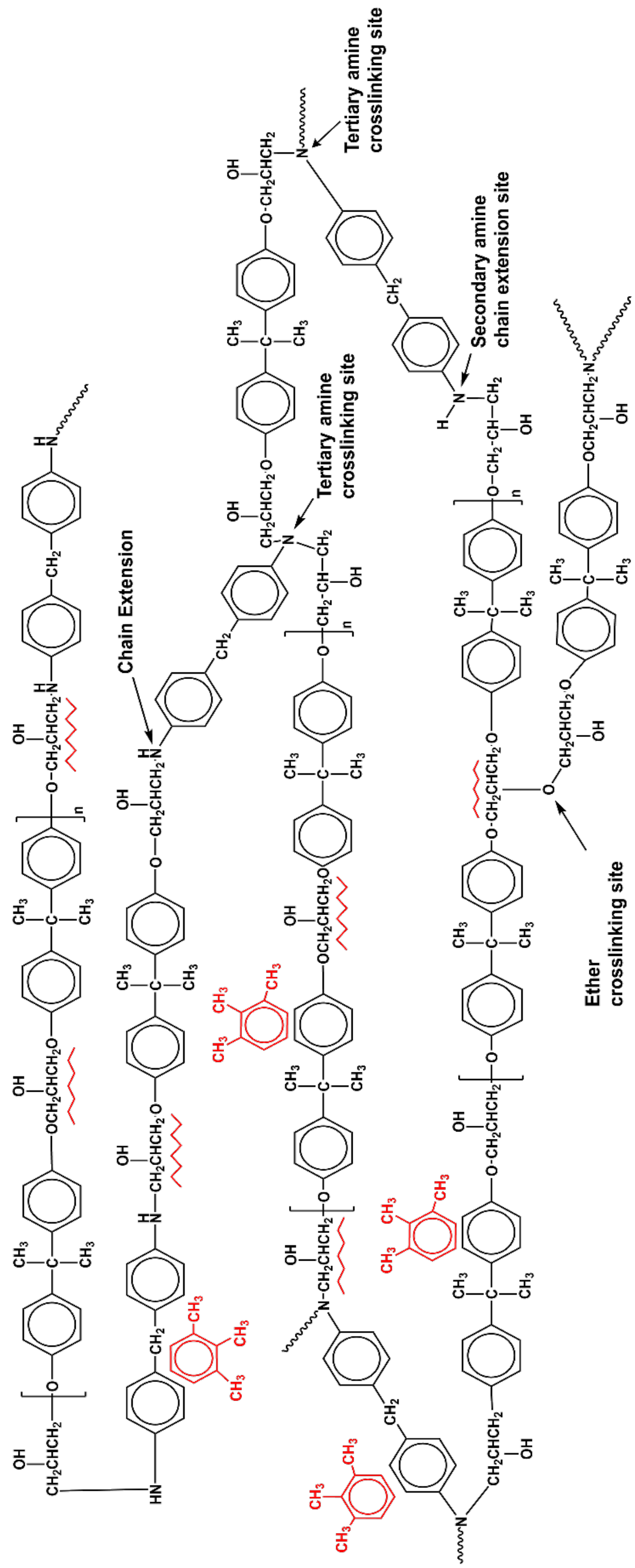

Figure 37. Epoxy resin after fuel components have diffused in it.

Water diffusion into the epoxy contrasts sharply with fuel diffusion. Water is a highly polar fluid that has a highly hydrogen bonded liquid structure. It forms hydrogen bonds to lone pair electrons on hydroxyl, carbonyl, carboxylic acid, and ether oxygens as well as to those on primary, secondary, and tertiary amine nitrogens. Due to water high polarity, it has significant permanent dipole-dipole attractive interactions. The hydrogen bonding and dipole-dipole attractions provide added attractive interactions in addition to Van der Waals attraction.

Upon spontaneous adsorption of water into a polymer, the overall entropy change increases since water and the polymer are proceeding from a more ordered state to a more disordered state, hence $\Delta S = (S_f - S_s) > 0$. This driving force permits water to diffuse into the polymer until equilibrium is reached. When diffusion occurs, attractive forces between water molecules in the starting state must be broken for them to leave this liquid state. Hydrogen bonding, dipole-dipole, and Van der Waals forces in the water bulk must be broken. This necessitates a higher energy input compared to breaking the attractive forces to free a fuel molecule at the starting state. Thus, this is endothermic process (H_s>0) costs more energy for water than fuel for a given weight. The diffusion of these water molecules into the polymer allows attractive forces between water and polymer components to from as well as between different water molecules that are diffused. These attractive forces are created by a combination of hydrogen bonding, dipole-dipole, and Van der Waals forces, which releases energy making it exothermic (H_f<0). At equilibrium, ΔG is zero. This requires that the overall change in enthalpy ΔH $(H_f - H_s)$ to be positive (endothermic) to counteract the magnitude of the $-T\Delta S$ term in Equation 21.

Water will diffuse to a larger extent in composites (fiber and matrix) compared to fuel. If the fiber used is oxidized to promote fiber to matrix adhesion, this will lead to the diffusion of water molecules into the fiber/matrix interface region. Here, water molecules will hydrogen bond to the oxygen atoms present on the fiber. This can act to lower the interfacial shear strength degrading composite properties (Figure 39).

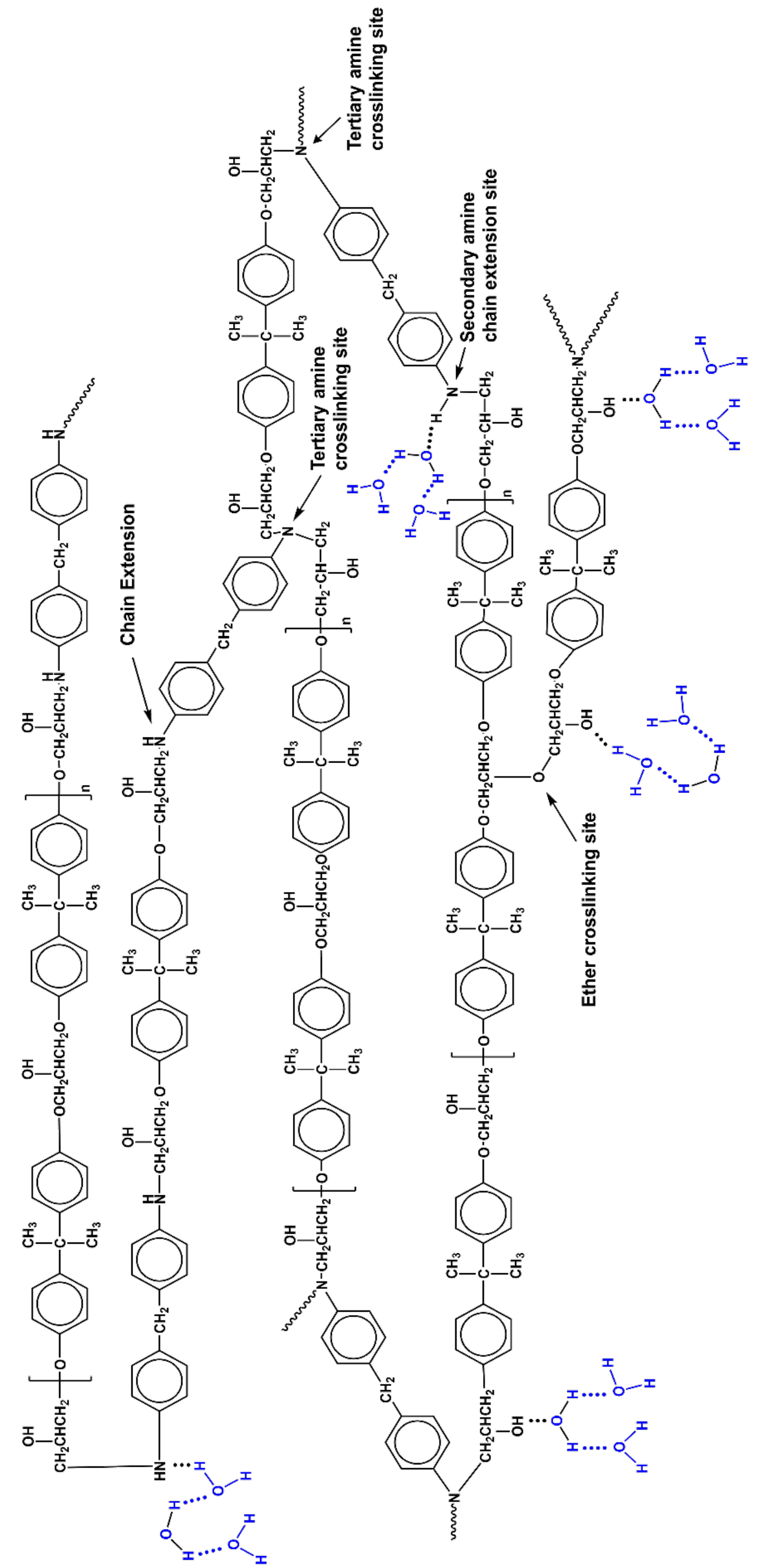

Figure 38. Full epoxy after water molecules have diffused in it.

A fluid's diffusion into thermoplastics or thermosets causes swelling. This swelling causes separations between polymeric chains allowing them to have more molecular mobility. This can be even more serious in thermoplastics, as increased molecular mobility can cause a type of non-elastic flow known as creep. In thermosets, such as epoxy resins, the diffusion of molecules past each other can never occur because crosslinks hold them together. However, enhanced mobility helps free some segmental motion between crosslinks (as illustrated in Figure 40), which may lower the glass transition temperature. This segmental motion occurs without permitting polymer chains to move past each other (because of the crosslinks). Therefore, the segments now in motion will never migrate apart, unlike the case of thermoplastics.

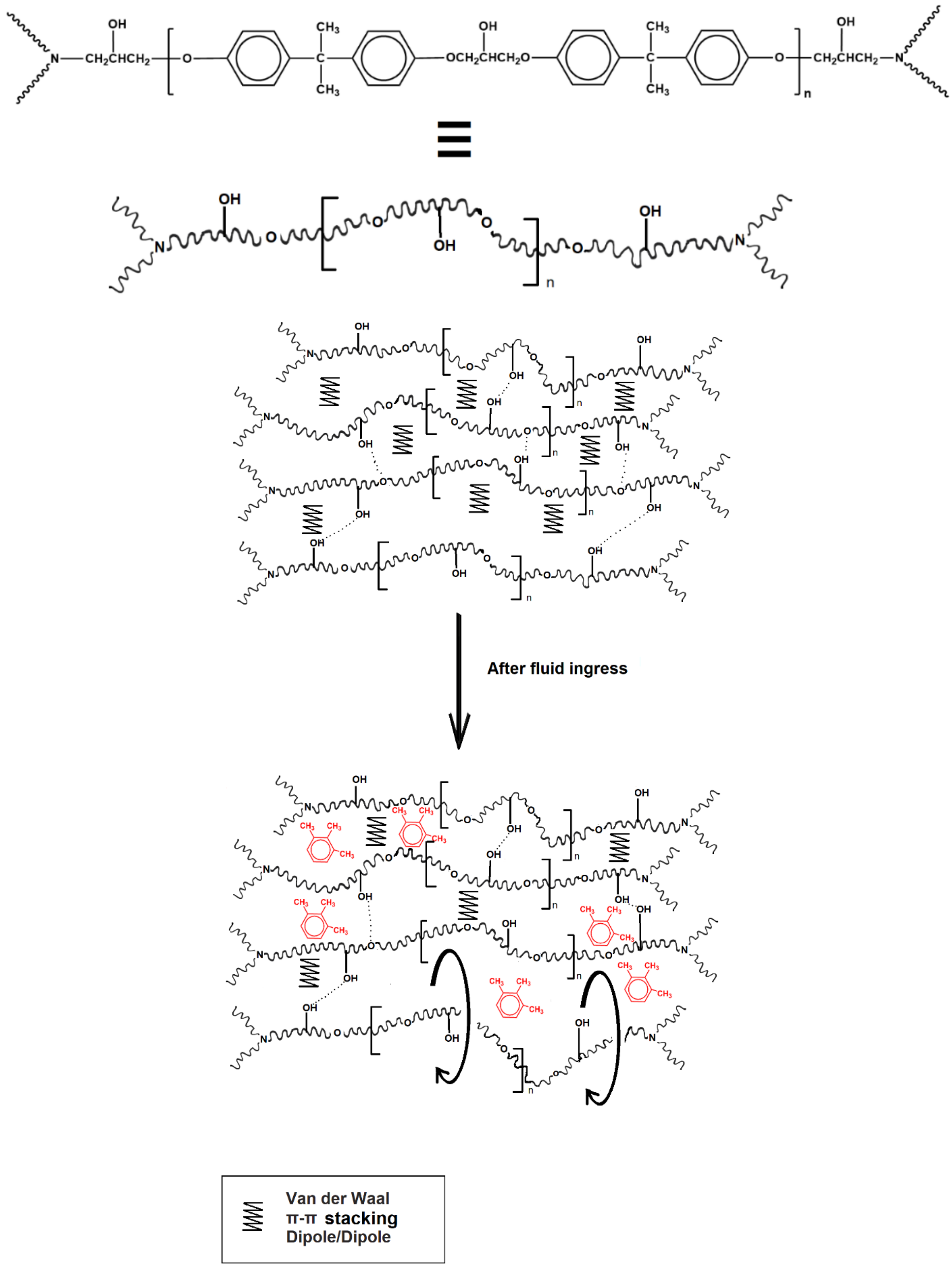

Figure 39. Effect of fluid ingress into an epoxy resin on chain mobility.

This swelling-induced higher mobility can directly affect glass transition temperatures. At low temperatures, amorphous polymers are in the glassy (sometimes referred to as vitreous) state where they are stiff. Upon warming, polymers undergo increased molecular motion that lowers stiffness (e.g., the storage modulus) in a distinctive temperature range known as the glass–rubber transition region. This differs in thermosets and thermoplastics. The glass transition temperature (T_g) range is critical since a material's properties can differ drastically as the temperature traverses and rises above the (T_g) range. The glass transition is a second-order transition. Instead of discontinuities in volume and enthalpy, their coefficients of expansion and heat capacity shift. Figures 41, 43, and 44 illustrate these principles. Amorphous thermosets and thermoplastics are both viscoelastic materials, which typically exhibit the five regions of viscoelastic behavior. This is illustrated in Figure 41 for thermoplastics. Figures 43 and 44 refer to thermosets. In the glassy phase, molecular motions mostly consist of short-range rotational movement and vibrational motion. In the glass transition phase, organized long-range molecular movement begins, involving longer chain segments that have achieved enough thermal energy to escape their confinements in the glassy region. These restrictions occur because attractive forces of all types between different chains (Van der Waal, π-π, dipole/dipole, H-bonding, etc.) hold chains in place. As temperature rises, these attractive forces are overcome, allowing chains to move with respect to each other. They are no longer frozen in place.

In the rubbery phase, as temperature rises, a different behavior is observed for thermoplastics and thermosets. In thermoplastics, the modulus slowly decreases, as illustrated in Figure 41. The molecular weight of the polymer controls the extent of the plateau width (the temperature range over which it exists). A higher molecular weight in linear polymers leads to a prolonged plateau. In the rubbery flow phase, the material will behave similarly to the rubbery phase. However, for extended periods under shear, the molecular motion induced by the higher temperature allows the organized movement of the chains (contingent upon the molecular weight), which can lead to flow of polymer molecules past one another and disentanglement of polymer chains from each other. Thus, flow can occur since molecules can begin to move past one another. In the liquid flow region, at even higher temperatures, the higher energy of the chains allows them to stretch and reptate out of entanglements and flow as separate molecules. This is seen in Figure 42. Viscous liquids become less viscous as temperature rises and flow can occur (Sperling, 2005). Upon stretching the polymer, chain deformation occurs, allowing larger elongations and creep.

Creep is a viscoelastic phenomenon where viscoelastic materials under a constant stress undergo a continual time-dependent permanent deformation (change in strain). Below the yield point, organized movement of the polymer chains proceeds, allowing polymer chains to stretch between the entanglement sites, allowing the material to regain its original shape after the stress is removed. Above the yield point, plastic deformation occurs, which is not completely recaptured when stress is no longer applied. This permanent deformation occurs through a permanent rearrangement of molecules. Creep is temperature and strain dependent. Higher temperatures will lead to more free volume between polymer chains, which will reduce secondary bonding and enhance chain mobility, allowing polymer chains to disentangle, leading to permanent deformation of the material. Higher strain rates will not grant polymer chains sufficient time to experience yielding, thus polymer chains will not occur.

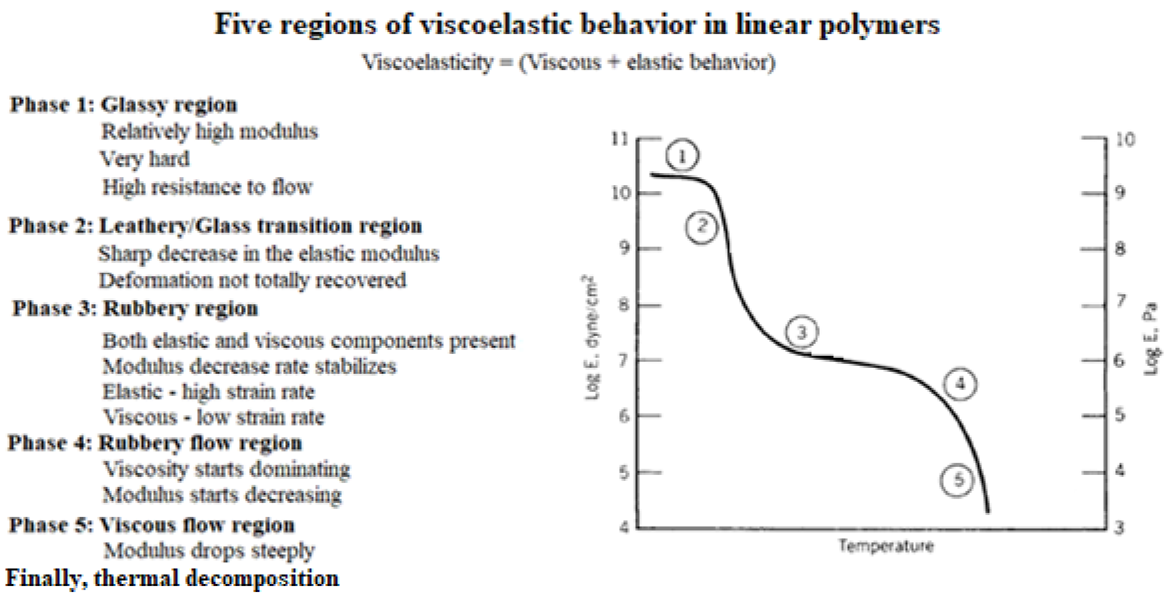

Figure 40. Five regions of viscoelastic behavior for a thermoplastic material (Sperling, 2005).

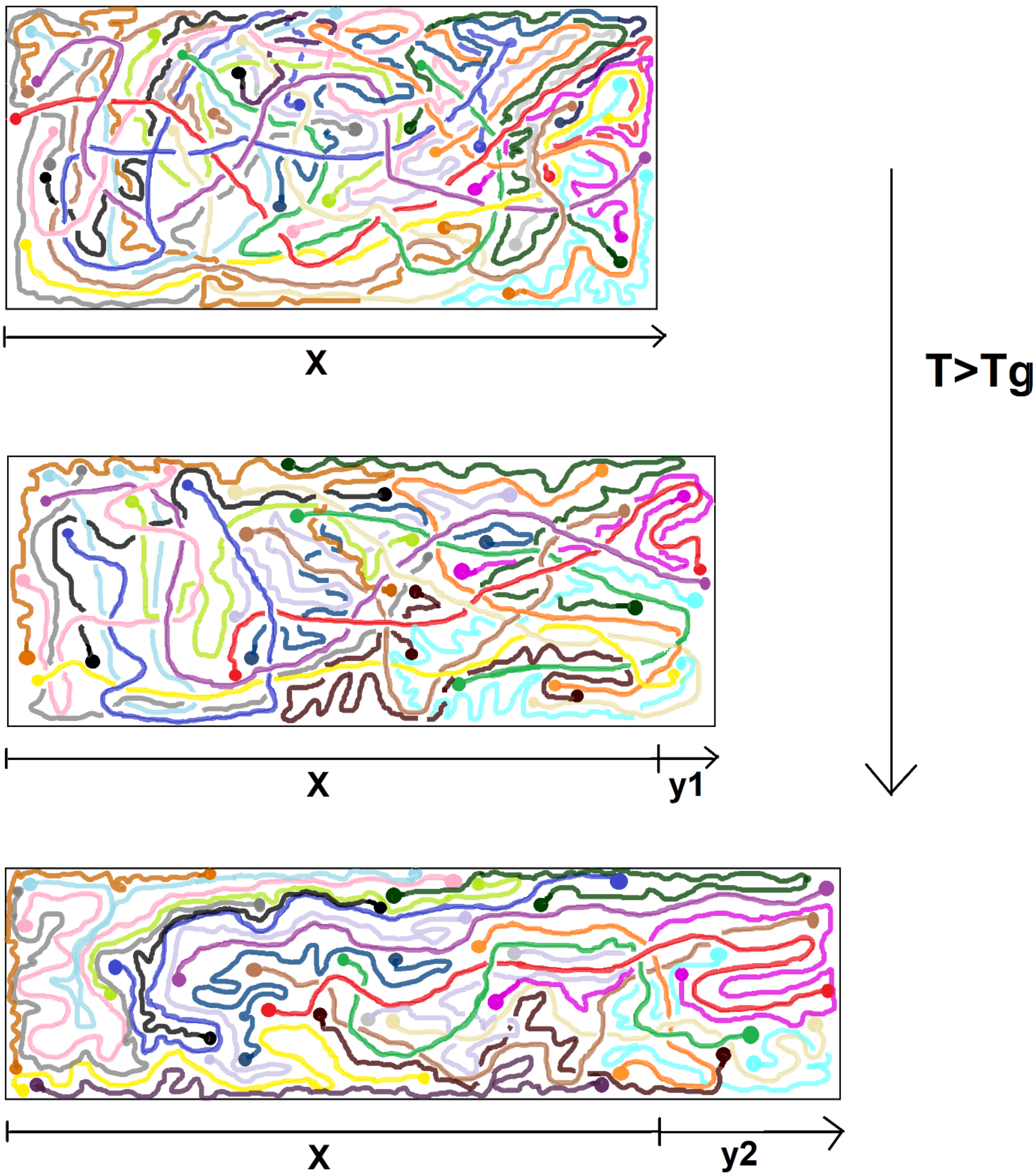

Figure 41. Stretching and reptation of linear polymer chains (different color for each chain).

In the rubbery phase of crosslinked polymers (e.g., epoxy resins), higher elasticity exists than in thermoplastics where decreased chain mobility of chain segments between crosslinks exists. This means the segments are now shorter and shorter segments have less ability to elongate and increase the actual distance between the crosslinking centers. Higher crosslink densities also impede the ability of fuel molecules to diffuse into the resin, which in turn, makes it harder to separate adjacent chain segments, which experience attractive interchain forces between these segments.

Neither the rubbery flow nor liquid flow regions occur in crosslinked polymers. Instead, and the rubbery phase remains present until decomposition of the thermoset occurs, as seen in Figure 43. The glass transition temperature responds to higher cross-link densities by rising T_g, as illustrated in Figure 44. This is due to a decreased chain mobility of chain segments between crosslinks because of increased covalent bonding between chains that reduces molecular freedom and often reduces the free volume. Hence, upon stretching the polymer, chain deformation occurs, as seen in Figure 45, allowing the thermoset to elongate slightly, as opposed to thermoplastics, which are susceptible to larger elongations and creep.

When a thermoset is subjected to a tensile stress at a temperature above T_g, the chemical crosslinks inhibit the molecules from flowing, yet there is sufficient molecular mobility for chain segments between crosslinks to relax, as seen in Figure 46. Thus, the polymer can be more flexible and “rubbery” and can elongate under tension until restricted by crosslinks. If the average distance between crosslinks is low, the elongation under a tensile stress will be greater. Conversely, at high crosslink density, elongation will be smaller.

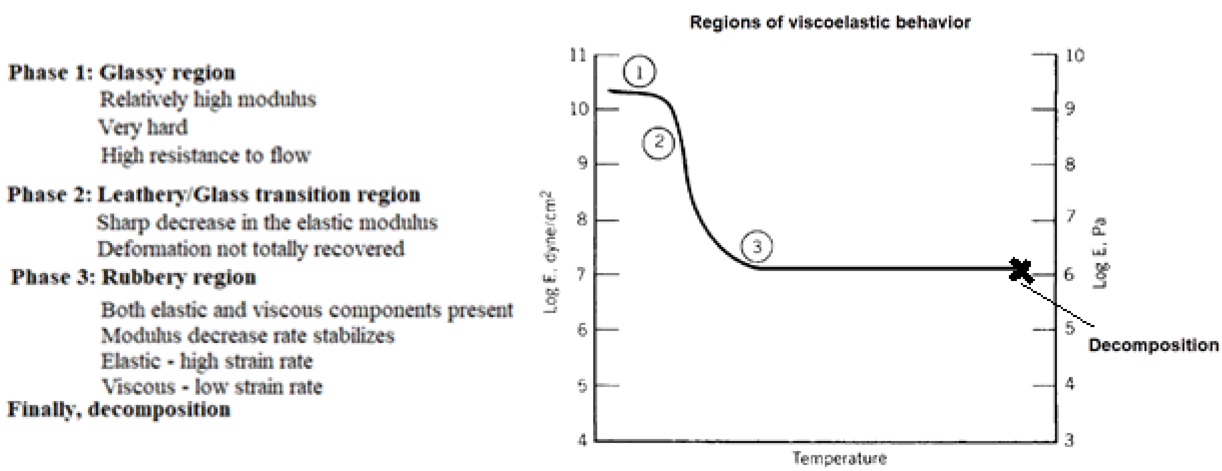

Figure 42. Regions of viscoelastic behavior for a thermoset polymer.

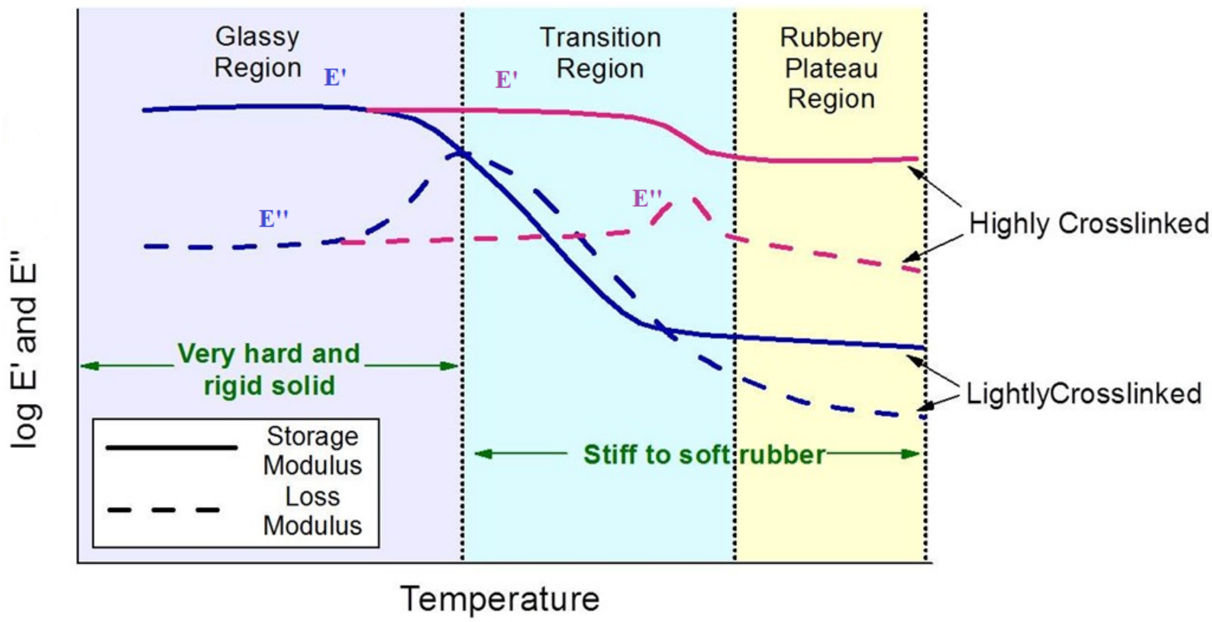

Figure 43. Change of storage and loss moduli with temperature for thermoset polymers (Bond & Smith, 2006).

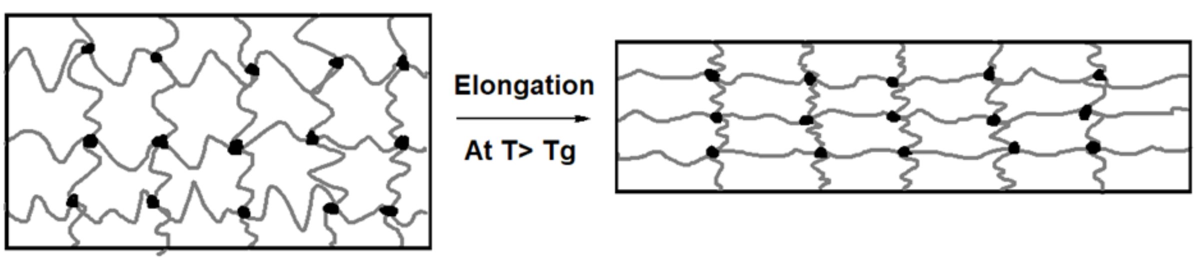

Figure 44. Stretching of crosslinked polymers.

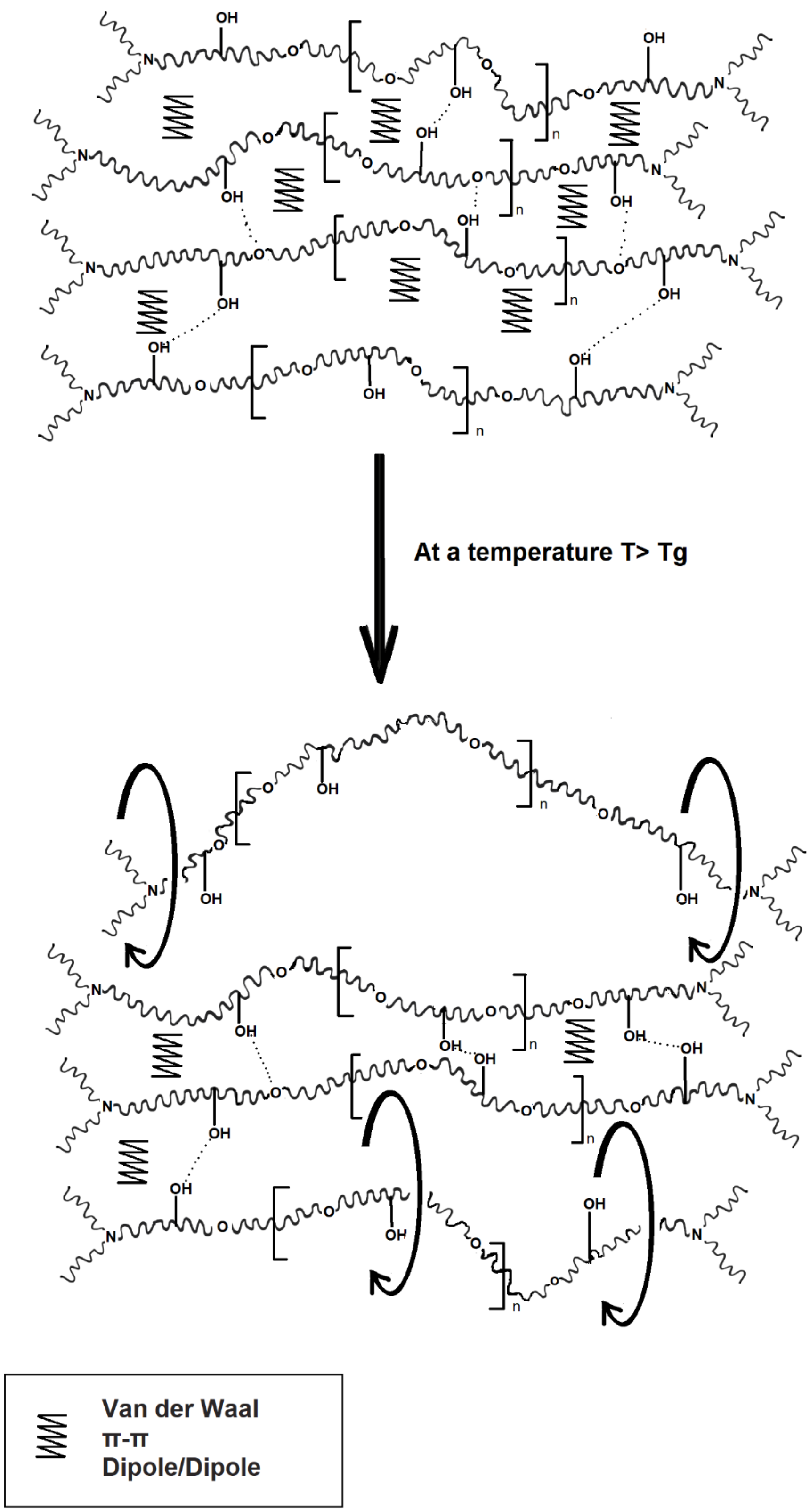

Figure 45. Increased chain mobility at temperatures above T_g.

2.4 Effects of fluid uptake by composites

The absorption of low-molecular-weight penetrants can significantly affect the matrix-dominated mechanical properties and thermomechanical properties of composite materials. One of the most commonly occurring low-molecular-weight penetrants that composite materials are exposed to is moisture in different forms, either liquid water or atmospheric moisture (e.g., from humid air) (Bond & Smith, 2006). The absorption of low-molecular-weight fluids contributes to matrix swelling (rearranging the polymer molecules), matrix cracking, and matrix plasticization (e.g., fuels, hydraulic fluids, etc.), as schematically shown in Figure 47. As discussed in the thermodynamics of diffusion section above, this matrix swelling and plasticization occur due to polymer interchain molecular polar bonds interference, which can affect the mechanical properties of the composite when subjected to matrix dominated loads, along with degrading the fiber/matrix interface (Bond & Smith, 2006). This section investigates the effects of moisture and aeronautical fluids absorption on polymer composites and polymers.

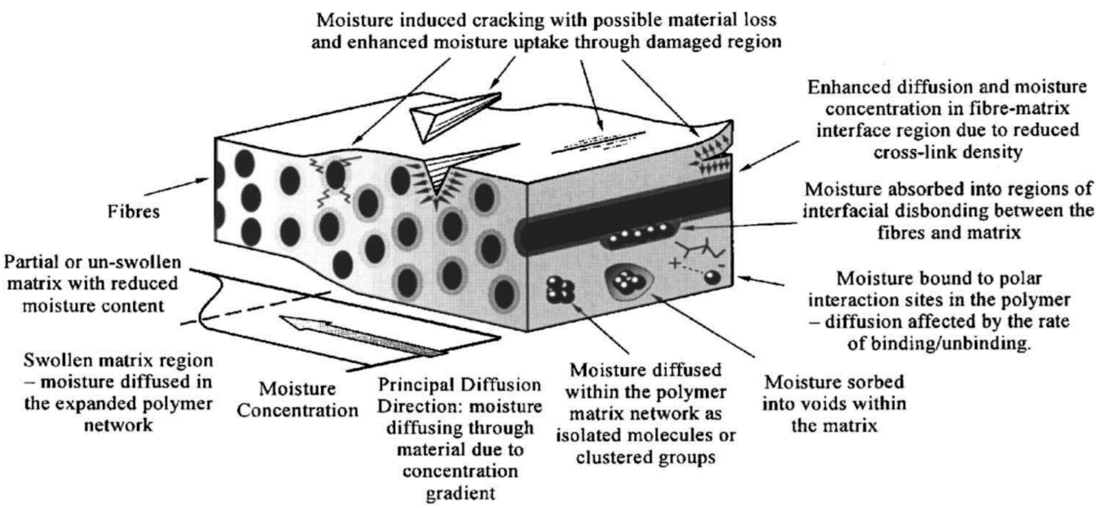

Figure 46. Schematic of the process of moisture absorption by composites (Bond & Smith, 2006).

2.4.1 Effects of moisture uptake by composites

The first noticeable effect of moisture absorption by the composite is swelling, which is a direct consequence of the uptake of moisture. This swelling can be tracked through weight gain of the composite. The weight tracking is generally realized periodically during the exposure time by taking the composites out of water, drying them, and weighing them. This weight gain is illustrated as a function of the square root of time and tends to follow a Fickian diffusion, where the curves have a steeper slope in the beginning and then reach a plateau of saturation, as discussed in the kinetics of diffusion section above (Ma, Lee, & Tai, 1992). To accelerate the diffusion process and reach saturation faster, immersion temperature can be increased with the condition that it remains below the glass transition temperature to increase the molecular motion of water. Such is the case for La Saponara et al. (La Saponara, 2011; Sugita, Winkelmann, & La Saponara, 2010) Feng et al. (Feng, et al., 2015), and Landry et al. (Landry, LaPlante, & LeBlanc, 2012), who studied the effects of environmental and chemical degradation of carbon/epoxy specimens for aerospace applications. In La Saponara et al., carbon/epoxy specimens were immersed in water at room temperature (RT), 70 °C, and 85 °C temperatures. Landry et al. and Feng et al. (Landry, LaPlante, & LeBlanc, 2012; Feng, et al., 2015) used two types of specimens with different thicknesses and immersed them in water at 70 °C (thick specimens were 3 mm and thin specimens were 2.25 mm), and two types of layups $[45/45/0/0/0/-45/90/45/45/0/0/0/-45/90]_s$ and $[0/0/45/0/0/-45/90/45/0/0/-45]_s$, respectively. In all studies mentioned, specimens' weight gain was tracked vs. the square root of time and the mass gain correlated with the Fickian diffusion model discussed in the kinetics of diffusion section (and the Langmuir model in La Saponara et al.'s work, as seen in Figure 48). Thicker specimens showed a higher weight gain than the thinner ones, reaching an overall value of 0.5% to 2% mass gain. Similar studies have been conducted using graphite/epoxy specimens.

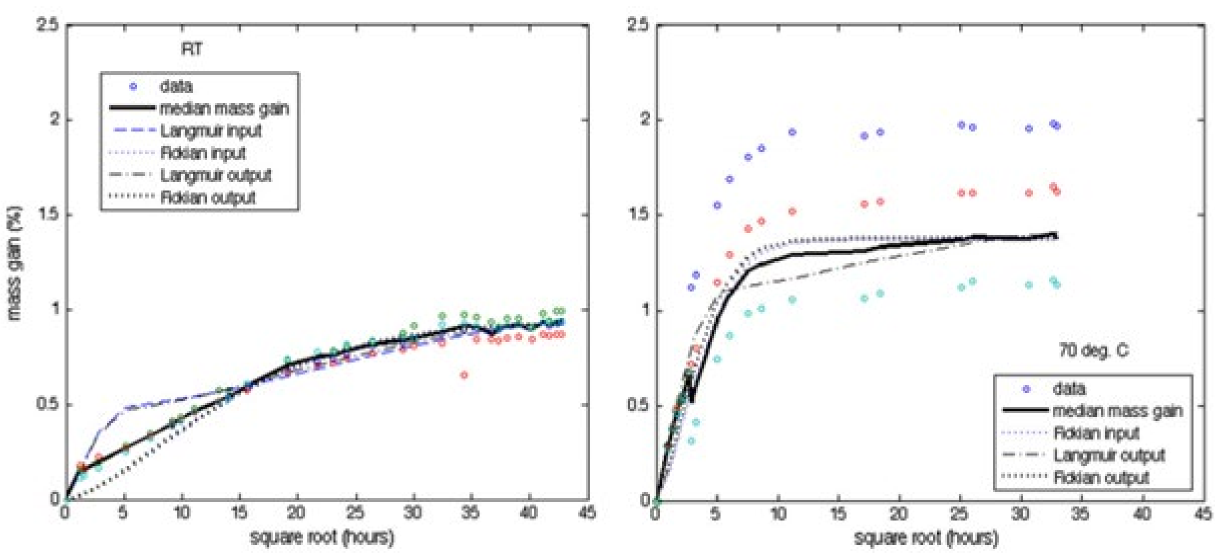

Figure 47. Median mass gain & diffusion models for water immersed carbon/epoxy specimens.

So far, it has been shown that the moisture diffusion in the epoxy systems depends on the hygrothermal conditions (such as varying temperatures of immersion in water), on the specimen thickness. Other studies have shown that the hygrothermal history can also play a role. Lin et al. (Lin & Chen, 2005)investigated the moisture sorption desorption–resorption process of DGEBA with dicyandiamide hardener DGEBA/DDA epoxy system, showing the effects of moisture on the mechanical behavior of the epoxy system. Desorption and resorption processes were faster than the sorption process, and resorption was the fastest among the three stages. The moisture diffusion coefficients of the epoxy system were independent on the thickness of the specimen, and the non-Fickian diffusion behavior became less noticeable with the specimen thickness increasing.

Loos et al. (Loos & Springer , 1979) investigated the effects of moisture absorption of graphite/epoxy composites (graphite fibers having a higher modulus and lower strength than carbon). Graphite/epoxy specimens were immersed in distilled and saturated salt water with three different soaking times (Loos & Springer , 1979), the composites masses increased as a function of both the immersion time and temperature. The final equilibrium weight gain was not affected by the difference in temperature. The higher the temperature, the faster saturation was reached for specimens immersed in distilled water and salt water (distilled water with 30g of sodium chloride per liter) (Loos & Springer , 1979). Other studies have investigated the effects of lowering the immersion temperature, such as Kim et al. (Kim & Takemura, 2011). In their work, pure cured epoxy resin and carbon/epoxy composites were immersed in water until reaching 1% weight gain, then some of these specimens were frozen to -20 °C without drying. Volume change showed that the pure epoxy absorbed more than the carbon/epoxy composites due to the carbon fibers reinforcement's hydrophobic nature or the presence of less amounts of matrix material compared to pure epoxy resin. The frozen specimens showed a higher volume change for both the epoxy and the carbon/epoxy due to the frozen water molecules.

Several studies investigated the effects of water uptake by cured epoxy resins. Zafar et al. (Zafar, Bertocco, Schjødt-Thomsen, & Rauhe, 2012) studied the long-term effects of moisture on carbon/epoxy composites and pure epoxy specimens (without fibers), and the effects of crosslinking degrees in pure epoxy resins. In the first study, the epoxy was based on DGEBA and Bisphenol F Diglycidyl Ether (DGEBF) with a diluent 2,3-epoxypropyl. Specimens made of carbon/epoxy were immersed in seawater and demineralized water between 40 to 300 days (long term). Both the composite and pure epoxy specimens followed a Fickian diffusion trend, reaching saturation after 56 days for the composites and 40 days for the pure cured epoxy resin. The composites' equilibrium moisture content (2.18% and 2.31% for sea and demineralized water, respectively) was higher than that of the pure epoxy (2.03% and 1.79% for sea and demineralized water, respectively). Specimens immersed in seawater showed lower equilibrium content than those immersed in demineralized water, which was explained by the presence of salt particles that weren't absorbed as much as water particles, and this can be verified by the degree of salinity of the water absorbed compared to the original seawater used. The second study focused on immersing highly cross-linked epoxy systems DGEBA and DGEBF (with DDS amine curing agent) in deionized water at two different temperatures 50 °C and 80 °C (Toscano, et al., 2016). After saturation was reached, desorption was performed at room temperature only for the samples immersed in 80 °C water. Water uptake and desorption were tracked through weight tracking. Both epoxy systems showed an increase following a Fickian diffusion trend, as seen in Figure 49.

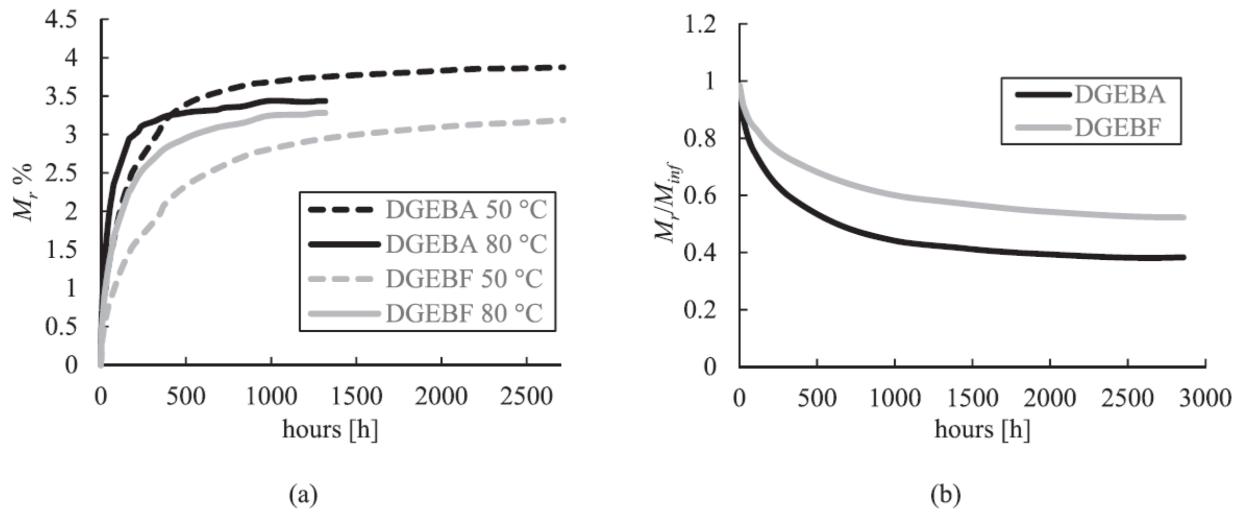

Figure 48. Mass tracking for epoxy specimens during a) absorption b) desorption (Toscano, et al., 2016).

For both exposure temperatures, DGEBA showed a higher weight gain at equilibrium than DGEBF, with a lower difference when exposed at 80 °C. DGEBA is known to have a higher cross-link density than DGEBF, explaining the high uptake for DGEBA by the presence of a higher free volume since the chain mobility is smaller for higher cross-linked epoxies. The difference in weight gain decreases when the temperature is increased, due to the increase in kinetics of water uptake, as discussed in kinetics and thermodynamics of diffusion section.

Thermal tests such as Differential Scanning Calorimetry (DSC), Thermogravimetric Analysis (TGA), and Dynamic Mechanical Analysis (DMA) can be performed to track changes of thermal properties. One of the most important properties for composites or polymers is T_g, which is the range of temperatures over which the transition from a hard-brittle state into a rubbery or viscous state occurs for polymers (Ma, Lee, & Tai, 1992). TGA is a method of thermal analysis in which the mass of a sample is measured over time as the temperature changes. DSC is a method used to study thermal transition (glass transition) of polymers by heating the specimens. In Zafar et al.'s work, DSC was used to determine T_g values of samples immersed for 300 days in seawater and demineralized water. Samples immersed in demineralized water had lower T_g values (56.7 °C) compared to the unimmersed specimens (79.1 °C), as shown in Figure 50. This difference in T_g was explained by the interaction of the hydroxyl groups present in the epoxy with water molecules that result in the plasticization of the epoxy by increasing the chain mobility (Zafar, Bertocco, Schjødt-Thomsen, & Rauhe, 2012).

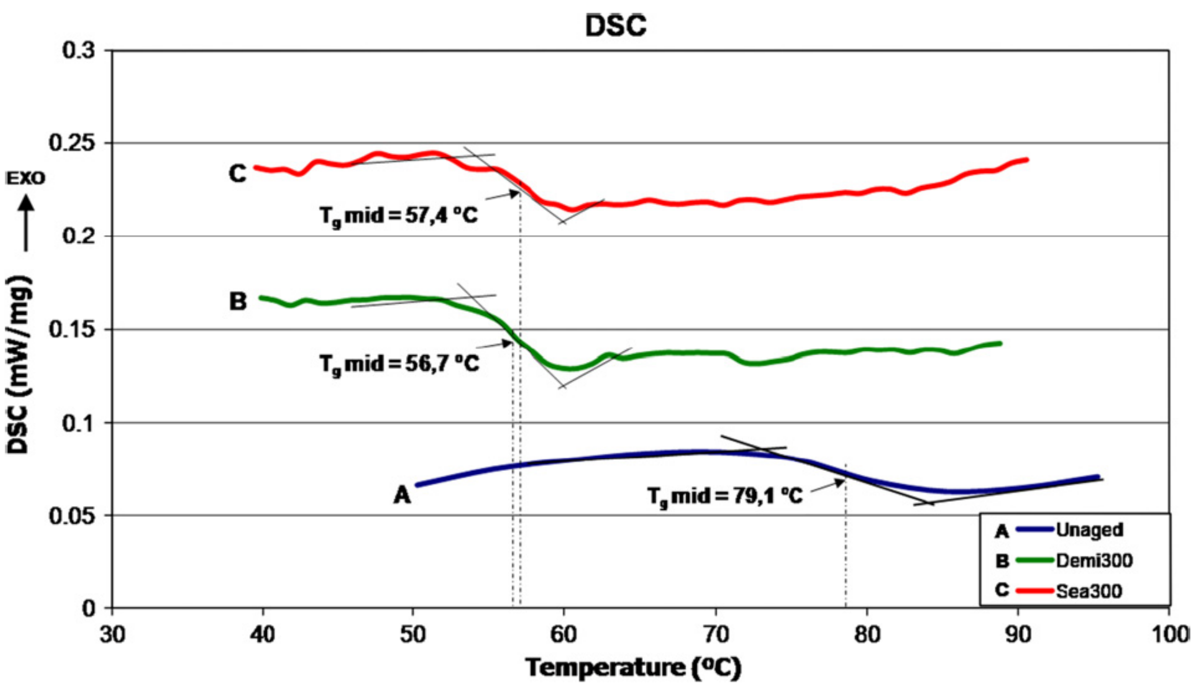

Figure 49. DSC results for unimmersed and water-immersed epoxy samples (Zafar, Bertocco, Schjødt-Thomsen, & Rauhe, 2012).

DMA is a material characterization technique that provides information on bulk properties and thermal transitions. At frequencies and temperatures of interest, an oscillatory strain (or stress) is applied to the material, and the resulting stress (or strain) developed in the material is measured (Barsoum, 2015). From these thermal tests, T_g decreased due to the uptake of water for both thermoplastics and thermosets, which constrains the possibility of high-temperature applications for these composite specimens. Vanlandingham et al. (Vanlandingham, Eduljee, & Gillespie Jr,

1999) found that the absorbed moisture could negatively affect the interfacial strength between the fiber and the epoxy matrix, hence reducing the performance of the composite material. Since the fibers and the matrix have a different thermal expansion, swelling induced by moisture can decrease mechanical interlocking between the fiber and matrix when temperature cooling down after the matrix is cured at high temperature. Therefore, water swelling could seriously alter the internal stress state in the interphase region. The absorbed moisture could also lead to a drop in T_g. This decrease in T_g could also be detrimental to the interphase region if the T_g of the wet interphase is exceeded during the composite's service. These detrimental effects on the interphase region can reduce the fiber/matrix adhesion and even cause failure at the fiber/matrix interface. This could then lead to the formation and propagation of microcracks and other types of damage, causing reductions in composite performance. Vanlandingham et al. (Vanlandingham, Eduljee, & Gillespie Jr, 1999) exposed epoxy specimens to the different conditioning environments (high temperature and high humidity), and found that moisture-induced swelling led to a decrease in T_g by 5-20 °C.

Effects of moisture absorption on composites and polymers' mechanical properties were further investigated using different types of testing, including tensile, compression, flexure, bending (Lin & Chen, 2005)(three-point or four-point), shear, and intralaminar tension or shear tests. These tests provide a range of properties such as tensile strength, elastic moduli, flexural strength, etc. After water uptake by the composites, these properties decrease within these specific composites, sometimes reaching critically low values. Landry et al. investigated the environmental effects on mode II delamination for aerospace-grade carbon/epoxy composites (Landry, LaPlante, & LeBlanc, 2012). After water saturation, carbon/epoxy specimens with different thicknesses were subjected to a four-point end-notched flexure test to study delamination. Water absorption decreased the delamination toughness by 20% along with increasing the delamination growth rate, due to the weakening of the fiber/matrix interface, leading to less energy necessary to initiate and propagate delamination (Landry, LaPlante, & LeBlanc, 2012). Zafar et al. (Zafar, Bertocco, Schjødt-Thomsen, & Rauhe, 2012) performed mechanical tests on moisture-saturated carbon/epoxy composites and pure epoxy specimens, which showed a deterioration of the mechanical properties after water uptake. Young's modulus of specimens immersed in both demineralized water and seawater for 40 days decreased by 5%. In specimens immersed for 300 days, Young's modulus decreased by 7.5% and 10% in demineralized water and seawater, respectively, as seen in Figure 51(a). The tensile strength also decreased by 20% for the specimens immersed in seawater for 300 days, while the other specimens showed a decrease between 15-18%, as seen in Figure 51(b). Therefore, seawater had more deteriorating effects on the epoxy than demineralized water, despite giving less total uptake, and the longer the specimens were immersed, the larger reduction in mechanical properties they experienced (Zafar, Bertocco, Schjødt-Thomsen, & Rauhe, 2012).

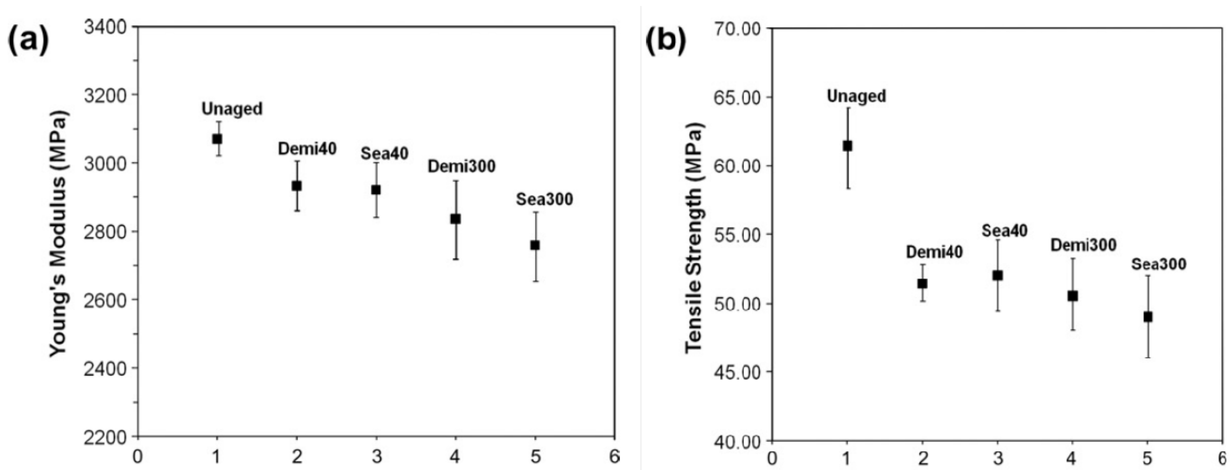

Figure 50. (a) Elastic modulus and (b) Tensile strength for different epoxy specimens under different water immersion conditions (Zafar, Bertocco, Schjødt-Thomsen, & Rauhe, 2012).

Studies have shown that the hygrothermal history also plays a role in affecting the mechanical properties of moisture-absorbed specimens. Lin et al. (Lin & Chen, 2005) performed Uniaxial tensile tests, and since specimens were hygrothermally aged, both the tensile elastic modulus and tensile strength of the studied epoxy system decreased. The extent of plasticization seems to increase noticeably with hygrothermal history, except that the tensile elastic modulus and tensile strength are slightly shifted back for the desorbed samples, as seen in Figure 52 (Lin & Chen, 2005).

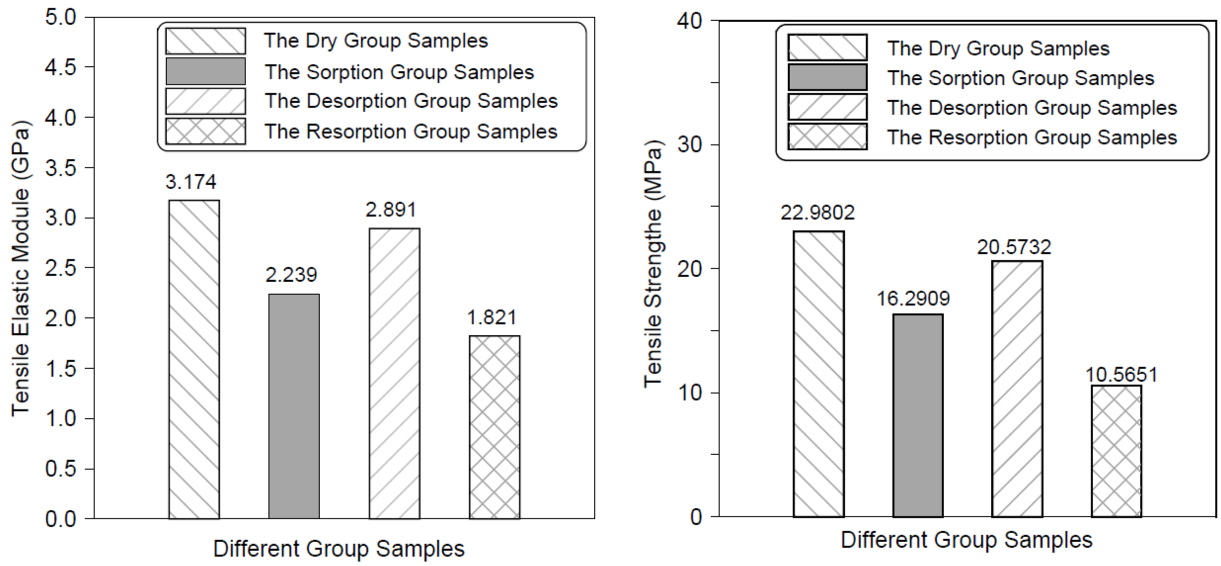

Figure 51. Water aging effects on the epoxy's tensile elastic modulus (left) and strength (right) (Lin & Chen, 2005).

Since moisture absorption does not lead to any physical damage in specimens, Scanning Electron Microscopy (SEM) is used to characterize the effects of moisture absorption on the microstructure of composites, and the moisture-induced failure mechanisms. Feng et al. (Feng, et al., 2015) performed SEM on the cross and side sections of the fractured surfaces of water-immersed and unimmersed panels, as seen in Figure 53(a-d). Figure 53(a) showed brittle fracture in the unaged panel's cross-section. Figure 53(b) shows the deleterious effect of moisture on the fiber/matrix interface, where debonding and gaps can be seen. Figure 53(c) showed good adhesion exists in the unaged panels' side section. Figure 53(d) showed pull-out fibers with smooth surface in the aged panels, with comparatively little matrix attached, indicating the interfacial debonding due to moisture saturation (Feng, et al., 2015).

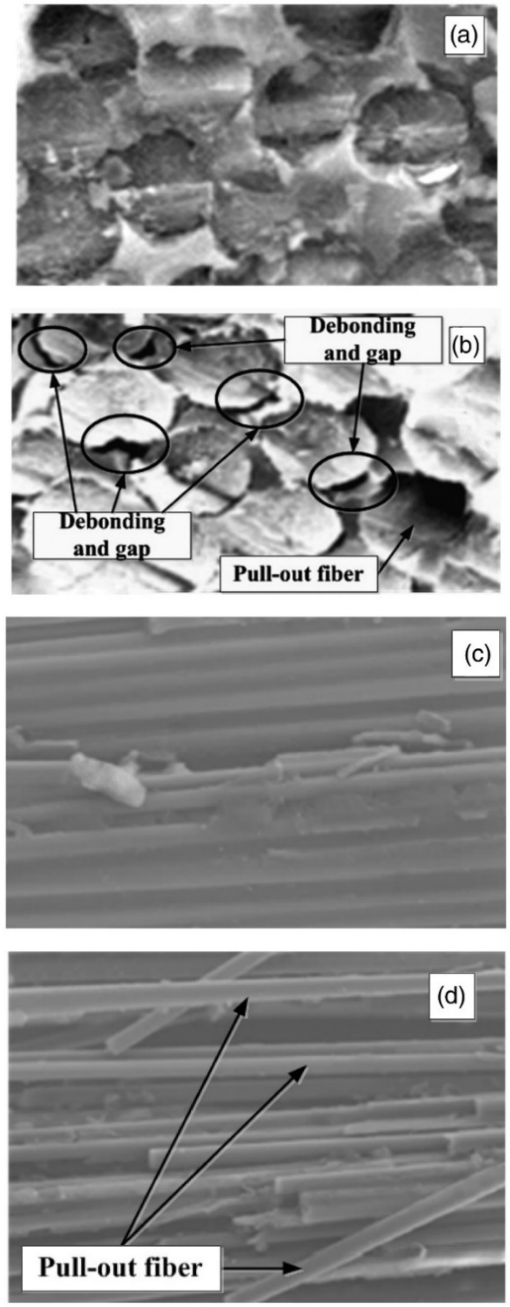

Figure 52. SEM micrographs of cross-section of (a) unaged and (b) aged panel; side-section of (c) unaged and (d) aged panel (Feng, et al., 2015).

In pure epoxy resin, different failure mechanisms can be observed on the microstructure level. In Lin et al.'s work (Lin & Chen, 2005), SEM imaging was performed on the fracture surface for unimmersed, moisture saturated, completely desorbed, and moisture re-saturated epoxy specimens, respectively, as seen in Figure 54, Figure 55, and Figure 56, respectively. From Figure 54, there was initially a relatively smooth fracture surface in the slow crack growth zone.

Spaced ‘rib’ markings perpendicular to the direction of crack growth can be seen in the crack speeding zones. With the crack propagating, the conic-shaped patterns arose in the rapid crack growth zone. For the saturated specimens, it can be seen from Figure 55 that a narrow shear band initially appeared in the slow crack growth zone. Irregular patterns were found on fracture surfaces in the rapidly moving crack zones, and a great number of fine circular or elliptical patterns can be seen on the fracture surface. Figure 56 showed a relatively smooth fracture surface and dissipated a relatively small amount of energy to generate new surfaces in the slow crack growth zone. In the rapid crack growth zone, the fracture surfaces had regularly spaced ‘rib’ markings perpendicular to the direction of crack growth. Compared to unaged samples, there were no dissimilar conic shaped patterns in the fracture surface of the desorbed specimens at 85 °C. Also, SEM images with the same magnification showed that the spaced ‘rib’ markings were more regular, finer, and narrow. These marking patterns indicated that the desorbed epoxy specimens became more brittle than the unimmersed ones when the specimens were preconditioned under the hygrothermal conditions and then desorbed.

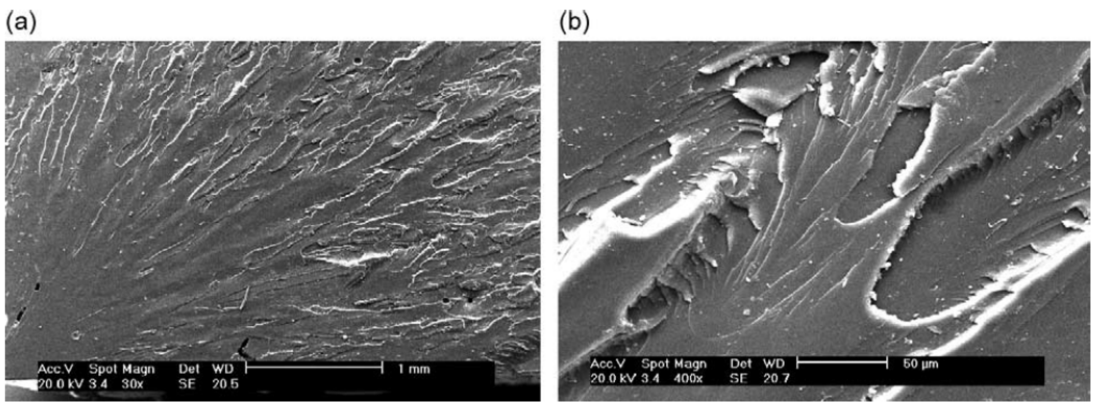

Figure 53. SEM micrographs of the fracture surface of unimmersed specimens at a magnification of : (a) (x30); (b) (x400) (Lin & Chen, 2005).

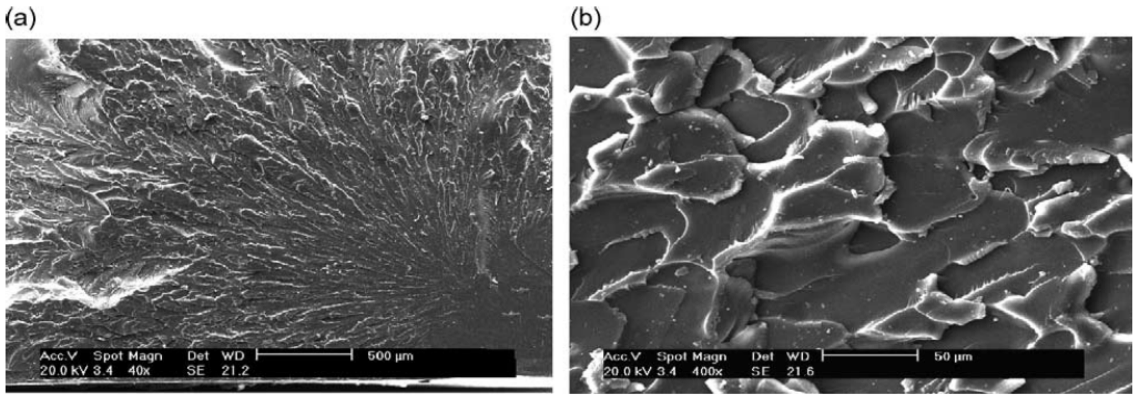

Figure 54. SEM micrographs of the fracture surface of saturated specimens under 85 °C/85%RH: magnification of (a) (x30); (b) (x400) (Lin & Chen, 2005).

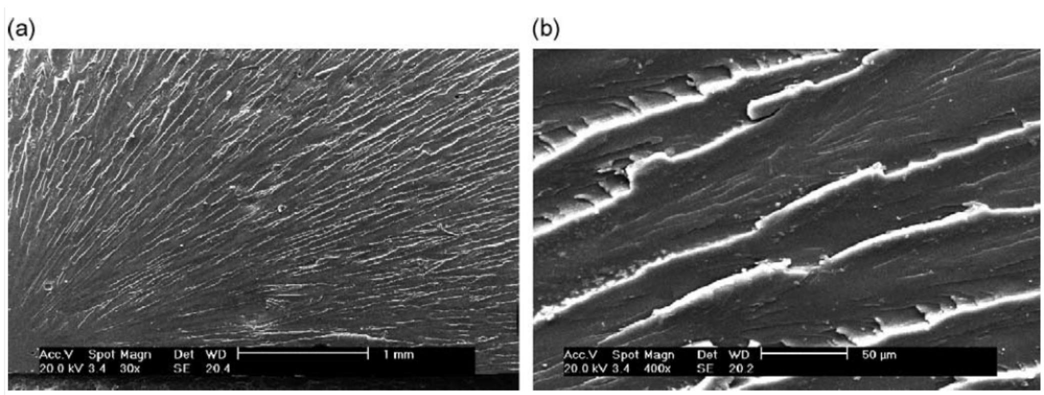

Figure 55. SEM micrographs of the fracture surface of completely desorbed specimens under thermal conditions, 85 °C, at a maginification of (a) (x30); (b) (x400) (Lin & Chen, 2005).

2.4.2 Effects of aeronautical fluids diffusion on composites

During their lifetime, composites used in the aviation industry can get into contact with different types of aeronautical fluids, such as anti-icing, hydraulic fluid, aviation fuel, etc. (Ma, Lee, & Tai, 1992). Each of these fluids will have a different interaction with composite specimens or pure polymeric specimens. This interaction mainly depends on the chemical composition of the fuels as well as the composite (or the polymers) as shown in Sections 2.1 and 2.2. Also, these different compositions will mainly control the degree of uptake of these aeronautical fluids by the composites (or polymers) as seen in Section 2.3.2.

A limited number of studies are reported on the exposure of composite structures to aeronautical fluids. Similar to moisture absorption, the first noticeable effect of fluid uptake by composites is swelling; many studies used weight tracking as a reliable method to follow the change in the overall weight of the composites. For most of aeronautical fluids, the rate of weight gain is higher during the first hours (or even days) until reaching a saturation plateau. As seen in section 2.3.1, it is following a Fickian diffusion trend.

In Curliss and Carlin (Curliss & Carlin, 1989; Curliss D. B., 1991), different aerospace grade composites were immersed in JP-4 fuel, these composite specimens ranged from carbon/PEEK (thermoplastic matrix) to carbon/epoxy and carbon/BMI (thermoset matrix). All these specimens followed a Fickian diffusion trend with the thermoplastics reaching a weight gain of 0.8% when saturated, while the thermosets reached a saturation weight gain of 0.1%.

Landry et al. (Landry, LaPlante, & LeBlanc, 2012) investigated aerospace-grade carbon/epoxy composites exposed to hydraulic fluid and deicing fluid. Weight tracking showed that specimens gained weight by absorbing a quantity of hydraulic fluid and deicing fluid. The weight gain was negative (-0.2%) for composites immersed in hydraulic fluid, as seen in Figure 57, which was explained by chemical degradation and loss of material. For deicing the weight gain reached 0.6%.

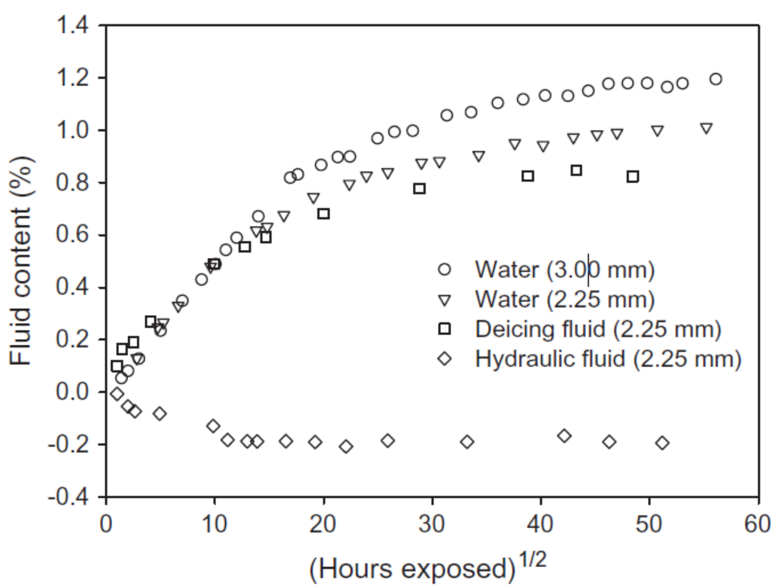

Figure 56. Weight gain curves for carbon/epoxy specimens immersed in different fluids (Landry, LaPlante, & LeBlanc, 2012).

In Ma et al. (Ma, Lee, & Tai, 1992), carbon/PEEK and carbon/PPS specimens were immersed in JP-4, hydraulic fluid, methylene chloride, and methyl ethyl ketone (MEK). Weight gain was illustrated as a function of the square root of time, following a Fickian diffusion trend. Methylene chloride was the most absorbed fluid by both carbon/PEEK and carbon/PPS with 7% and 5% weight gain, respectively.

Arzak et al. investigated the sorption of methylene chloride of two types of PEEK films, amorphous films, and highly crystalline films (Arzak, Eguiazabal, & Nazabal, 1994). From the weight gain tracking, the amorphous specimens reached saturation faster compared to the crystalline specimens, with a higher amount (60% more) of absorbed fluid. These results corroborate the fact that the solvent affects amorphous specimens more than crystalline ones, due to the inactive crystalline phase that acts as a barrier to the absorption of a solvent.

Cornélis et al. exposed an amorphous (PEEK) film sample to acetone at room temperature until equilibrium saturation in fluid uptake was reached, and then dried the film sample in a vacuum oven at 70 °C temperature to desorb the acetone from the PEEK film (Cornélis, Kander, & Martin, 1996; Stober & Seferis, 1988). The PEEK film showed a Fickian diffusion pattern with saturation reached after 12.5 days and an equilibrium weight gain of 14%.

Stober et al. exposed PEEK films to a wide range of different fluids (acetone, benzene, methylene chloride, etc.) with different Solubility Parameter and Hydrogen Bonding Index. The weight gain was higher in specimens exposed to fluids with lower hydrogen bonding index, and these specimens showed the highest swelling percentages and induced crystallinity. In addition, different PEEK film specimens were fabricated with different cooling rates to affect the initial crystallinity of the specimens: the higher the cooling rate, the lower the crystallinity. These film specimens were exposed to methylene chloride, and the higher the crystallinity, the lower the weight gain, and absorption of methylene chloride. Crystallinity increased for all specimens, with the biggest change in the initial crystallinity value, implying that low initial crystallinity specimens were more susceptible to have solvent-induced crystallization.

In another study, the fluid uptake and loss by PEEK films of different crystallinities were investigated to study the effects of temperature and initial crystallinity on the absorption process (Wolf & Grayson, 1993). Three different specimens were used an amorphous (0% of crystallinity %C), a PEEK film with 11.5% of crystallinity and a PEEK film with 29% crystallinity (%C). All these specimens were immersed in two different solvents toluene and carbon disulfide (CS_2). These films were immersed at a constant temperature in CS_2 and showed that the rate of absorption decreased as the crystallinity of the PEEK films increased. Also, the equilibrium weight gain decreased with the increase in crystallinity. The PEEK film immersed in toluene had different immersion temperatures showing the same result that even with the increase of temperature, the rate and equilibrium amount decreased with the increase of crystallinity. CS_2 showed higher absorption rates for the cases with similar properties (temperature and %C) than toluene, which was due to the difference in their chemical structure; CS_2 has a longer linear molecule with a smaller diameter compared to toluene, which has a cylindrical shape.

From Equation 14 (the Arrhenius equation section 2.3.1), diffusion is a process that is highly dependent on temperature at which immersion happens. It is assumed that the higher the temperature of immersion the higher the rate of diffusion. Some studies proved that for some of the aeronautical fluids, this statement is true (La Saponara, 2011; Sugita, Winkelmann, & La Saponara, 2010), while others showed that in a small range no clear changes in the rate of diffusion was observed (Loos & Springer , 1979).

In Sugita et al. (Sugita, Winkelmann, & La Saponara, 2010) and LaSaponara (La Saponara, 2011), carbon/epoxy specimens were immersed in Jet fuel, anti-icing additives, and hydraulic fluid at three different temperatures (room temperature, 70 °C and 85 °C), jet fuel was used only at room temperature for safety reasons. The weight gain data for anti-icing fluid, showed an increase in the rate of absorption where specimens reached saturation faster than at room temperature, around 20 days at room temperature compared to 10 and 5 days for 70 °C and 85 °C, respectively. The saturated weight gain for anti-icing was around 35% for all three temperatures. Anti-icing and hydraulic fluid were more readily absorbed than jet fuel, showing a higher weight gain. The weight gain followed a Fickian diffusion trend only for room temperature, with different trends observed when the temperature was increased.

In Loos and Springer (Loos & Springer , 1979), three different graphite/epoxy composite specimens were immersed in jet A fuel, diesel fuel, and aviation oil at three different temperature (27 °C, 38 °C, 49 °C). Specimens immersed showed no changes with temperature; it is believed that this temperature range will not affect absorption rates for these fluids. Also, the saturation weight gain for all three fluids was in the range of 0.5-0.6%, with jet fuel showing the lowest weight gain among them.

The presence of intralaminar cracks is believed to serve as an absorption path for any type of fluid that the specimen encounters. Other than cracks, the presence of drilled hole used for lap joints or other use, represent also an easier path for fluids to ingress into the specimens. In Sala (Sala, 2000), pristine, impacted, and drilled carbon/epoxy and aramid/epoxy specimens were immersed in jet fuel, Skydrol, and dichloromethane. The impact tests were realized to induce intralaminar cracks due to matrix shear and bending, interfacial pullout, interlaminar delamination, and fiber failure (Sala, 2000). These low energy impacts had a maximum specific energy of 1.5 J/mm. Drilled specimens showed higher weight gain due to fluid uptake than the impacted and original specimens. Carbon/epoxy specimens showed lower weight gain compared to aramid/epoxy, since carbon fibers is known to be a non-hygroscopic fiber compared to aramid fibers.

In another study (Horn, Soeganto, & Shaikh, 1989), graphite/PEEK composites were exposed to jet fuel, hydraulic fluids, brine, ethylene glycol, and paint stripper under uniaxial tension (10% and 20% of ultimate strength). The goal was to mimic the effect of in-flight load conditions on fluid uptake (Horn, Soeganto, & Shaikh, 1989). Specimens labelled T are 16-ply quasi-isotropic no-hole tensile specimens, with $[+45/90/-45/0/0/-45/90/+45]_s$ layup. The main purpose of the T specimens is to determine the stiffness and strength of the material in tension. Other specimens labelled R/C were used, they are open hole specimens, with a similar layup as T specimens. R specimens were used in tension to failure and C in compression to failure tests. Also, specimens labeled I with 18-ply $[+45/90/-45/+45/-45/0/0/0/0]_s$ layup these were used for interlaminar shear. From weight gain results, R/C specimens showed the highest weight gain for all the fluids used, followed by T specimens and then I specimens. This shows that the presence of holes in the geometry increases the rates of absorption, and a higher thickness decreases the final saturation amount. Weight gain of all used fluids were compared for T specimens, where paint stripper showed the highest weight gain reaching a saturation weight gain of 2.5%, while for jet fuel it was around 1%.

The absorption of aeronautical fluids by composites (or polymers), is known to degrade mechanical properties of such composites (or polymers). This degradation can affect mechanical properties such as tensile strength, elastic moduli, flexural strength, etc. Different tests can be done to investigate changes in these mechanical properties such as tensile, compression, flexure, shear, and intralaminar tension or shear tests. Thermomechanical properties, such as T_g, decrease as well with fluid absorption and swelling of these composites (or polymers) explained in Section 2.3.2.

In some cases (Ma, Lee, & Tai, 1992), the flexural strength of specimens (carbon/PEEK) immersed in JP-4 fuel increases because of the swelling of the composites. Both composites (carbon/PEEK and carbon/PPS) displayed a degradation in mechanical strengths as a function of fluid uptake, and a reduction in T_g of up to 20 °C. For carbon/PEEK composites, the changes in strength were modest. In contrast, carbon/PPS composites displayed a significant decrease in tensile and flexural strengths (Ma, Lee, & Tai, 1992). Flexural moduli and strengths were seen to decrease for carbon/epoxy and carbon/BMI when exposed to JP-4 (Curliss & Carlin, 1989;

Curliss D. B., 1991). These decreases were attributed to the changes in the fiber/matrix interface and/or adhesion. The ultimate strengths in tension and compression of specimens immersed in fluids and loaded to *20%* of ultimate strength decreased more than those exposed to the fluids in the unloaded state (Horn, Soeganto, & Shaikh, 1989). The average strength of unloaded specimens exposed to water and hydraulic fluid increased. The modulus of the unloaded specimens was mostly less than that of the loaded specimens after being immersed in the same fluid for 60 days. Even though none of the specimens reached their equilibrium saturation condition for any of the investigated fluids, jet fuel, and paint stripper had a profound effect on composite mechanical properties, as seen in Table 7 and Table 8 (Horn, Soeganto, & Shaikh, 1989).

Table 7. Effect of fluid uptake on the mechanical properties of fluid-immersed graphite/PEEK composites with no load conditioning (table reproduced from (Horn, Soeganto, & Shaikh, 1989)).[2]

Chemical agent	**Mechanical properties**				
	Ultimate strength in tension (f_T) for T specimens	**Open-hole ultimate strength in tension (f_{OT}) for R specimens**	**Open-hole ultimate strength in compression (f_{OC}) for C specimens**	**Young's modulus in tension (E_T) for T specimens**	**Interlaminar shear strength (f_S) for I specimens**
	(ksi)	**(ksi)**	**(ksi)**	**(ksi)**	**(ksi)**
Baseline	125.04 ± 9.46	72.17 ± 1.86	55.71 ± 2.35	6.8 ± 0.53	5.64 ± 0.33
Paint stripper	107.34 ± 6.58	64.79 ± 1.23	47.7 ± 0.76	6.59 ± 0.64	6.12 ± 0.18
Brine	119.28 ± 7.84	71.54 ± 3.01	57.49 ± 0.35	6.65 ± 0.44	6.34 ± 0.32
Water	119.92 ± 7.25	72.71 ± 4.26	53.02 ± 1.85	6.55 ± 0.34	6.33 ± 0.43

[2] Each column in the two tables contains the mean of the assessed mechanical property and their standard deviation for up to five specimens exposed to each fluid for almost 60 days.

Chemical agent	Mechanical properties				
	Ultimate strength in tension (f_T) for T specimens	Open-hole ultimate strength in tension (f_{OT}) for R specimens	Open-hole ultimate strength in compression (f_{OC}) for C specimens	Young's modulus in tension (E_T) for T specimens	Interlaminar shear strength (f_S) for I specimens
	(ksi)	(ksi)	(ksi)	(ksi)	(ksi)
Ethylene glycol	121.06 ± 0.91	69.79 ± 2.23	54.48 ± 2.49	6.77 ± 0.22	6.1 ± 0.53
Hydraulic fluid	123.6 ± 7.99	73.75 ± 4.36	54.22 ± 2.13	6.98 ± 0.46	5.97 ± 0.35
Jet fuel	126.53 ± 3.03	68.18 ± 0.51	55.88 ± 1.35	7.03 ± 0.22	6.06 ± 0.34

Table 8. Effect of fluid uptake on the mechanical properties of fluid-immersed graphite/PEEK composites under a uniaxial load during immersion (table reproduced from (Horn, Soeganto, & Shaikh, 1989)).

Chemical agent	Mechanical properties				
	Ultimate strength in tension (f_T) for T specimens	Open-hole ultimate strength in tension (f_{OT}) for R specimens	Ultimate strength in tension (f_T) for T specimens	Young's modulus in tension (E_T) for T specimens	Ultimate strength in tension (f_T) for T specimens
	(ksi)	(ksi)	(ksi)	(ksi)	(ksi)
Baseline	125.04 ± 9.46	72.17 ± 1.86	55.71 ± 2.35	6.8 ± 0.53	5.64 ± 0.33
Paint stripper	121.83 ± 2.88	71.29 ± 1.89	54.88 ± 2.36	6.73 ± 0.51	5.56 ± 0.36
Brine	117.62 ± 5.16	70.8 ± 0.99	51.94 ± 2.84	6.83 ± 0.35	5.75 ± 0.27

Chemical agent	Mechanical properties				
	Ultimate strength in tension (f_T) for T specimens	Open-hole ultimate strength in tension (f_{OT}) for R specimens	Ultimate strength in tension (f_T) for T specimens	Young's modulus in tension (E_T) for T specimens	Ultimate strength in tension (f_T) for T specimens
	(ksi)	(ksi)	(ksi)	(ksi)	(ksi)
Water	117.49 ± 1.83	71.33 ± 2.81	54.39 ± 2.36	6.76 ± 0.39	5.96 ± 0.27
Ethylene glycol	129.69 ± 0.00	69.05 ± 3.83	53.91 ±2.9	7.07 ± 0.42	5.69 ± 0.28
Hydraulic fluid	124.53 ± 5.66	69.77 ± 3.14	53.82 ± 1.15	7.22 ± 0.18	6.1 ± 0.37
Jet fuel	114.09 ± 0.00	67.39 ± 2.62	51.11 ± 1.45	7.13 ± 0.23	5.57 ± 0.63

Changes in mechanical properties of carbon/epoxy and aramid/epoxy specimens immersed in different types of fluids were investigated. For the [+/-45°] ply configuration, the stiffness reduction for carbon/epoxy composites was not as pronounced as that of aramid/epoxy composites, due to plasticization of the hygroscopic aramid fiber composite matrix. Exposure to water and Skydrol resulted in a reduction of tensile stiffness values for aramid/epoxy composites, while the tensile stiffness and compressive stiffness for the fuel exposed specimens increased. Aramid composites' tensile and compressive strength decreased after exposure to all types of fluids, as seen in Table 9. In terms of maximum fatigue stress, the conditioned specimens showed lower values than the plain ones with more drastic decreases in properties for the impacted ones.

Table 9: Static characteristics of fluid-conditioned aramid laminates (Sala, 2000).

Conditioning	Dry (control specimens)	Water	Dichloromethane	Jet fuel	Skydrol
Tensile stiffness (GPa)	62.9	52.4	63.3	67.2	56.4

Conditioning	**Dry (control specimens)**	**Water**	**Dichloromethane**	**Jet fuel**	**Skydrol**
Compressive stiffness (GPa)	60.0	50.3	57.1	64.3	49.6
Tensile strength (MPa)	188.3	177.2	169.9	174.1	147.6
Compressive strength (GPa)	96.6	62.3	73.1	73.6	58.3

Landry et al. (Landry, LaPlante, & LeBlanc, 2012) investigated mode II delamination. All specimens showed decreases in certain properties, delamination toughness decreased by order of 20-25% for water and deicing fluid, and only a 4% decrease for the hydraulic fluid case. The delamination growth rate increased for the specimens, with higher values related to water and deicing fluid (125% and 327%, respectively), compared to hydraulic fluid (60%).

In a different study, the effects of acetone (a component in paint-stripper) exposure on the thermomechanical properties of *i*) PEEK, *ii*) amorphous poly (etherimide) (PEI), and *iii*) a 50/50 blend of PEEK/PEI have been investigated (Browne, Forsyth, & Goodwin, 1997). A drop in T_g for all specimens was observed. Specimens made of PEEK/PEI showed drastically reduced solvent uptake compared to the PEI homopolymer. Both polymers showed substantial decreases in Young's modulus, yield stress, and tensile strength, as seen in Table 10. In contrast, the properties of PEEK were relatively unaffected by acetone exposure; this was attributable to PEEK's high degree of crystallinity, low net mass increase after fuel absorption/desorption, and relatively low plasticization.

Table 10: Mechanical properties of PEEK, PEI, and 50 wt% PEEK/PEI blend (Browne, Forsyth, & Goodwin, 1997).

Conditions	**Specimen**	**Tensile strength (MPa)**	**Yield stress (MPa)**	**Young's modulus ($x10^2$ MPa)**	**% Strain at break**
Untreated	PEEK	56 ± 2	41 ± 1	13.4 ± 0.5	245 ± 15
	PEI	91 ± 4	50 ± 2	14.0 ± 0.9	14 ± 1
	Blend	70 ± 4	45 ± 2	13.4 ± 0.07	50 ± 50
Immersed at 25 °C	PEEK	33 ± 2	27 ± 2	9.60 ± 0.5	286 ± 35
	PEI	1.5 ± 0.9	0.6 ± 0.6	0.83 ± 0.9	4 ± 2
	Blend	16 ± 0.9	15 ± 0.9	5.0 ± 0.3	17 ± 6
Immersed at 45 °C	PEEK	38 ± 4	32 ± 2	1.0 ± 0.2	6.8 ± 0.5
	PEI	5 ± 3	5 ± 3	0.3 ± 0.2	304 ± 12
	Blend	28 ± 3	24 ± 5	1.0 ± 0.2	5 ± 1

Cornélis et al. (Cornélis, Kander, & Martin, 1996) exposed an amorphous (PEEK) film sample to acetone at room temperature until equilibrium saturation in fluid uptake was reached. The vacuum dried film (acetone desorbed) was compared to the initial film using DSC, Wide-Angle X-ray Scattering (WAXS), Small-Angle X-ray Scattering (SAXS), and infra-red spectroscopy. DSC results showed that the amorphous PEEK film has an exothermic crystallization peak and an endothermic melting peak while the exposed PEEK film the melting point is visible but not the crystallization peak meaning that the acetone crystallizes the exposed PEEK film, as seen in Figure 58.

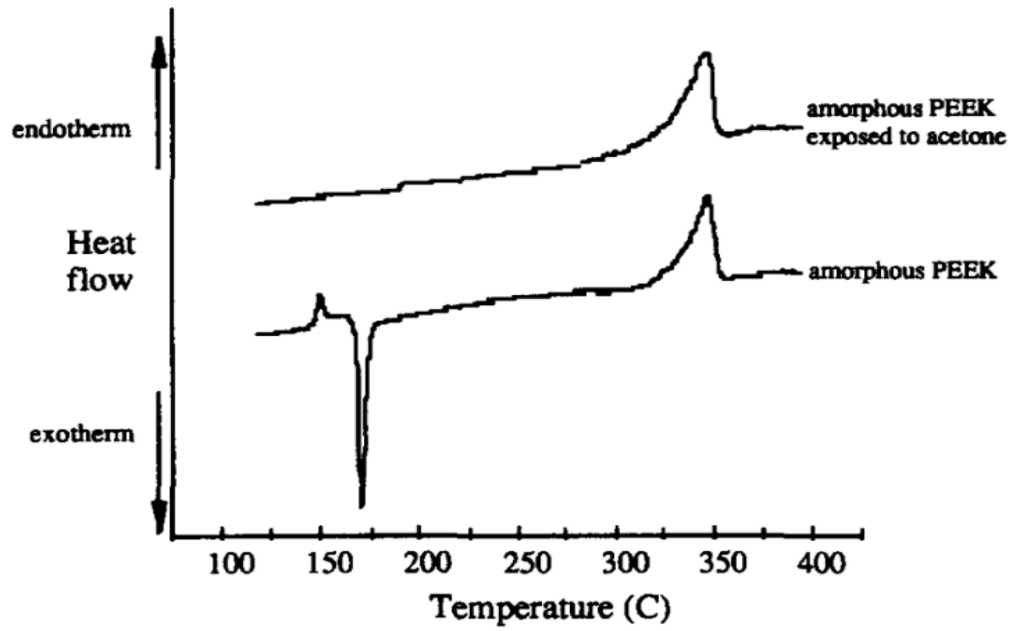

Figure 57. DSC curves of amorphous PEEK unexposed and exposed to acetone.

The WAXS results correlated the DSC result by affirming that a solvent induced crystallization with small crystal morphology was happening, which was due to the plasticization of the polymeric chains. From the WAXS curves seen in Figure 59, the curves of the acetone exposed PEEK show sharp peaks compared to the unexposed film, implying solvent induced.

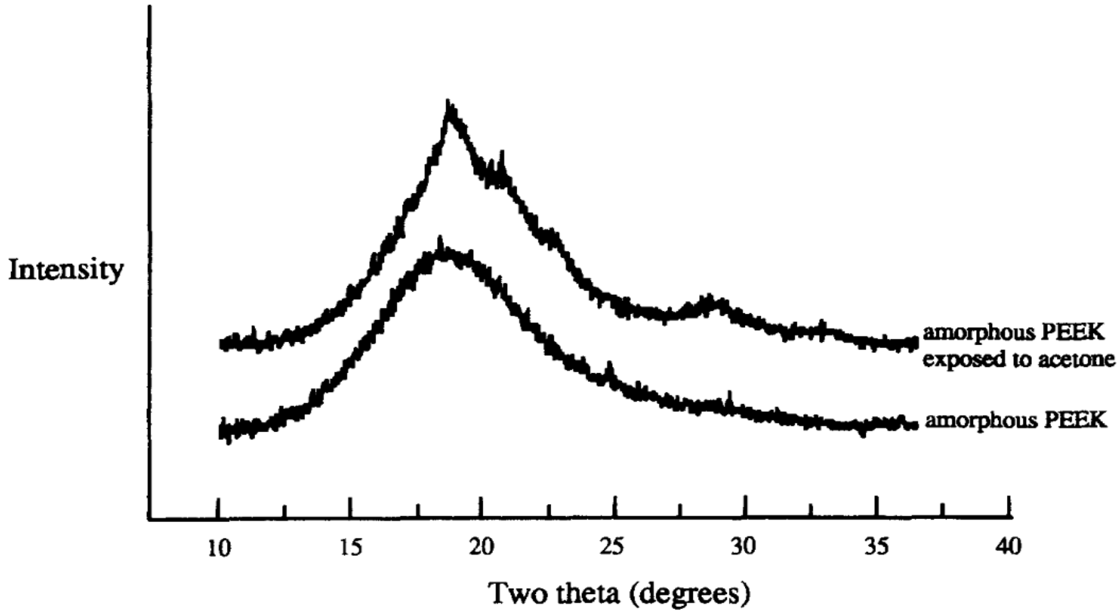

Figure 58. WAXS curves of amorphous PEEK unexposed and exposed to acetone.

To investigate the interaction between JP-4 and polymer components, test specimens that were immersed were heated, and volatiles were collected (condensate) using a cold trap (Curliss & Carlin, 1989; Curliss D. B., 1991). The condensate was then diluted and analyzed using gas chromatography (GC)-mass spectrometry (MS). The GC separated different components of the condensate, and MS was used to identify those components. The condensate composition was different than that of the fuel, indicating leaching of small molecules from the matrix and/or degradation of the matrix, as seen in Table 11 (Curliss & Carlin, 1989; Curliss D. B., 1991).

Table 11: Comparison between components of JP-4 and the fuel desorbed from APC (Curliss D. B., 1991).

No.	JP-4	A/A0	Desorbed	A/A0
1	2,3-dimethylpentane	2.3	Octane	1.0
2	Heptane	1.9	1,2-dimethlybenzene	8.9
3	Methylcyclohexane	1.4	1-ethyl-3-methylbenzene	31.8
4	Octane	1.0	1-ethyl-2-methylbenzene	9.4
5	2,6-dimethylheptane	0.1	1,2,3-trimethylbenzene	34.4
6	Ethylcyclohexane	0.5	1,2,4-trimethylbenzene	17.9
7	2-methyloctane	0.4	1-methyl-3-propylbenzene	8.8
8	1,2-dimethylbenzene	0.5	1,4-diethylbenzene	32.2
9	nonane	1.0	1-ethyl-1,4-dimethylbenzene	21.8
10	3,4,4-trimethyl-2hexene	0.1	1,2,4,5-tetramethylbenzene	31.8

With a limited number of studies reported on the exposure of composite structures to low aromatic content alternative jet fuels, the impact of using these fuels in systems that evolved for use with petroleum fuels has not yet been well defined. Boeing has examined the effect of SPK and SPK/Jet-A fuel blends (up to 50%) on nonmetallic materials used in commercial aircraft fuel systems. Some of the test materials used were a fluorocarbon O-ring material, epoxy coatings, nylon films, a rubber O-ring material, a polythioether, and a polysulfide sealant. Volume swell was determined for dry materials immersed in different Jet-A fuels (containing a range of 8.7% to 23.1% aromatic contents) and SPK fuels (0% aromatics) for 40 hours at room temperature. In certain cases, the volume swell of the test materials did not reach equilibrium by the end of the 40-hour aging period. Nonetheless, the progression of the volume swell was deemed enough to determine the relative response of each material to the test fuel (Graham, 2011). The volume swell of the test materials was assessed using TGA and thermal desorption gas chromatography-mass spectrometry (TD-GC–MS) tests. These tests showed that swelling increased with higher aromatic contents in the fuel and that the test materials reacted differently to the aromatics of the fuel. Volume swell increased with the decreased molar volume of the fuel components, and with increasing polarity. Polarity and hydrogen bonding also had effects on the volume swell of the test materials. Moreover, the impact of hydrogen bonding was considerably higher than that of polarity, meaning that the volume swell of test materials due to jet fuel will increase as the boiling range decreases to lower temperatures (lower molecular weight), and as polarity and hydrogen bonding increase. Since Jet-A fuels and all regular SPKs are paraffinic and thus non-polar, the polarity and hydrogen bonding of the fuel will be governed by the aromatics (Graham, 2011).

The Air Force Civil Engineer Support Agency (AFCESA) investigated the effects of a 50% hydro-treated renewable JP-8 jet fuel (HRJ) blend in existing fuels systems by immersing test materials for a total of 28 days in this fuel blend. (Pond & Company, Inc., 2012). This fuel blend could lead to the reduction of the life expectancy of some Nitrile rubber components in fuel systems, namely control valves where elasticity is an important property. The blends can also lead to shrinkage in some seals, which can result in short term leakage when the new fuel is introduced into a current system (Pond & Company, Inc., 2012).

Baeza et al. (Baeza, et al., 2014), investigated the compatibility of biokerosene blends of coconut, babassu, and palm kernel with commercial Jet A-1, testing airplane polymeric materials, metals, and composites. The composites tested were ribs and wings from an Airbus company airplane, and which were mainly made of carbon fibers, electrically isolated titanium screws, yellow paint on the surface, and phenylene polysulphide joints sealing joints. The compatibility of the fuel blends with these composite materials was investigated through a different method. Instead of determining the differences in the composite's properties due to the immersion in the fuel blends, the effect of this immersion was measured on the fuels (Baeza, et al., 2014). The specimens were immersed in several blends for 90 days (2160 hours) at a temperature of 50 °C. The fuel degradation was evaluated through an analysis of the oxidation and nitration bands resulting from the compatibility tests measured with Fourier Transform Infrared Spectroscopy (FTIR). Four samples were taken, the first one at the beginning of the test and the others every 30 days. All fuel samples were below the maximum acidity given by the ASTM standard D1665 (Standard Test Method for Engler Specific Viscosity of Tar Products). The acidity even decreased when the composite specimens were immersed in coconut-biokerosene and babassu-biokerosene blends. The density of the fuel samples was also within the allowed range of the standard and was higher than Jet A fuel's density. The kinematic viscosity decreased slightly after the immersion test and was far below the maximum established by standard ASTM D1655 for all fuel samples. Color tests demonstrated no variation from the initial color, meaning that no fuel degradation occurred during testing (Baeza, et al., 2014). Additionally, all fuel samples met the standard for aviation fuel DEF STAN 91-91, which requires kerosene, used in aviation to be colorless and clear. Through FTIR analysis, the oxidation and nitration bands were measured to investigate the degradation of the composites, but the spectra did not display any trace of oxidized compounds. Therefore, it was concluded that composite specimens studied were compatible with the alternative jet fuel blends tested (Baeza, et al., 2014).

3 Conclusion

This literature review surveys the effects of aeronautical fluids on aerospace composites with applications to general aviation and commercial transport aircrafts. The literature review includes a comprehensive overview of *i*) the different aeronautical fluid composite materials may encounter, *ii*) the possible material combination used in aerospace grade composites, *iii*) the thermodynamics and kinetics of diffusion, and *iv*) experimental techniques used to assess progressive degradation in composite's thermal and mechanical properties as a function of different commercially available conventional jet fuel/ alternative jet fuel blends, exposure times and exposure temperatures.

Aeronautical fluids effects on aerospace composites comprise swelling, gain in weight, mechanical property degradation (e.g., stiffness, tensile strength, flexural strength, compressive strength, etc.), thermal degradation (e.g., T_g), and can lead to the degradation of the structural integrity of the composite (e.g., delamination, fiber/matrix debonding, matrix cracking, etc.).

Alternative fuels, which are known to have low to no aromatic content, are approved under the same certification guidelines as traditional fuel, and as such, are expected to have similar interactions with composite materials. The diffusion and thermo-mechanical properties of a selection of alternative fuel blends were studied over a limited duration and showed no significant difference compared with those of conventional jet fuel [Ref of Final-Report].

However, long term effects of new alternative fuels on composite structures are not extensively available in the literature. It is recommended to further investigate the extended exposure of new alternative jet fuels or pure aliphatic model fluids to aerospace composites.

4 References

Abdelkader, A., & White, J. (2005). Water absorption in epoxy resins: The effects of the crosslinking agent and curing temperature. *Journal of applied polymer science, 98*(6), 2544-2549.

Aircraft Hydraulic Fluids Types, Intermixing, Contamination, Flushing and Handling. (n.d.). Retrieved 2019, from aircraftsystemstech: https://www.aircraftsystemstech.com/p/types-of-hydraulic-fluids.html

Akay, M., Mun, S. K., & Stanley, A. (1997). Influence of moisture on the thermal and mechanical properties of autoclaved and oven-cured Kevlar-49/epoxy laminates. *Composites science and technology, 57*(5), 565-571.

Allen, D., & Ishida, H. (2001). Thermosets: Phenolics, Novolacs, and Benzoxazine.

Arzak, A., Eguiazabal, J., & Nazabal, J. (1994). Effects of methylene chloride sorption on the properties of poly (ether ether ketone). *Journal of Polymer Science Part B: Polymer Physics, 32*(2), 325-331.

ASTM. (2019). *International Research Report RR:D02-1914 CHJ Pathway.*

ASTM International. (2011). ASTM D7566-11a, standard specification for aviation turbine fuel containing synthesized hydrocarbons. *ASTM 2008 Annual Book of Standards*.

ASTM International. (2012). ASTM D4054-09, Standard Practice for Qualification and Approval of New Aviation Turbine Fuels and Fuel Additives. *ASTM International West Conshohocken, PA*.

ASTM International. (2012). D5229/D5229M-12" Standard Test Method for Moisture Absorption Properties and Equilibrium Conditioning of Polymer Matrix Composite Materials.".

ASTM International. (2013). ASTM D6415 / D6415M - 06a, Standard Test Method for Measuring the Curved Beam Strength of a Fiber-Reinforced Polymer-Matrix Composite.

ASTM International. (2014). ASTM D1665-98, Standard Test Method for Engler Specific Viscosity of Tar Products.

ASTM International. (2015). ASTM D7028 - 07, Standard test method for glass transition temperature (DMA Tg) of polymer matrix composites by dynamic mechanical analysis (DMA).

ASTM International. (2020). D1655-20c, Standard Specification for Aviation Turbine Fuels.

ATAG. (2009). Beginners Guide to Aviation Biofuels. Switzerland.

Aviation Biofuel. (n.d.). Retrieved 2018, from Wikipedia: https://en.wikipedia.org/wiki/Aviation_biofuel

Aviation fuel: Jet fuel. (n.d.). Retrieved 2018, from Wikipedia: https://en.wikipedia.org/wiki/Aviation_fuel#Jet_fuel

Aviation Maintenance Technician Book Vol. 2 (Vols. FAA-H-8083-31). (2012). US Department of Transportation, Federal Aviation Administration.

Baeza, A.-l., Maria, A., Llamas Lois, A., Bolonio Martin, D., Canoira Lopez, L., Sanz Perez, F., & Lapuerta , M. (2014). Airplane materials compatibility with blends of fossil kerosene jet A1 with biokerosenes from babassu, palm kernel and coconut oils. *Global nest journal, 16*(6), 1066-1075.

Baeza, A.-l., María, A., Llamas Lois, A., Bolonio Martín, D., Canoira López, L., Sanz Pérez, F., & Lapuerta, M. (2014). Airplane materials compatibility with blends of fossil kerosene jet A1 with biokerosenes from babassu, palm kernel and coconut oils. *Global nest journal, 16*(6), 1066-1075.

Bao, L.-R., & Yee, A. F. (2002). Effect of temperature on moisture absorption in a bismaleimide resin and its carbon fiber composites. *Polymer, 43*(14), 3987-3997.

Barsoum, R. G. (2015). *Elastomeric Polymers with High Rate Sensitivity: Applications in Blast, Shockwave, and Penetration Mechanics.* William Andrew.

Bassou, R., Harich, N., Kundu, S., Priddy, M. W., Lacy, T. E., & Pittman, C. U. (2019). *DOT/FAA/TC-20/22 - Effect of Jet Fuels Exposure on Aerospace Composites - Literature Review.* Federal Aviation Administration. Atlantic City International Airport, NJ: FAA William J. Hughes Technical Center.

BENEFITS, A. L. (2009). CONFERENCE ON AVIATION AND ALTERNATIVE FUELS. *Transportation Research*.

Berens, A., & Hopfenberg, H. (1979). Induction and measurement of glassy-state relaxations by vapor sorption techniques. *Journal of Polymer Science: Polymer Physics Edition, 17*(10), 1757-1770.

Biofuels for Aviation: Technology Brief. (2017). Retrieved 2018, from http://www.irena.org/documentdownloads/publications/irena_biofuels_for_aviation_2017.pdf

Boinard, E., Pethrick, R. A., Dalzel-Job, J., & Macfarlane, C. J. (2000). Influence of resin chemistry on water uptake and environmental ageing in glass fibre reinforced composites-polyester and vinyl ester laminates. *Journal of materials science, 35*(8), 1931-1937.

Bond, D., & Smith, P. (2006). Modeling the transport of low-molecular-weight penetrants within polymer matrix composites. *Applied Mechanics Reviews, 59*(5), 249-268.

Brown, A. (2013). *The Decomposition Behavior of Thermoset Carbon Fiber Epoxy Composites in the Fire Environment.* Sandia National Lab.(SNL-NM), Albuquerque, NM (United States).

Browne, M., Forsyth, M., & Goodwin, A. A. (1997). The effect of solvent uptake on the relaxation behaviour, morphology and mechanical properties of a poly (ether ether ketone)/poly (etherimide) blend. *Polymer, 38*(6), 1285-1290.

CAAFI Frequently Asked Questions. (n.d.). Retrieved 2019, from www.caafi.org/resources/faq.html

CAAFI Fuel Qualification. (n.d.). Retrieved 2019, from http://www.caafi.org/focus_areas/fuel_qualification.html

Carter, H. G., & Kibler, K. G. (1978). Langmuir-type model for anomalous moisture diffusion in composite resins. *Journal of Composite Materials, 12*(2), 118-131.

Cheng, Y.-S., Zhou, Y., Chow, J., Watson, J., & Frazier, C. (2001). Chemical composition of aerosols from kerosene heaters burning jet fuels. *Aerosol Science & Technology, 35*(6).

Chua, J., & Tu, Q. (2018). A Molecular Dynamics Study of Crosslinked Phthalonitrile Polymers: The Effect of Crosslink Density on Thermomechanical and Dielectric Properties. *Polymers, 10*(1), 64.

Collyer, A. (1989). High temperature engineering thermoplastics. *Progress in rubber and plastics technology, 5*(1), 36-87.

Comparison of Thermoset Versus Thermoplastic Materials. (n.d.). Retrieved 2019, from https://www.thomasnet.com/articles/plastics-rubber/thermoset-vs-thermoplastics/

Cornélis, H., Kander, R. G., & Martin, J. P. (1996). Solvent-induced crystallization of amorphous poly (ether ether ketone) by acetone. *Polymer, 37*(20), 4573-4578.

Crank, J. (1979). *The mathematics of diffusion.* Oxford university press.

Curliss, D. B. (1991). *The effect of Jet fuel exposure on advanced aerospace composites I: Thermal and Chemical Analysis.* WRIGHT LAB WRIGHT-PATTERSON AFB OH.

Curliss, D., & Carlin, D. (1989). *Effect of jet-fuel exposure on advanced aerospace composites, II: Mechanical properties. Final report,.* Air Force Wright Research and Development Center, Wright-Patterson AFB, OH (USA).

Daniel, I. (1978). Failure mechanisms in fiber-reinforced composites.

Defence Standard. (2002). 91-91/4: Turbine Fuel. *Aviation Kerosine Type, A-1 NATO code: F-35 Joint Service Designation: AVTUR*.

Demeuse, M., & Kiss, G. (2014). Liquid crystal polymers (LCPs) as a reinforcement in high temperature polymer blends. In *High Temperature Polymer Blends* (pp. 141-164). Elsevier.

Edwards, J., Shafer, L., & Klein, J. (2012). *US Air Force hydroprocessed renewable jet (HRJ) fuel research.* AIR FORCE RESEARCH LAB WRIGHT-PATTERSON AFB OH PROPULSION DIRECTORATE ….

Ethanol feedstocks. (n.d.). Retrieved 2019, from https://afdc.energy.gov/fuels/ethanol_feedstocks.html

Feedstocks for Biofuel Production. (2019). Retrieved 2019, from https://farm-energy.extension.org/feedstocks-for-biofuel-production/#Sugar_and_Starch_Crops

Fellet, M. (2016). *Now Boarding: Commercial Planes Take Flight with Biobased Jet aFuel*. Retrieved 2018, from cen.acs.org/articles/94/i37/boarding-Commercial-planes-take-flight.html

Feng, Y., He, Y., An, T., Cui, R., Shao, Q., & Fan, C. (2015). Effect of hygrothermal condition on buckling and post-buckling performance of CCF300/5228A aero composite stiffened panel under axial compression. *Journal of Reinforced Plastics and Composites, 34*(12), 989-999.

Five Jet Biofuels Now Approved, FAA Says. (2016). Retrieved 2018, from www.aopa.org/news-and-media/all-news/2016/april/14/five-jet-bio-fuels-now-approved-says-faa

Grace, L. R., & Altan, M. (2013). Non-fickian three-dimensional hindered moisture absorption in polymeric composites: Model development and validation. *Polymer Composites, 34*(7), 1144-1157.

Grace, L. R., & Altan, M. (2014). Three-dimensional anisotropic moisture absorption in quartz-reinforced bismaleimide laminates. *Polymer Engineering & Science, 54*(1), 137-146.

Graham, J. (2011). Impact of Alternative Jet Fuel and Fuel Blends on Non-Metallic Materials Used in Commerical Aircraft Fuel Systems. *Federal Aviation Administration and The Boeing Company, Technical Report DTFAWA-10-C-0030*.

Handbook, M. (2002). MIL-HDBK-17-2F: Composite materials handbook. *Polym Matrix Compos Mater Usage Des Anal, 17*.

Horn, W., Soeganto, A., & Shaikh, F. (1989). Degradation of mechanical properties of advanced composites exposed to aircraft environment. *AIAA journal, 27*(10), 1399-1405.

Huang, X. (2009). Fabrication and properties of carbon fibers. *Materials, 2*(4), 2369-2403.

Hydraulic fluid: Aircraft hydraulic systems. (n.d.). Retrieved 2018, from Wikipedia: https://en.wikipedia.org/wiki/Hydraulic_fluid#Aircraft_hydraulic_systems

Iredale, R. J., Ward, C., & Hamerton, I. (n.d.). Modern advances in bismaleimide resin technology: a 21st century perspective on the chemistry of addition polyimides. *Progress in Polymer Science, 69*, 1-21.

Jacobs, P., & Jones, E. (1989). Diffusion of moisture into two-phase polymers. *Journal of materials Science, 24*(7), 2343-2347.

Johnson, T. (2019). *Composites in Aerospace*. Retrieved 2019, from https://www.thoughtco.com/composites-in-aerospace-820418

Kim, H., & Takemura, K. (2011). Influence of water absorption on creep behaviour of carbon fiber/epoxy laminates. *Procedia Engineering, 10*, 2731-2736.

Korkees, F., Alston, S., & Arnold, C. (2018). Directional diffusion of moisture into unidirectional carbon fiber/epoxy Composites: Experiments and modeling. *Polymer Composites, 39*(S4), E2305-E2315.

La Saponara, V. (2011). Environmental and chemical degradation of carbon/epoxy and structural adhesive for aerospace applications: Fickian and anomalous diffusion, Arrhenius kinetics. *Composite Structures, 93*(9), 2180-2195.

La Scala, J., & La Scala, J. (2005). Property analysis of triglyceride-based thermosets. *Polymer, 46*(1), 61-69.

Landry, B., LaPlante, G., & LeBlanc, L. (2012). Environmental effects on mode II fatigue delamination growth in an aerospace grade carbon/epoxy composite. *Composites Part A: Applied Science and Manufacturing, 43*(3), 475-485.

Li, M., Gu, Y.-Z., Liu, H., Li, Y.-X., Wang, S.-K., Wu, Q., & Zhang, Z.-G. (2013). Investigation the interphase formation process of carbon fiber/epoxy composites using a multiscale simulation method. *Composites Science and Technology, 86*, 117-121.

Lin, Y., & Chen, X. (2005). Moisture sorption–desorption–resorption characteristics and its effect on the mechanical behavior of the epoxy system. *Polymer, 46*(25), 11994-12003.

Loos, A., & Springer , G. (1979). Moisture absorption of graphite-epoxy composites immersed in liquids and in humid air. *Journal of Composite Materials, 13*(2), 131-147.

Ma, C.-C., Lee, C.-L., & Tai, N.-H. (1992). Chemical resistance of carbon fiber-reinforced poly (ether ether ketone) and poly (phenylene sulfide) composites. *Polymer composites, 13*(6), 435-440.

Mangalgiri, P. (1999). Composite materials for aerospace applications. *Bulletin of Materials Science, 22*(3), 657-664.

Mazumdar, S. (2001). *Composites manufacturing: materials, product, and process engineering.* CrC press.

Melton, G. H., Peters, E. N., & Arisman, R. K. (2011). Engineering Thermoplastics. In *Applied Plastics Engineering Handbook* (pp. 7-21). Elsevier.

Menard, K., & Menard, N. (2002). *Dynamic mechanical analysis in the analysis of polymers and rubbers.* Encyclopedia of Polymer Science.

Michel, J. (2016). Work Package 5, D5. 2: Final Report on Technical Compatibility, Certification and Deployment.

Moses, C., & Roets, P. (2009). Properties, characteristics, and combustion performance of sasol fully synthetic jet fuel. *Journal of Engineering for Gas turbines*.

National Academies of Sciences, E. (2016). *Commercial aircraft propulsion and energy systems research: reducing global carbon emissions.* National Academies Press.

New alternative jet fuel approved. (2016). (FAA) Retrieved 2018, from https://www.faa.gov/news/updates/?newsId=85425

O'Neil, G. W., Knothe, G., & Reddy, C. M. (2019). Jet biofuels from algae. In *Biofuels from Algae* (pp. 359-395). Elsevier.

Office of Energy Efficiency & Renewable Energy. (n.d.). *Alternative Aviation Fuels: Overview of Challenges, Opportunities, and Next Steps*. Retrieved 2019, from Energy.gov: https://www.energy.gov/eere/bioenergy/downloads/alternative-aviation-fuels-overview-challenges-opportunities-and-next-steps

Parts, L. (1979). *Assessment of the flammability of aircraft hydraulic fluids.* MONSANTO RESEARCH CORP DAYTON OH DAYTON LAB.

Phenolic novolac and resole resins. (n.d.). Retrieved 2019, from https://www.plenco.com/phenolic-novolac-resol-resins.htm

Pillard, D., & DuFresne. (1999). Toxicity of formulated glycol deicers and ethylene and propylene glycol to Lactuca sativa, Lolium perenne, Selenastrum capricornutum, and Lemna minor. *Archives of environmental contamination, 37*(1), 29-35.

Pires, A., Han, Y., Kramlich, J., & Garcia-Perez, M. (2018). Chemical composition and fuel properties of alternative jet fuels. *BioResources, 13*(2), 2632-2657.

Polyether ether ketone. (n.d.). Retrieved 2019, from Wikipedia: https://en.wikipedia.org/wiki/Polyether_ether_ketone

Pond & Company, Inc. (2012). *Investigative Study to Determine Effects of Hydro-Treated Renewable JP-8 Jet Fuel Blend in Existing Fuels Infrastructure.*

Puhan, D., & Wong, J. S. (2019). Properties of Polyetheretherketone (PEEK) transferred materials in a PEEK-steel contact. *Tribology International, 135*, 189-199.

Rahmes, T., Kinder, J., Crenfeldt, G., LeDuc, G., Abe, Y., McCall, M., . . . Lewic, C. (2009). Sustainable bio-derived synthetic paraffinic kerosene (Bio-SPK) jet fuel flights and engine tests program results. *9th AIAA aviation technology, integration, and operations conference (ATIO) and aircraft noise and emissions reduction symposium (ANERS)*, (p. 7002).

Renner, A., & Kramer, A. (1989). Allylnadic-imides: A new class of heat-resistant thermosets. *Journal of Polymer Science Part A: Polymer Chemistry, 27*(4), 1301-1323.

Roy, S., Xu, W., Park, S., & Liechti, K. (1999). Anomalous moisture diffusion in viscoelastic polymers: modeling and testing. *J. Appl. Mech., 67*(2), 391-396.

Sala, G. (2000). Composite degradation due to fluid absorption. *Composites Part B: Engineering, 31*(5), 357-373.

Shell. (n.d.). *AEROSHELL HYDRAULIC FLUIDS*. Retrieved 2019, from https://www.shell.com/business-customers/aviation/aeroshell/knowledge-centre/the-aeroshell-book/_jcr_content/par/textimage_1433441235.stream/1519764659863/50dd52fd4fce5d8a22ec69e7db85f0d7d26c50ca/aeroshell-book-6hydraulics.pdf

Shen, C.-H., & Springer, G. S. (1976). Moisture absorption and desorption of composite materials. *Journal of composite materials, 10*(1), 2-20.

Singh, A. K., Panda, B. P., Mohanty, S., Nayak, S. K., & Gupta, M. K. (2017). Thermokinetics behavior of epoxy adhesive reinforced with low viscous aliphatic reactive diluent and nano-fillers. *Korean Journal of Chemical Engineering, 34*(11), 3028-3040.

Soloiu, V., Muinos, M., Harp, S., Naes, T., & Gaubert, R. (2016). Combustion and Emissions Characteristics of Dual Fuel Premixed Charge Compression Ignition with Direct Injection of Synthetic FT Kerosene Produced from Natural Gas and Port Fuel Injection of n-Butanol.

Sperling, L. H. (2005). Introduction to physical polymer science.

Stenzenberger, H. (1988). Recent advances in thermosetting polyimides. *British Polymer Journal, 20*(5), 383-396.

Stenzenberger, H. (1990). Chemistry and properties of addition polyimides. In *Polyimides* (pp. 79-128). Springer.

Stober, E. J., & Seferis, J. C. (1988). Fluid sorption characterization of PEEK matrices and composites. *Polymer Engineering & Science, 28*(9), 634-639.

Sugita, Y., Winkelmann, C., & La Saponara, V. (2010). Environmental and chemical degradation of carbon/epoxy lap joints for aerospace applications, and effects on their mechanical performance. *Composites Science and Technology, 70*(5), 829-839.

The race is on to repurpose garbage. (2019). Retrieved 2019, from https://cen.acs.org/business/biobased-chemicals/race-repurpose-garbage/97/i42

Toscano, A., Pitarresi, G., Scafidi, M., Di Filippo, M., Spadaro, G., & Alessi, S. (2016). Water diffusion and swelling stresses in highly crosslinked epoxy matrices. *Polymer Degradation and Stability, 133*, 255-263.

Vanlandingham, M., Eduljee, R., & Gillespie Jr, J. (1999). Moisture diffusion in epoxy systems. *Journal of applied polymer science, 71*(5), 787-798.

What are phenolic resins? (n.d.). Retrieved 2019, from https://www.hexion.com/en-us/chemistry/phenolic-resins/overview

What is PPS? (n.d.). Retrieved 2019, from http://www.dic-global.com/en/products/pps/about.html

Wilson, D., Stenzenberger, H. D., & Hergenrother, P. M. (1990). *Polyimides.* Springer.

Wolf, C. J., & Grayson, M. A. (1993). Solubility, diffusion and swelling of fluids in thermoplastic resin systems. *Polymer, 34*(4), 746-751.

Wyman, O. (2017). *Aviation 2.0: Why The Next Airplane You Fly On May Be Using BioFuels*. (Forbes, Producer) Retrieved 2018, from Forbes Magazine.

Yang, H., & Lee, L. J. (2002). Effects of resin chemistry on redox polymerization of unsaturated polyester resins. *Journal of applied polymer science, 84*(1), 211-227.

Yuan, M., Galloway, J. A., Hoffman, R. J., & Bhatt, S. (2011). Influence of molecular weight on rheological, thermal, and mechanical properties of PEEK. *Polymer Engineering & Science, 51*(1), 94-102.

Zafar, A., Bertocco, F., Schjødt-Thomsen, J., & Rauhe, J. (2012). Investigation of the long term effects of moisture on carbon fibre and epoxy matrix composites. *Composites Science and Technology, 72*(6), 656-666.

Zhang, Y. (2014). Production and Applications of Formaldehyde-Free Phenolic Resins Using 5-Hydroxymethylfurfural Derived from Glucose In-Situ.